OPTICAL ACCESS NETWORKS BASED ON 1.5-μm VCSELS

JINGJING ZHOU

NATIONAL UNIVERSITY OF SINGAPORE

2016

OPTICAL ACCESS NETWORKS BASED ON 1.5-μm VCSELS

JINGJING ZHOU

(*B. Eng., Northeastern University at Qinhuangdao*)

A THESIS SUBMITTED

FOR THE DEGREE OF DOCTOR OF PHILOSOPHY

DEPARTMENT OF ELECTRICAL AND COMPUTER ENGINEERING

NATIONAL UNIVERSITY OF SINGAPORE

2016

Declaration

I hereby declare that this thesis is my original work and it has been written by me in its entirety. I have duly acknowledged all the sources of information which have been used in the thesis.

This thesis has also not been submitted for any degree in any university previously.

Jingjing Zhou

August 5, 2016

Acknowledgement

I feel very fortunate to have had the opportunity to work with and learn from many remarkable people during my Ph.D candidature at the National University of Singapore (NUS). This thesis would not have been possible without their kind help and support.

First of all, I would like to express my deepest gratitude and sincere appreciation to my advisors Prof. Kim Hoon, Prof. Changyuan Yu and Prof. Mohan Gurusamy for their valuable guidance, helpful support and kind encouragement throughout my Ph.D study. Prof. Kim has set an example of both a great scholar with the spirit of adventure and a responsible mentor. Prof. Yu and Mohan, who constantly give me their support and trust, are not only erudite scholars, but also very patient and considerate mentors.

I thank many of our group members and visitors in both Optical Communication and Communication and Network Labs, with whom I had the best fortune to collaborate. I also thank all my friends since childhood, from NEUQ and those I met during these four years, for their friendship, company and encouragement.

Lastly, and most importantly, I would like to express my deepest gratitude to my beloved family members: my parents and younger brother, for their sacrifices, support and encouragement throughout my entire life. My special thanks go to my boy friend L, who has been consistently encouraging and supporting me. It is their love and support that make my life colorful!

Table of Contents

Summary

In order to reduce the cost of optical access networks which cover the "last mile" area and serve numerous business and residential users, inexpensive and energy-efficient optical sources, such as vertical-cavity surface emitting lasers (VCSELs), are becoming more and more desirable. Recent advancement in reliability and performance of 1.5-μm VCSELs has made this feasible and promising. However, there are still some problems that need to be properly addressed. Direct modulation-induced frequency chirp makes the generated signals from VCSELs suffer from severe chromatic dispersion (CD)-induced distortions when transmitted over standard single-mode fiber (SSMF). This thesis is devoted to investigating various methods to improve the dispersion tolerance of 1.5-μm VCSEL-based access link and to increase the bit-rate length (BL) product of the system.

This thesis starts with the performance investigation on 10.7-Gb/s VCSEL-based optical access link. The frequency-shift keying (FSK) modulation is first utilized by making good use of the frequency chirp in VCSELs, then a delay interferometer (DI) is inserted in the transmission link for FSK to amplitude-shift keying (ASK) conversion. Different DC-balanced line codings are tested in Chapter 3 to combat with the pattern-dependent signal distortions caused by the non-uniform frequency modulation (FM) response of VCSELs at low frequencies (i.e., $<$10 MHz). By taking

into account the insertion loss of the DI, we achieve a power budget improvement by >5 dB with the utilization of on-off keying (OOK) modulation format and DI, when compared with a conventional OOK VCSEL link without DI. In addition, 50- and 60-km transmissions over SSMF are successfully achieved with PIN and avalanche photodiode (APD) receivers, respectively. Then, we present a systematic study on the transmission performance of 10.7-Gb/s OOK and 4-pulse amplitude modulation (PAM) signals generated by a directly modulated 1.5-μm VCSEL in Chapter 3. With the optimized extinction ratio (ER) of signals and the use of receiver-side electrical dispersion compensation (EDC), we are able to achieve 80- and 40-km transmissions over SSMF by using the OOK and 4-PAM signals, respectively.

In the second part of this thesis, we explore the possibility of utilizing 1.5-μm, 10G-class VCSEL in 25-Gb/s optical access networks for the cost-effective implementation. Simple modulation formats (i.e., OOK and 4-PAM) and direct detection are employed. As for OOK signal, two different transmitter schemes: with and without a DI at the output of the VCSEL are investigated. When the DI is used, the FSK signal is converted into the OOK signal with an improved ER. The EDC technique is employed for dispersion and VCSEL's band-limitation compensation. With the optimized ER and receiver-side EDC, 35- and 45-km transmissions over SSMF by utilizing 25-Gb/s 4-PAM and OOK signals are successfully achieved, respectively. Moreover, the power budget of the 25-Gb/s OOK system is improved up to 25 km at the expense of the cost of the DI, compared to the case without DI.

We believe that inexpensive and energy-efficient 1.5-μm VCSELs could be used for short- or intermediate haul (e.g., < 50 km) transmission links and cost-sensitive optical access networks with low splitting ratios, supporting up to 25 Gb/s.

List of Figures

LIST OF FIGURES

List of Tables

List of Abbreviations

AM	Amplitude Modulation
AMI	Alternate Mark Inversion
APD	Avalanche Photodiode
ASE	Amplified Spontaneous Emission
ASK	Amplitude-Shift Keying
AWG	Array-Waveguide Grating
BER	Bit-Error Ratio
BL	Bit-Rate Length
B2B	Back-to-Back
CD	Chromatic Dispersion
CO	Central Office
CW	Continuous Wave
DBR	Distributed Bragg Reflectors
DCF	Dispersion Compensation Fiber
DCM	Dispersion Compensation Module
DFB	Distributed Feedback
DFE	Decision-Feedback Equalizer

DI	Delay Interferometer
DML	Directly Modulated Laser
DSP	Digital Signal Processing
EAM	Electro-Absorption Modulator
EDC	Electronic Dispersion Compensation
ER	Extinction Ratio
EXOR	Exclusive-Or
FEC	Forward Error Correction
FFE	Feed-Forward Equalizer
FFT	Fast Fourier Transform
FM	Frequency Modulation
FP	Fabry-Perot
FSK	Frequency Shift Keying
FSR	Free Spectral Range
FTTC	Fiber to the Curb
FTTCab	Fiber to the Cabinet
FTTEx	Fiber to the Exchange
HDTV	High-Definition Television
IC	Integrated Circuit
IDF	Inverse Dispersion Fiber
ISI	Inter-Symbol Interference
LMS	Least Mean Square
LPF	Low Pass Filter
MLSE	Maximum Likelihood Sequence Estimation

LIST OF ABBREVIATIONS

MMF	Multi-Mode Fiber
MUX	Multiplexer
MZM	Mach-Zehnder Modulator
NDF	Negative Dispersion Fiber
NRZ	Non-Return-to-Zero
OFDM	Orthogonal Frequency Division Multiplexing
OIL	Optical Injection Locking
OMA	Optical Modulation Amplitude
OOK	On-Off Keying
PAM	Pulse Amplitude Modulation
PON	Passive Optical Network
PRBS	Pseudo-Random Binary Sequence
QPSK	Quadrature Phase Shift Keying
QW	Quantum Well
RMS	Root Mean Square
SNR	Signal-to-Noise Ratio
SSBN	Signal-to-Signal Beating Noise
SSMF	Standard Single-Mode Fiber
TO	Transistor Outline
VCSEL	Vertical-Cavity Surface Emitting Laser
WDM	Wavelength Division Multiplexing

List of Publications

Journal Papers

- Z. Al-Qazwini, J. Zhou, and H. Kim, "1.5-μm, 10-Gb/s VCSEL link for optical access applications", *IEEE Photon. Technol. Lett.*, vol. 25, no. 22, pp. 2160-2163, Nov. 2013.

- J. Zhou, C. Yu, and H. Kim, "Transmission performance of OOK and 4-PAM signals using directly modulated 1.5-μm VCSEL for optical access network", *J. Lightwave Technol.*, vol. 33, no. 15, pp. 3243-3249, Aug. 2015.

- J. Zhou, C. Yu, G. Mohan and H. Kim, "25-Gb/s OOK transmission using 1.5-μm 10G-Class VCSEL for optical access network", *J. Lightwave Technol.*, vol. 34, no. 16, pp. 3790-3795, Jun. 2016.

Conference Papers

- J. Zhou, C. Yu, and H. Kim, "10-Gb/s, 20-km VCSEL optical access link at 1.5-μm with 23-dB power budget", *in Proc. OFC*, San Francisco, CA, Mar. 2014, paper W2A.2.

LIST OF PUBLICATIONS

- J. Zhou, C. Yu, and H. Kim, "1.5-μm, 10-Gbps 4-PAM VCSEL transmission for optical access networks", *in Proc. COIN*, Jeju, Korea, Aug. 2014, paper FA2-3.
- J. Zhou, C. Yu, and H. Kim, "1.5-μm, 21.4-Gbps 4-PAM VCSEL link for optical access applications", *in Proc. OFC*, Los Angeles, CA, Mar. 2015, paper Th2A.54.
- J. Zhou, C. Yu, G. Mohan and H. Kim, "25-Gb/s OOK and 4-PAM transmission over >35-km SSMF using directly modulated 1.5-μm VCSEL", *in Proc. OFC*, Anaheim, CA, Mar. 2016, paper Th1G.7.
- J. Zhou, C. Yu, G. Mohan and H. Kim, "Power budget improvement of 25-Gb/s optical link based on 1.5-μm 10G-Class VCSEL", *in Proc. OECC*, Niigata, Japan, Jul. 2016, paper ThB2-5.

Chapter 1

Introduction

1.1 Overview

With the rapid increase in the demand for faster telecommunication network (orders of magnitude increase in bit-rate length (BL) product), the traditional telephone network based communication system is not able to fulfill the requirements. The use of the optical waves as the carrier for telecommunication becomes necessary. The research phase of fiber-optic communication began at around 1975 and the commercial deployment of lightwave systems followed closely. The progress has been incredible and an increase in the bit rate by a factor of 100,000 is achieved over a period of less than 25 years. In addition, the transmission distance is also extended from 10 to 10,000 km over the same period [1]. As entering the 21st century, the fiber-optic communication systems have been deployed worldwide, and revolutionized the technology behind telecommunications. It is reported that nearly 99% of the total voice and data traffic is presently carried worldwide by cost-effective submarine cables (i.e, optical fibers) that creates "a global village" [2].

Nowadays, the explosive growth of triple play service (data, voice and video), Internet and other emerging broadband applications (e.g., high-definition television (HDTV), interactive games, etc.) are keeping imposing a huge demand for network bandwidth on the underlying telecommunication infrastructure [3], which is consequently pushing existing copper-based access networks and hybrid fiber systems like FTTCab (Fiber to the Cabinet), FTTC (Fiber to the Curb), and FTTEx (Fiber to the Exchange) to their limits [4]. The optical access networks, which cover the "last mile" area and serve numerous residential and small business users, also need to be scaled up commensurately and to avoid being the bandwidth bottleneck between end users and backbone networks [3].

In order to alleviate the bottleneck in optical access network, effective solutions should not only provide more bandwidth to end users, but also meet several requirements: e.g., supporting longer reach options, raising the splitting ratio (subscribers per fiber) with minimal total expense, and maintaining low-complexity system [3, 4]. Therefore, high-speed cost-effective optical access networks (10 Gb/s and beyond) have drawn lots of attention on both academic and commercial sides. Passive optical network (PON) has been considered as an attractive method to meet these requirements, thanks to its easy maintenance and considerable flexibility [5]. In particular, directly modulated lasers (DMLs) (e.g., vertical-cavity surface emitting lasers (VCSELs))-based optical transmitters offer enormous advantages compared with other transmitter options in PONs, such as Mach-Zehnder modulators (MZMs) [6] and electro-absorption modulators (EAMs) [7].

VCSELs can not only reduce system complexity and cost by getting rid of external modulators, but also preserve many appealing properties such as small footprint,

high modulation bandwidth, low cost, array integration capability and high energy efficiency at low driving currents [8, 9]. These properties make VCSELs widely accepted as the preferred light sources for very short-reach interfaces including data server links and optical interconnects [10,11]. Excellent performance at high data rates for such applications has already been achieved by using 0.8-μm VCSELs [10, 12]. Thanks to the reliability and performance improvement of long-wavelength VCSELs (e.g., 1.5 μm), they are now also considered as the attractive optical sources for optical access networks.

Unfortunately, there are also some limitations on the use of 1.5-μm VCSELs for the optical access applications. VCSELs usually emit low output power due to the small active volume [1] and it is also highly susceptible to fiber dispersion. The frequency chirp caused by the directly modulation of VCSELs together with the inherent low output power of VCSELs not only severely limit the power budget of optical access networks but also limit the transmission distance over widely deployed standard single-mode fiber (SSMF) at 1550 nm [13].

This thesis is devoted to addressing the issue mentioned above and finding out effective methods to alleviate the dispersion-induced distortions in 1.5-μm VCSEL-based optical access links. The remaining sections in this chapter are organised as follows: Section 1.2 introduces the research motivation. Section 1.3 gives an overview of the organization of this thesis. The contributions of the thesis are highlighted in Section 1.4.

1.2 Research Motivation

In this section, I present some issues in the long wavelength VCSEL-based optical access networks, which need to be properly addressed and can potentially be exploited for improving the power budget of optical access networks.

When considering applying long-wavelength VCSELs as the transmitters in optical access networks with bit rates of 10 Gb/s and above, chromatic dispersion (CD) becomes a major problem in these high-speed systems, which is because of the inherent frequency chirp associated with the direct modulation of semiconductor lasers [8]. Direct current modulation of the VCSELs always accompanies a large frequency chirp originating from the dependence of the refractive index on the carrier density inside the lasers. A short cavity length of VCSELs, compared to edge-emitting lasers, causes high current density inside the gain media and makes the devices very sensitive to the refractive index changes induced by the current modulation. Due to the frequency chirp and CD effects, the pulse width will be considerably broadened when transmitting through the 1550-nm SSMF, which introduces severe inter-symbol interference (ISI) and therefore leads to severe performance degradation during high-speed modulation [14].

One straightforward way of reducing frequency chirp effect in directly modulated VCSELs is to operate VCSELs with a high bias current (i.e., far beyond the threshold current). In this way, the extinction ratio (ER) of the signal is reduced, and both the transient and adiabatic chirps are also reduced. However, this method is not helpful in improving the power budget of access networks, due to its poor back-to-back (B2B) receiver sensitivity. Several other approaches have also been proposed to overcome the chirp-induced performance degradation, which include the use of injection locking

[14–16], dispersion compensation modules (DCMs) [17, 18], inverse-dispersion fiber (IDF) [19, 20], and narrow optical filtering [8, 21]. These approaches, however, either introduce added cost and complexity to the system, or have been demonstrated using short pseudo-random bit sequence (PRBS) lengths which do not represent real data.

In this thesis, I propose and investigate several methods to improve the transmission distance and power budget of long-wavelength (i.e., 1.5-μm) VCSEL-based optical access link.

1.3 Thesis Outline

This thesis consists of 5 chapters as follows:

Chapter 1: Introduction provides an overview of the thesis followed by research motivation, thesis outline and the contribution of this thesis.

Chapter 2: Literature Review reviews literatures on direct modulation and direct modulated VCSELs-based optical transmission system. In particular, I first review the basic characteristics and key features of VCSELs in Section 2.1. Then, in Section 2.2, I discuss the direct intensity modulation of VCSELs and the corresponding approaches have been proposed to mitigate the frequency chirp problem associated with the intensity modulation of VCSELs. At last, the frequency-shift keying (FSK) modulation of VCSELs is introduced in Section 2.3, and I also compare several approaches reported to combat with the performance degradation caused by the non-uniform frequency modulation (FM) response of the VCSELs in this section.

Chapter 3: 10-Gb/s Signals Transmission over 1.5-μm VCSEL-based Optical Access Link firstly proposes to utilize the FM of VCSELs, which takes good use of the frequency chirp in directly modulated VCSELs. The VCSEL generates binary

FSK-formatted signals, which are then converted into amplitude-shift keying (ASK) signals by a delay interferometer (DI). However, there exists a problem in this approach: the non-uniform FM response of the VCSEL at low frequency region (usually below 10 MHz) will introduce severe pattern-dependent signal distortions [22]. We utilize DC-balanced line codings to deplete the low-frequency spectral contents of the signal and then utilize the flat region of the FM response at higher frequency region. Compared with other methods on combating non-uniform FM response on lasers (e.g., modification of laser structure [23], electrical equalization [24] and narrow optical filtering [25], etc.), this approach offers a fully digital solution and relatively simplified solution: no optical devices (e.g., transmitter, fiber links or receivers) need to be modified or replaced in the existing systems. In this work, we test and investigate different line codes to find a line coding which is suitable for 10-Gb/s directly modulated systems (i.e., with relatively small overhead, while maintaining sufficiently low DC characteristics).

Another method to improve the transmission performance of 10.7-Gb/s VCSEL-based optical access link is to consider multi-level modulation formats (e.g., 4-pulse amplitude modulation (PAM)) and electrical equalization at the receiver side. Multilevel modulation format is a promising solution to make the signal less susceptible to fiber dispersion, since it shows higher spectral efficiency and also allows us to use band-limited devices to accommodate high-speed data [9, 26–28]. Electrical dispersion compensation (EDC) has been introduced as an alternative means of compensating fiber dispersion in the electrical domain. It has been shown that post-detection EDC can improve the receiver sensitivity of dispersion-limited optical link effectively [12,27,29,30]. In the second part of Chapter 3, we present a systematic

study and comparison on the transmission performance between 10.7-Gb/s on-off keying (OOK) and 4-PAM signals generated by a 1.5-μm VCSEL. The ERs of the 10.7-Gb/s OOK and 4-PAM signals are optimized and the electrical equalization technique is applied in this work.

Chapter 4: 25-Gb/s Signals Transmission Using 1.5-μm 10G-Class VCSEL for Optical Access Network explores the possibility of utilizing a highly cost-effective transistor-outline-can (TO-can) packaged 10G-class 1.5-μm VCSEL for optical access networks based on 25-Gb/s signal transmission, which might be realized by using spectrally efficient 4-PAM signal and electrical dispersion compensation. Note that it is also possible to transmit 25-Gb/s OOK signal in 10G-class VCSEL-based optical access link. However, in this case, the electrical equalization technique is necessary to be employed at the receiver side to compensate for the dispersion-induced signal distortions and band-limitation of the VCSEL. In sum, in this chapter, we investigate and compare the transmission performances of 25-Gb/s 4-PAM and OOK signals obtained from two different transmitter schemes: with and without a DI at the output of the directly modulated VCSEL. When the DI is used, the FSK signal from the VCSEL is converted into the OOK signal having an improved ER. The electrical equalization is employed at the receiver side to compensate for the dispersion-induced signal distortions and band-limitation of the VCSEL.

Chapter 5: Conclusions and Future Works summarizes the research findings of this thesis and suggests future works.

1.4 Thesis Contribution

The major contributions of this thesis are summarized as follows:

1.4.1 Dispersion Tolerance Improvement of 10-Gb/s VCSEL-based Optical Access Link

In the first part of Chapter 3, we experimentally demonstrate the power budget improvement of a 10-Gb/s VCSELs link by utilizing the OOK modulation format with DI, and also optimize the free-spectral range (FSR) of DI. In addition, among tested line codings, it is shown that 9B/10B and scramble-and-select line codings have outstanding performance on combating with non-uniform response of VCSEL, but with low overhead added. Compared to a conventional OOK VCSEL link without DI, $>$ 5-dB improvement in the power budget is achieved by using dispersion-resilient OOK modulation format with improved ER and low-overhead 9B/10B line coding, when the insertion loss of the DI is taken into account. 60-km transmission over SSMF with less than 0.5-dB power penalty is successfully achieved with the use of an avalanche Photodiode (APD) receiver. The results in Chapter 3 show that the application of DI successfully improves the power budget and dispersion tolerance of 1.5-μm VCSEL-based optical access link.

1.4.2 Outstanding Performance of OOK Signal than 4-PAM Signal in 10-Gb/s VCSEL-based Optical Access Link

In the second part of Chapter 3, a systematic study and comparison on the transmission performance of a 10.7-Gb/s OOK and 4-PAM signals generated by a directly modulated 1.5-μm VCSEL are presented. With the optimized ER and receiver-side EDC, 40-km transmission over SSMF is successfully achieved by 4-PAM signal. The maximum transmission distance is further extended to 80 km with the application of

OOK modulation, which, to best of our knowledge, is the longest transmission distance ever achieved by using 10G-class VCSEL without optical dispersion compensation. The better transmission performance of OOK signal is due to its duobinary-like phase characteristics, which does not present for 4-PAM signal transmission and is known to be resilient to fiber chromatic dispersion. This work indicates that the OOK format is better suited for 1.5-μm 10-Gb/s VCSEL based optical access networks since not only it outperforms the 4-PAM format in terms of tolerance to CD but also the OOK transceivers are much simpler to implement than the 4-PAM counterparts.

1.4.3 25-Gb/s Signal's Transmission on 1.5-μm 10G-Class VCSEL-based Optical Access Network

In Chapter 4, 25-Gb/s signals' transmission is successfully achieved in 1.5-μm, 10G-class VCSEL-based cost-effective optical access networks. Simple modulation formats (i.e., OOK and 4-PAM) and direct detection are employed. 35- and 45-km transmissions over SSMF are successfully achieved by utilizing 25-Gb/s 4-PAM and OOK signals with optimized ER and electrical equalization at the receiver side, respectively. Thus, we achieve a BL product of 1125 Gb/s·km without using optical dispersion compensation. We believe this is the highest BL product ever reported for directly-detected VCSELs. The use of DI successfully improves the power budget of 25-Gb/s OOK VCSEL-based transmission link up to 25 km: $>$11 dB power budget is achieved up to 20 km with a 25-GHz DI, even though the maximum transmission distance is limited to 33 km. This work indicates the possibility of utilization of 25-Gb/s OOK signal in 10G-class VCSEL-based optical access link by taking advantage of the duobinary characteristic of the OOK signal using a

limited-band VCSEL. In addition, the use of DI can improve the power budget in short transmission distance. Thanks to the periodicity of the DI's transmittance with respect to wavelength, a single DI can be shared among multiple channels in wavelength-division-multiplexed optical access networks.

Chapter 2

Literature Review

2.1 Directly Modulation and VCSELs

2.1.1 Introduction of Directly Modulation

In general, there are two ways of imposing electrical information onto the light: direct modulation and external modulation [1]. Specifically, in direct modulation [see Fig. 2.1(a)], the electrical information signal is directly driven into the laser diode which results in a series of optical pulses. The laser diode switches between ON and OFF states depending on the change of logical 1 and 0, respectively. As for the external modulation [see Fig. 2.1(b)], a continuous wave (CW) is generated by a laser source and then the external modulators (like EAMs [7] and MZMs [6]) will let the light transmit through whenever the data correspond to 'marks' and block them whenever the signals are 'spaces' [31]. Compared with external modulators, DML-based optical transmitters offer many advantages: they not only reduce the transmitter's complexity and cost by getting rid of external modulators, but also show easy integration with driver integrated circuits (ICs) owing to their semiconductor-based structures [32]. In

addition, DMLs usually require low driving current and have low power consumption, compared with external modulators, which allow the use of low-cost drivers for signal generation, therefore, the system cost is saved.

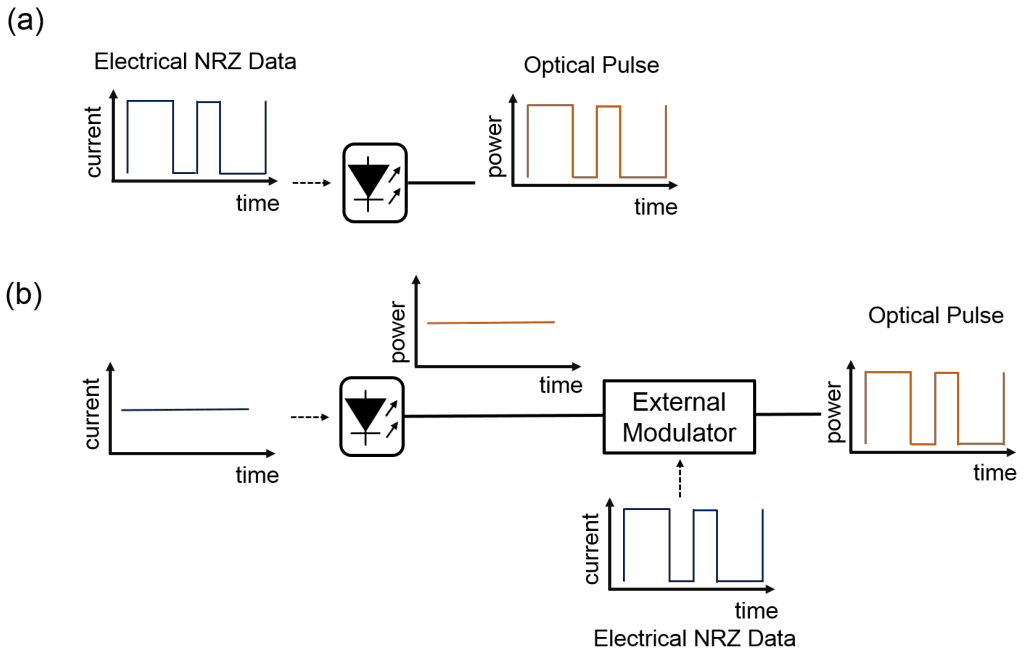

Figure 2.1: Illustration of (a) direct modulation and (b) external modulation.

2.1.2 Introduction of VCSELs

In today's fiber optical transmission systems, there are basically two types of lasers used: edge-emitting and surface-emitting lasers. The most popular high-speed edge-emitting lasers are Fabry-Perot (FP) and distributed feedback (DFB) lasers. The beam emission for these devices is parallel to the substrate. In the case of surface-emitting lasers (e.g., VCSELs), the light is emitted vertical to the substrate.

VCSELs emerged at around 1990s and have shown many potential applications and a number of unique advantages compared with other types of laser diodes [14].

The light from VCSEL is traveling and bouncing in the vertical direction inside the laser cavity and emitting typically from the top surface of the device, which is different to the edge-emitting lasers that the light is emitting from both facets on the sides. The fabrication of VCSELs requires growth of multiple thin layer mirrors on a substrate. The active gain region of the VCSELs is composed of one or several layers of quantum wells (QWs), which are sandwiched between two high-reflectivity ($> 99.5\%$) distributed Bragg reflectors (DBRs). Each DBR mirror is made through growing many pairs of alternating AlAs and GaAs layers with $\lambda/4$ thick, where λ is the VCSEL's emitted wavelength [33]. A wafer-bonding technique is sometimes applied for 1.5-μm VCSELs to accommodate the InGaAsP active region [34].

VCSELs offer many advantages [33]:

• All the processing and testing steps can be completed on the wafer level thanks to the top emitting design. This enables very cost-effective fabrication and wafer-scale testing process. However, for edge emitting lasers, they must be cleaved into individual devices before they can be operated and tested, which increases processing cost and decreases yields significantly.

• VCSELs (e.g., 1.5-μm) usually operate in a single longitudinal mode, which is because of their extremely short cavity length (in the order of 1 μm). In addition, the emission wavelength can be continuously adjusted over a relatively wide spectral range by tuning the current or temperature. As for edge emitting lasers, single longitudinal mode operation requires difficult and expensive process steps.

• VCSELs can be fabricated in the form of two dimensional arrays, which shows potential to be used for parallel data processing or image displays.

• For VCSELs, the laser beam emitting from the symmetric aperture is in a narrow

circular shape with small amount of divergence, which is ideal for direct fiber coupling. No expensive optics is needed.

• VCSELs exhibit a relatively low threshold ($\sim$1 mA or less). The small active volume of a VCSEL leads to a very low threshold current and low power consumption.

Table 2.1 shows a comparison among VCSELs, DFBs and FPs, where we can also observe the above-mentioned characteristics of VCSELs. In terms of the applications of these laser sources, FPs and short-wavelength (e.g., 850-nm) VCSELs are mainly used for short-range transmissions (e.g., data center [35, 36]) due to their relative wide spectral and multi-longitudinal modes. Since the spectral width of DFBs is generally narrow and a single longitudinal mode can be achieved, DFBs can be used for high data rate long-distance transmission. For example, 51.56-Gb/s OOK signal is successfully transmitted through 15-km SSMF by using directly-modulated 1.55-μm DFB laser (bandwidth=25.6 GHz) [37]. The authors in [38] successfully demonstrate error free 25.78-Gb/s transmission over 10-km SSMF under all temperature conditions by using a 1.3-μm TO-can package DFB. With the help of asymmetric narrow-band filtering, 40-Gb/s transmission over 25-km negative dispersion fiber is achieved by using a commercial directly modulated DFB laser in [39]. In addition, thanks to the reliability and performance improvement of long-wavelength (e.g., 1.5-μm) VCSELs, they are now also considered as the attractive optical sources for optical access networks [40, 41].

However, there are also some disadvantages of using VCSELs as laser sources. Firstly, VCSELs usually can only emit less than a few milliwatts of power due to the small active volume [1], which limits the transmission distance of VCSEL-based data transmission link. In addition, the direct modulation of the VCSEL is always

Table 2.1: Comparison among VCSELs, DFBs and FPs technologies

Attribute	VCSEL	DFB	FP
Cost	Low	High	High
Optical Output Power	Low	High	High
Power Consumption	Low	High	High
Size	Small (vertical construction)	Large (planar construction)	Large (planar construction)
Mode Stability	Good	Fair	Fair
Testing	On Chip	Packaged assembly	Packaged assembly
Manufacturing	Easy (20,000 devices on 3-inch wafer)	Difficult	Difficult
Packaging	Easy	Difficult	Difficult
Coupling to Fiber	Efficient	Inefficient	Inefficient
Drive circuit	Simple	Complicated	Complicated
Reliability	Good	Good	Neutral

accompanied by FM, which introduces a large frequency chirp effects and therefore limits the fiber transmission speed and distance in fiber-optic communication systems. Especially in the long-wavelength VCSEL (e.g., 1.5-μm)-based optical transmission system, the interaction between the frequency chirp and chromatic dispersion in SSMF (e.g., SMF-28 fiber) at 1550 nm causes severe signal distortions during the transmission and severely limits the transmission distance over SSMF [21]. Moreover, the modulation bandwidth of long-wavelength VCSEL is usually limited to less than 20 GHz, which is because of the nonlinear gain effect and the carrier transport lifetime of the material system at 1550 nm [14].

2.1.3 Frequency Chirp

In [42], the authors pointed out that the direct intensity modulation causes certain variation of carrier concentration in the laser active region, which affects the refractive index governed by the linewidth enhancement factor α [1]. To be more specific, the laser intensity modulation caused frequency chirp ($\triangle\ \nu(t)$) can be expressed as [8]:

$$\triangle\ \nu(t) = \frac{\alpha}{4\pi}\{\frac{d}{dt}ln[P_L(t)] + \kappa P_L(t)\} \tag{2.1}$$

which makes the instantaneous frequency shift from its steady-state value (ν_0). In Eq. (2.1), $P_L(t)$ is the laser output power, κ is the adiabatic chirp coefficient, which relates to the nonlinear gain compression coefficient ε and is given in [43]:

$$\kappa = \frac{2\Gamma}{\eta h\nu V}\varepsilon \tag{2.2}$$

where Γ is the optical confinement factor, η is the differential quantum efficiency, h is Planck's constant, ν is the optical frequency, and V is the volume of the active layer.

The first term in right side of Eq. (2.1) describes the *transient chirp* (also called dynamic chirp). The transient chirp is laser structure independent and only relates to the time derivative of the changing instantaneous optical power at rising and falling pulse edges [8,44], which means that it represents the wavelength shift associated with the 'ON' and 'OFF' states. The transient chirp dominates the frequency chirp when dP_L/dT is large due to either a large output power swing or fast changing rise-time or fall-time current pulses [43]. The second structure-dependent term in Eq. (2.1), called *adiabatic chirp*, is directly proportional to the instantaneous optical power and leads to a wavelength shift between high- and low-power points in the optical waveforms

[44, 45]. As observed from the adiabatic chirp coefficient κ in Eq. (2.2), this adiabatic chirp is caused by the nonlinear gain effect, which depends on the cavity volume, photon lifetime, etc.

Fig. 2.2 provides an illustration of the interaction between the laser chirp and fiber dispersion. In Fig. 2.2(a), only adiabatic chirp is considered and it is observed that the adiabatic chirp is directly proportional to the optical power. If the fiber dispersion coefficient is positive, like in SSMF at 1.55-μm window, the group velocity of signal's rising edge increases, while the speed of the falling edge gets slower. Consequently, the rising time decreases, which results in the overshoot in the output pulse, and the falling time is extended as displayed in Fig. 2.2(a). As for the transient chirp effect [see Fig. 2.2(b)], the frequency deviations occur at the slopes of the pulse. Because of the positive derivative in the rising edge, it propagates faster than the flat region, which suffers no transient chirp effects because of the constant optical power. Vice versa, the falling edge propagates slower in the SSMF because of the negative frequency deviation as shown in Fig. 2.2(b). Hence, the output pulse after transmission is broadened. In addition, it is noted that according to the first term in the right side of Eq. (2.1), the transient chirp is proportional to derivative of the natural logarithm of the pulse power, which means it is sensitive to the actual shapes of the pulse slopes. Consequently, the distorted output waveforms may be considerably different for supposedly similar input ones. The combination of both adiabatic and transient chirp effects is displayed in Fig. 2.2(c) and it shows that the output pulse after transmission through SSMF is distorted [44].

In conclusion, the frequency chirp in directly modulated VCSELs not only limits the data rate of the signal but also limits the transmission distance over SSMF.

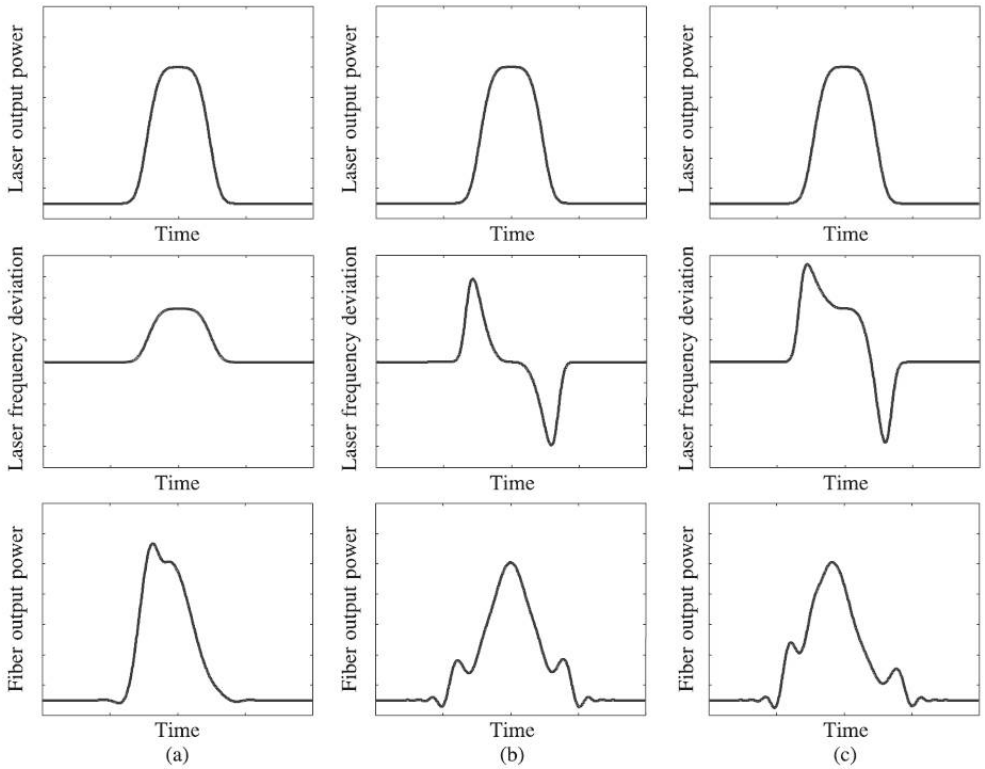

Figure 2.2: Illustration of chirp-dispersion induced pulse distortion for (a) adiabatic chirp, (b) transient chirp, and (c) both chirp components [44]. (reproduced with permission)

Therefore, the BL product is usually limited in the directly modulated VCSEL-based optical transmission systems. In the following section, I am going to review several methods in the literature to combat with frequency chirp and dispersion-induced signal distortions in VCSEL-based transmission links.

2.2 Approaches for Addressing Frequency Chirp in Directly Intensity Modulation

According to Eq. (2.1), it is firstly observed that a possible way to reduce the transient chirp in VCSELs is to bias the VCSELs with a high bias current and reduce the ER of the output signal. When the ER of the signal is reduced, the output power swing between 'ON' and 'OFF' states is accordantly reduced. Consequently, the transient chirp, which is proportional to the optical power changing, is also reduced. Otherwise, the high-ER signals with large current modulation will lead to the large frequency chirp. However, it is noted that the low-ER signal is not beneficial for long distance transmission, due to its poor signal-to-noise ratio (SNR) after transmission.

The following subsections review several approaches that have been reported to combat with the frequency chirp effect in VCSELs. These approaches can be categorized into either device-based or system-based approaches. Moreover, different system-based approaches including transmitter/ receiver compensation and optical dispersion compensation will be introduced.

2.2.1 Device Approaches

As mentioned in previous section, direct current modulation of VCSELs always accompanies a large frequency chirp originating from the dependence of the refractive index on the carrier density inside the lasers: the refractive index is governed by the linewidth enhancement factor α and the frequency chirp is proportional to α as shown in Eq. (2.1). In [46–48], the authors proposed to use transverse coupled cavity VCSEL to improve the modulation bandwidth of VCSEL and reduce the frequency

chirp. The detuned loading effect in the transverse coupled cavity VCSEL successfully increases the differential modal gain, which is achieved by introducing dispersive loss mechanism with detuning of the laser frequency away from the loss minimum. Since the linewidth enhancement factor α is inversely proportional to the differential modal gain, an increased effective differential modal gain contributes to the reduction of the chirp. For example, the linewidth enhancement factor of a conventional VCSEL is supposed to be 4 [46]. The frequency chirp is reduced by a factor of more than 2 for the transverse coupled cavity VCSEL at the strongest coupling strength in [46]. In addition, the 3-dB bandwidth is successfully increased by a factor of 3 by using the bow-tie shape transverse coupled cavity VCSEL in [47].

Even though the use of transverse coupled cavity VCSEL can effectively reduce the frequency chirp at some extent, they require to modify the laser structure in order to achieve low frequency chirp, which is not easy to be realized and also increases the cost and complexity of the transmitter.

2.2.2 System Approaches

In addition to modifying the structure of VCSELs, there are many system-based methods have been proposed to alleviate the chirp effects and improve the BL product in VCSEL-based optical transmission systems, which are listed as following:

2.2.2.1 Transmitter Pre-compensation

As mentioned in Section 2.1, when a signal pulse with a positive chirp transmits through a SSMF, its blue-shifted leading edge will travel faster than the main portion of the pulse and make the pulse be broadened after travelling through SSMF as shown

in Fig. 2.3 (a) and (b), which introduces significant chirp-induced power penalty due to severe ISI and consequently limits the maximum achievable transmission distance of the system. Electronic pre-compensation (also called pre-chirping) technique is one possible way to compensate this chirp effect in the electrical domain at the transmitter side [49–51]. The working principle of electronic pre-compensation is trying to delay the spreading of the bit in adjacent slots by taking advantage of the linearity of the fiber dispersion in the optical domain. It tries to arrange the light in the leading edge of the pulse to have lower frequency, while that in the trailing edge of the pulse to have higher frequency, which is opposite to the positive chirp effects. Consequently, when the pulse with negative chirp passes through the SSMF, its low-frequency content in the leading edge passes through the entire pulse slot before it starts interacting with the trailing edge and can successfully avoid errors [see Fig. 2.3 (c)-(f)] [52].

Another electronic pre-compensation is realized by applying electronic equalizer (e.g., feed-forward equalizer (FFE)) at the transmitter side. In [53], 64-Gb/s VCSEL-based optical link over 57-m OM4 multi-mode fiber (MMF) is successfully achieved, with 2-tap FFE wireboned to VCSEL at the transmitter side and another 2-tap FFE incorporating with receiver's output. In [54], 50 Gb/s non-return to zero (NRZ) modulation is successfully achieved in an 850-nm VCSEL-based transmission link with transmitter pre-compensation from 30 °C to 90 °C. 56- and 50-Gb/s NRZ signal transmissions at back-to-back and over 2-km large effective area fiber are successfully achieved by using a 1530-nm VCSEL and active transmitter equalization (i.e., a 2-tap FFE driver IC directly wirebonded to the VCSEL) in [55, 56], respectively. 32-Gb/s 4-PAM signal can be transmitted over MMF links by using a 0.85-μm VCSEL, which is realized by applying a 5-tap transversal electrical filter at the transmitter side for

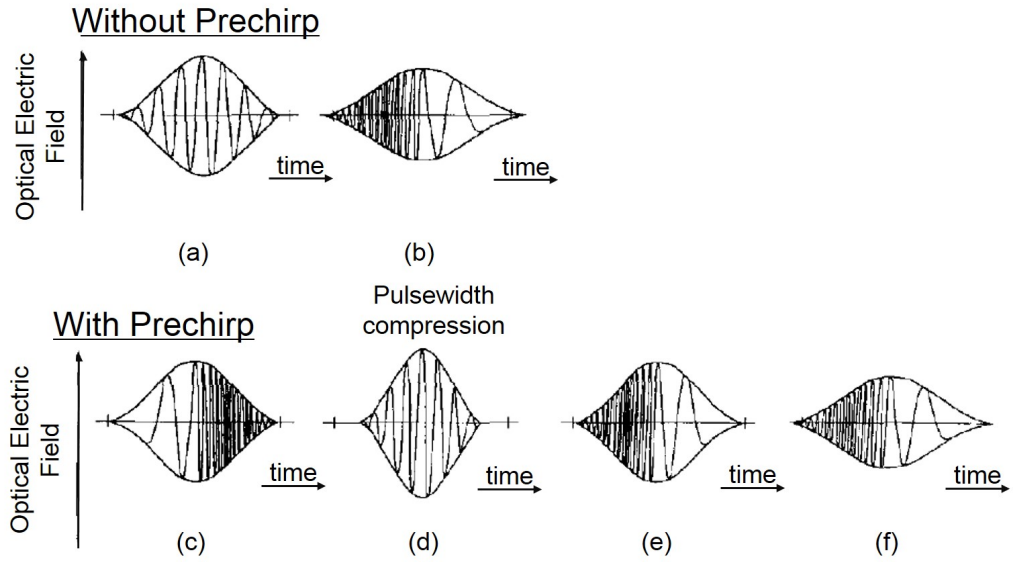

Figure 2.3: Principle of prechirp (a) ideal intensity modulated waveform, (b) received optical waveform, (c) prechirped optical waveform, (d)-(e) middle of a transmission fiber, and (f) received optical waveform [51]. (reproduced from permission)

signal predistortion [27].

However, when applying the above methods, the pre-chirping parameters need to be carefully chosen based on the span length of the transmission system, in order to make sure that the pulse is suitably compressed in the middle of the transmission. This consequently increases the complexity at the transmitter side. In addition, each transmitter needs to be re-adjusted whenever the span length changes.

2.2.2.2 Receiver Post-compensation

EDC implemented at the receiver side is also an effective way to combat with fiber dispersion in the electrical domain. Adaptive equalizer, which automatically adapts to the time-varying properties of communication channel, is attractive for networks with

dynamic channel variation. One advantage of EDC at the receiver side is that there is no need to obtain the knowledge of fiber length and other span characteristics in advance. Therefore, receiver-side EDC is well suitable for various system design with different fiber spans and characteristics.

With the help of EDC, the transmission distance is extended to 40 km in a 1.5-μm VCSEL-based transmission link, which is 4 times of that without EDC at $< 10^{-3}$ bit error rate (BER). With the aid of a decision-feedback equalizer (DFE) at the receiver, 10-Gb/s OOK and 4-PAM transmissions over 300-meter polymer optical fiber were achieved by using a 0.85-μm VCSEL [30]. A record 55-Gb/s transmission of 0.85-μm OOK VCSEL signal was also demonstrated by using the electrical equalization at both the transmitter and receiver sides [12]. For 1.5-μm VCSELs, error-free transmissions of 10-Gb/s OOK signals over 40-km SSMF were reported by using the maximum likelihood sequence estimation (MLSE)-based EDC at the receiver side [29].

Receiver-side electronic equalization can effectively alleviate the dispersion-induced signal distortions in the transmission system with SSMF, which is at the expense of the additional electronic logic circuits.

2.2.2.3 Optical Compensation

Besides the electrical dispersion compensation techniques implemented at the transmitter or receiver side that mentioned above, there are also many optical compensation methods implemented to alleviate the dispersion-induced signal distortions in the fiber span. In this subsection, I will review three existing methods of optical compensation: IDF, dispersion compensation fiber (DCF), optical injection locking (OIL).

a.) Inverse dispersion fiber

As mentioned before, the interaction between the positive chirp generated in the directly modulated VCSELs and the positive dispersion of conventional SSMF not only introduces signal distortions but also limits the maximum achievable transmission distance. The chirp affects the pulse propagation by making the leading and trailing edges of the pulses have different frequencies and hence different group velocities. In particular, after transmission through the positive dispersion fiber (e.g., SMF-28), the blue-shifted leading edge of the pulse preserves a larger group velocity compared with the red-shifted falling edges, which makes the pulses broadened and results in severe ISI [57]. Besides the electrical dispersion compensation methods mentioned in previous section, there also exists all-optical, fiber-based solutions to reduce this dispersion-induced signal distortion, which can be achieved by a special fiber, known as IDF. The IDF is a kind of fiber with negative dispersion: if the pulses pass through this fiber, the blue-shifted components of the pulse will have a smaller group velocity compared with the red-shifted components. The pulse is compressed after transmission through IDF. Consequently, significant transmission performance improvement can be achieved by utilizing the IDF along with SSMF together [57].

In [19], the authors successfully demonstrated 10.7-Gb/s signal transmission (at BER=10^{-9}) over 50-km transmission distance (composed of 15-km IDF and 35-km SSMF) in an uncooled VCSEL-based access link. 10 Gb/s optical signal's transmission over an un-amplified 99.7-km dispersion-matched link is successfully achieved in [20], in which a field-deployable IDF was used for dispersion compensation. In [5], a 20 km 60 Gb/s two-way PON based on directly modulated two-state injection-locked 1.55-μm VCSELs transmitter and negative dispersion fibers (NDFs) is proposed and

demonstrated.

Although the implementation of IDF in the optical access network could effectively alleviate the dispersion-induced signal distortions, it requires the replacement of the existing fiber links, which are commonly implemented by SSMF. This replacement will introduce the additional cost and complexity. Therefore, there is a trade-off between the cost-effectiveness and dispersion compensation by using IDF.

b.) Dispersion compensation fiber

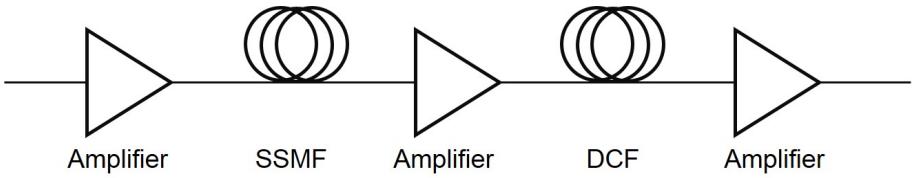

Figure 2.4: Typical transmission system with DCF.

DCF modules are also introduced to deal with the dispersion-induced degradation of the optical signal [1] and a special kind of fiber with negative dispersion coefficient can used for this purpose. The DCF module which is composed of specific-length DCF is usually connected with optical amplifiers (spaced apart by 60-80 km) to upgrade the existing lightwave systems operating over SSMF as shown in Fig. 2.4. This kind of combination is necessary for compensating the relative high loss (attenuation coefficient α=0.4$\sim$0.6 dB/km) that DCFs have. Even though the insertion loss of DCF module can be compensated by increasing the amplifier gain, which is at the expense of enhanced amplified spontaneous emission (ASE). Therefore, the input power needs to be carefully controlled to avoid the nonlinear effects of the amplifiers and the transmission distance is accordantly limited. In addition, the fiber span length of the

DCF needs to be carefully considered and designed in advance to ensure a proper compensation of the positive dispersion in SSMF.

The application of DCF module for dispersion tolerance improvement of VCSEL-based transmission systems have been investigated a lot [17, 58]. In [58], 25- and 80-km transmissions with 0.7- and 1.6-dB power penalties are successfully demonstrated in VCSEL-based transmission link, respectively. 10-Gb/s NRZ signal is successfully transmitted through 29-km fiber span with SMF and DCF in a 1.5-μm VCSEL-based optical link [17]. Though the dispersion tolerance of transmission link can be successfully improved with the utilization of DCF modules, the design of dispersion-management schemes of DCF and the utilization of amplifiers need to be carefully considered in order to satisfy specific cost and effectiveness requirement.

c.) Injection locking

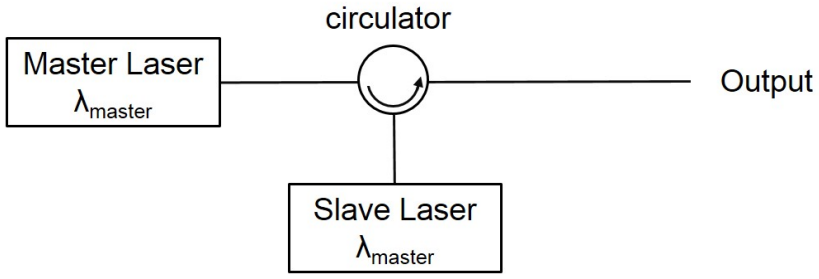

Figure 2.5: Typical experimental setups of optical injection locking.

Optical injection locking refers to a state that the frequency and phase of a laser oscillator (i.e., slave laser) are locked through the direct coupling light injection from another laser oscillator (i.e., master laser) and the typical experimental setup of optical injection locking is shown in Fig. 2.5. It has been proved as an effective technique to enhance the dynamic performance of slave laser on reducing chirp and chirp-induced

performance degradation [16, 59]. The injection-locked frequency chirp of the slave laser can be effectively controlled by varying the wavelength detuning and the power injection ratio between the master and slave lasers. Moreover, the changing of the chirp sign can also be obtained by suitable tuning the injection ratio and wavelength offset [60]. In addition, using injection locking VCSELs is possible to increase the cut-off and resonance frequency of a long wavelength VCSEL [59].

Many different laser sources have been utilized for injection locking VCSELs to reduce the chirp effects, such as: VCSLE-to-VCSEL injection locking [16, 60], cascaded injection locking using DFB lasers and VCSELs [61], etc. In [60], by means of VCSEL-to-VCSEL injection locking at 1.55-μm at 10-Gb/s modulation bit rate, the experimentally generated chirp inversion successfully overcomes the limitations in the propagation performance due to the large spectrum induced by the direct modulation. Furthermore, 40-km uncompensated transmission over SSMF is achieved for error free transmission (at BER of 10^{-6}). 60-Gb/s signal transmission over 20-km NDF is successfully achieved in a two-stage injection-locked 1.55-μm VCSEL-based two-way PON [5].

However, the injection locking technique would inevitably increase the system cost, since it needs additional laser sources to play the role of master laser. This cost increase is more obvious when applying injection locking in the wavelength division multiplexing (WDM) systems, where multiple master lasers are required to be placed at the central office (CO) to fulfil the requirements of different-wavelength slave lasers. Furthermore, the performance and properties (e.g., the 3-dB bandwidth) of the directly modulated slave lasers are very sensitive to the applied OIL conditions including optical injection power, wavelength detuning range, polarization, temperature and so

on [62]. All of these parameters need to be carefully optimized to achieve desirable performance. Note that there also exists a tradeoff between the injection ratio and signal's ER [60].

2.3 FSK Modulation of VCSELs

The approaches reviewed in Section 2.2 all deal with the chirp effects in the directly modulated VCSEL-based transmission system. Besides direct intensity modulation, FSK is another modulation format can be implemented on directly modulated VCSELs. By taking the advantage of the frequency chirp, the generated FSK signal can improve the dispersion-limited transmission distance [63]. The FSK modulation of lasers can be realized by operating the laser far beyond the threshold with a small modulation current. In this method, a FM to amplitude modulation (AM) converter at either transmitter or receiver side is required for signal detection, such as, narrow optical filter or a DI [32].

However, the main problem of using the FSK modulation on VCSELs is that VCSELs usually exhibit non-uniform frequency modulation response at low frequencies (usually from a few Hz up to 10 MHz) [22,64], which in turn, causes severe pattern-dependent signal degradation. The non-uniform FM response in VCSELs can be explained as follows: the temperature and carrier density in the active layer are changing with the modulating injection current, which in turn causes a change in the refractive index and thus affects the oscillation frequency. The thermal effect is observed to be dominant only at low frequencies, usually below 10 MHz. In contrast, the carrier effect makes the refractive index change in opposite to the thermal effect, which has a roughly flat response up to 1 GHz with a resonance peak at much higher

frequency [65]. The combined thermal and carrier effects make a "dip" or an enhanced response at low frequencies as appeared in the FM response of a laser diode [64].

The FM response of the VCSEL [13] used in our works will be shown next.

2.3.1 FM Response of VCSEL

The FM response of the VCSEL we used in our experiment is displayed in Fig. 2.6. It was measured based on the frequency domain network analysis approach by using an optical FM discriminator [13]. The inset of Fig. 2.6(a) shows the experimental setup: the intensity modulation generated by a directly modulated laser diode is always accompanied with frequency modulation and can be removed from the interference data by making two measurements, each on an opposite slope of the FM discriminator, which is a 25-GHz FSR DI [66]. The measured FM response of the VCSEL is compared with the FM response of an edge-emitting DFB laser housed in a butterfly package. The DFB laser is biased at 60 mA (i.e., 6 times the threshold current) and the temperature is controlled at 20 $^{\circ}C$. According to [67], the typical FM response of DFBs is first governed by the thermal effect up to around 1 MHz and then by the carrier-induced FM effect from 1 MHz and beyond. It is observed in Fig. 2.6(b) that there is a $\pi-$phase shift around 1 MHz caused by the thermal effect with respect to the carrier-induced FM effect. The combined effects of the above two different properties make the FM response of the edge-emitting DFB laser non-uniform up to $\backsim$10 MHz. In comparison, the VCSEL has a similar but slightly different FM response. It is observed from Fig. 2.6(a) that the VCSEL also has a non-uniform FM response, which is similarly due to the combination of the thermal and carrier-induced FM effects. Except for a magnitude dip and π-phase jump at 35 kHz, the thermal response is gradually

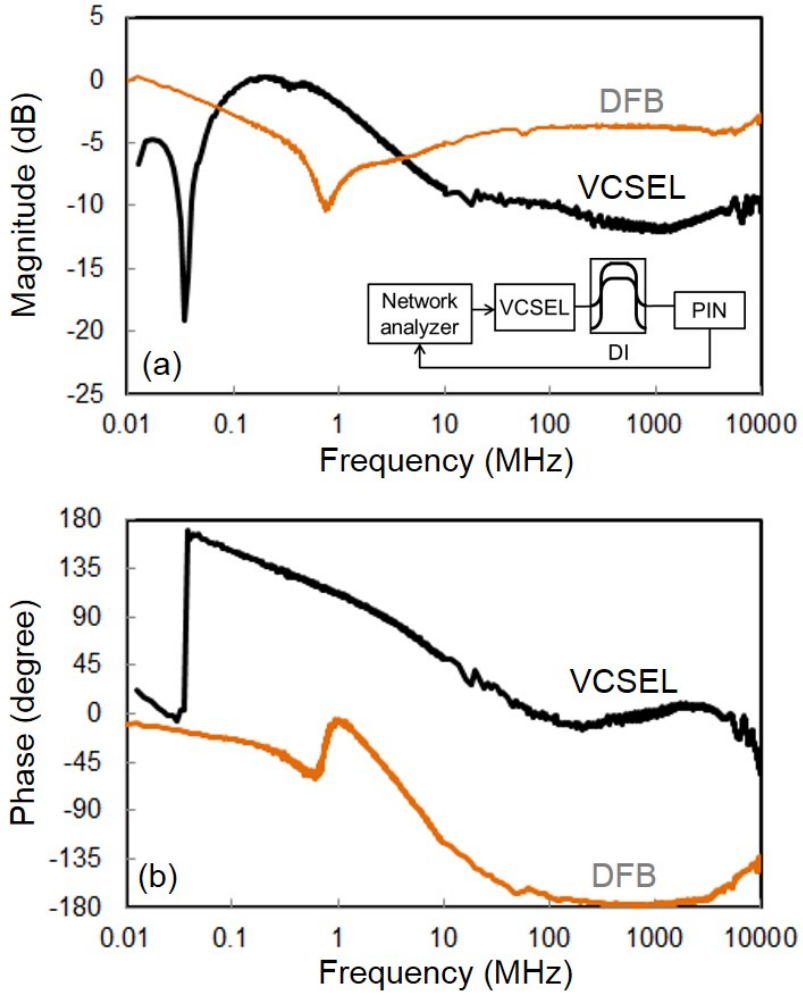

Figure 2.6: FM response of a VCSEL: (a) magnitude and (b) phase. Also shown in the figure for comparison is the FM response of an edge-emitting DFB laser [13]. (reproduced with permission)

minified as the frequency increases. However, the thermal response is nearly 10 dB larger than the carrier-induced FM effect and stretches to tens of MHz because of the small size of the gain medium and uncooled operation of the VCSEL. Nevertheless, both the VCSEL and DFB lasers exhibit flat FM response from tens of MHz up to 10 GHz.

The non-uniform FM response of the directly-modulated laser sources will result in a severe pattern dependency and the power penalty will be increased with longer PRBS length [68,69]. This can be explained as follows: if the PRBS length is relatively short (e.g., 2^7-1), the lowest frequency component of the signal is relatively high (e.g., $=$10 GHz$/127=$78.7 MHz), so that the signal only occupies the uniform region of the lasers' FM response. However, as the pattern length increases, the low-frequency contents of the signal may be affected by the non-uniform FM response because of the narrowing spectral space, which consequently introduces the signal distortions.

Thus, it is necessary to figure out approaches to counteract the performance degradation associated with the non-uniform FM response in VCSELs and improve the transmission performance of FSK-modulated VCSEL-based transmission system.

2.3.2 Optical Filtering

In directly modulated system, the frequency chirping or time evolution of wavelength change usually induce the optical spectrum broadening and signal degrading along the fiber link. Moreover, the broadened spectrum is asymmetric and the obtained spectrum density is considered as a convolution of the data AM spectrum and a related chirp-induced FM term [70]. Optical filtering has been widely applied in high speed externally modulated communication systems for narrowing the signal spectrum and improving the spectral efficiency [71]. It can also improve the transmission performance in directly modulated system via two main mechanisms: converting chirp-induced FM to AM for transmission and narrowing or reshaping the broadened spectrum [8, 70], as shown in Fig. 2.7.

Since there are many unwanted frequency components in the broadened spectrum

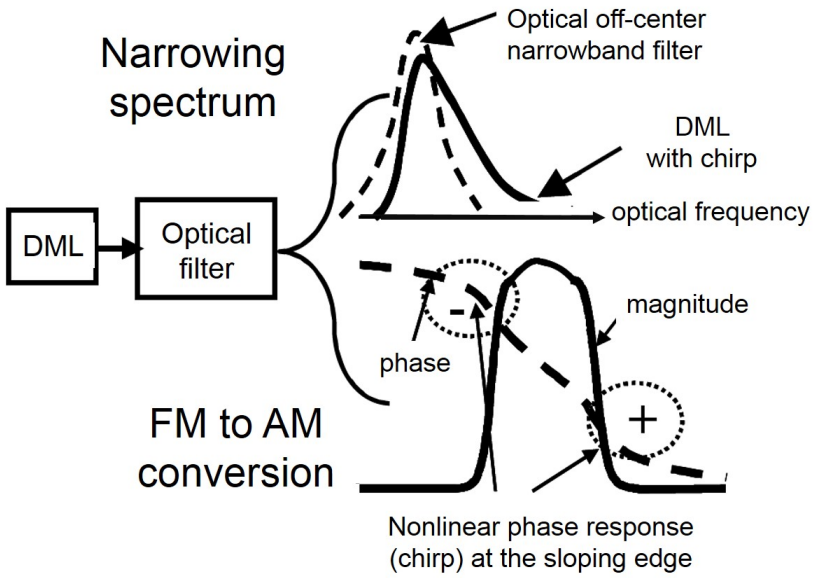

Figure 2.7: Conceptual diagram of asymmetric filtering in directly modulated system [70]. (reproduced with permission)

of the output signals, it is necessary to use an optical filter with a bandwidth narrower than the broadened spectrum to remove these frequency components and reshape a "cleaner" signal for longer distance transmission. It is worth noting that the filter should be placed asymmetrically with the center of the optical spectrum, due to the asymmetric chirp-induced broadened spectrum. In addition, the asymmetric filtering can cut more off some low driving current induced frequency components (i.e., reducing '0' level more than '1' level) and the ER of the signal will be improved. Thanks to the higher immunity to the optical noise, the signal with improved ER is better for long-haul transmission. In addition, in order to interact with laser chirp and dispersion along the fiber link and convert the frequency modulation into amplitude modulation, the grating filter needs to have pre-designed chirp or dispersion. Since

most of the chirp or dispersion of an optical filter is related to the sloping edge's nonlinear phase response, asymmetric filtering is also necessary [70].

In [8], it is pointed out that when the modulation depth increases, the spectrum of the modulated signal will shift to higher wavelength due to the adiabatic chirp, and the wavelength separation between '1'and '0' levels will increase under the combined effects of adiabatic and transient chirp. Therefore, there is a tradeoff between the signals' ER and chirp effects. To reduce the chirp effects while at the same time achieve a desirable ER of modulated signal, a tuneable Gaussian filter with 0.38-nm 3-dB bandwidth was used for optical filtering in [8]. By setting 336-pm filter offset between the filter and the signal spectrum, the attenuation of the '0' level is greater than that of the '1' level. Because of the power decrease on '0' level, the ER of the signal increases and the signal's '0' level dispersion distortion of the signal decreases. It is further shown that by applying optical filtering with optimized offset, more than twofold increase in the 10-Gb/s VCSEL-based network reach can be achieved, i.e., extending the reach from 11.7 km to 25.8 km for a dispersion margin of 4 dB. With the help of an optical bandpass filter, 40-Gb/s long-wavelength VCSEL-based optical interconnect is successfully achieved in [72].

Even though the use of optical filtering can effectively improve the transmission performance of directly FM-based transmission link, the system's cost and complexity will inevitably increase, especially in WDM transmission systems, which is because each independent channel requires a filter for narrow filtering. In addition, when implementing the off-center optical filtering, the offset between the filter and the center of signal spectrum also needs to be well controlled and maintained. This also increase the complexity of the transmission system.

2.3.3 Approaches to Overcome Non-uniform FM Response

2.3.3.1 Electronic Equalization

As mentioned in Section 2.3, a problem with a direct FSK modulation is that most semiconductor lasers usually have non-uniform FM response over the bandwidth of the modulation signal. This non-uniform FM response introduces the pattern-dependent signal distortion. Excessive frequency drift is observed along with a corresponding increase in BER, when the data sequence contains long strings of ones or zeroes is transmitted. In order to deal with the effects of a non-uniform FM transfer function, FM equalization has been utilized by either active or passive means through different mechanisms (e.g., pre-distortion, post-distortion, feedback, etc.) to make the overall system's FM response relative uniform along the frequency [24].

In [73], a passive equalization network at the transmitter side was developed to shape the injection current modulation waveform for suppressing the low-frequency enhancement. The equalization network is realized by the cascade of a second-order highpass filter and a diode laser model, whose parameters need to be computer-optimized to obtain a flat response. The result shows that the equalized diode laser approximates a flat FM sensitivity of 40 MHz/mA, which was originally from 3 GHz/mA at low frequencies to 50 MHz/mA at high frequencies [73].

The applied electrical equalization circuits can effectively shape the laser driving signal and hence the FM response of the laser diode. However, proper adjustment depending on the device's FM characteristics is necessary for electrical equalization, which requires additional analog circuits and thus increases the complexity of transmitter.

2.3.3.2 DC-balanced Line Coding

Utilization of DC-balanced line coding is another way to address the signal performance degradations caused by the non-uniform FM response of VCSELs. The authors in [74] pointed out that the temperature modulation of the laser causes drifts in the optical frequency when there is long strings of zeros or ones in the NRZ direct modulation formats. The resulting baseline wander in the received signal would cause erroneous detection for long PRBS patterns, even if at low data rate. By utilizing the DC-balanced line coding, the low frequency contents of the signals can be depleted such that only the uniform region of the FM response at higher frequency range is exploited, which thus effectively mitigates the signal distortion caused by the non-uniform FM response.

Many kinds of DC-balanced line codings have been proposed and implemented, such as Manchester coding [75–77], alternate mark inversion (AMI) coding [78, 79] and 8B/10B line coding [80], etc.

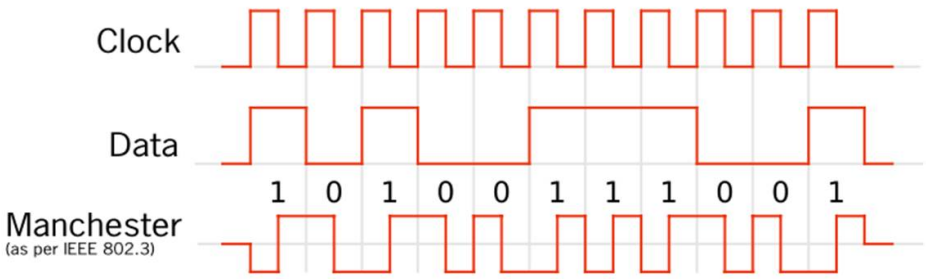

Figure 2.8: The Manchester coding signal format.

Fig. 2.8 shows the illustration of Manchester coding (i.e., biphase coding). If the NRZ signal is assumed to be digital with levels '0' and '1', the Manchester coding can be realized by applying an exclusive-or (EXOR) operation between the original NRZ

signal and a digital clock (CLK) as follows:

$$\text{BIPHASE} = \text{NRZ} \oplus \text{CLK(digital)} \tag{2.3}$$

From Fig. 2.8, the transitions happen at the midpoint of one period and the direction of the mid-bit transition indicates the encoded data: a '0' is expressed by a high-to-low transition and a '1' is presented by a low-to-high transition. Note that the transitions at the period boundaries do not carry any information, which is necessary to place the signal in the correct state for the mid-bit transition. Furthermore, the information non-carrying transitions allows the signal to be self-clocking and the receiver to be aligned correctly. However, the price of applying the Manchester coding is the doubled bandwidth compared to NRZ coding schemes [77].

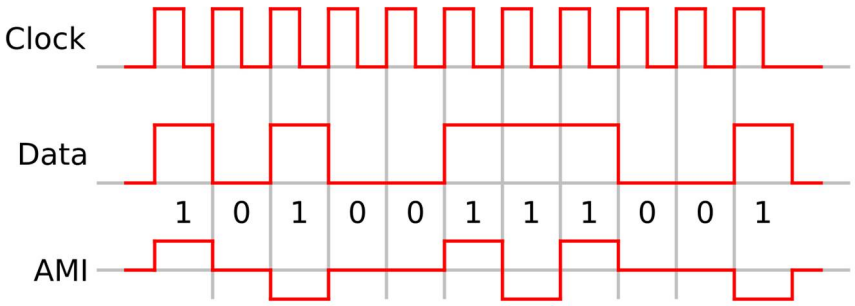

Figure 2.9: The AMI coding signal format.

As shown in Fig. 2.9, the AMI coding is realized by representing a binary '0' using zero voltage and a binary '1' using a positive or a negative voltage alternately [81]. AMI coding also requires additional 50% bandwidth increase due to the ternary symbol used for signal transmission, which in turn introduces higher requirement for lasers' modulation bandwidth. Moreover, in order to generate the ternary signal, the driving condition becomes more complicated and the optical spectrum is substantially

broadened [80].

Table 2.2: DC-balanced line codings in comparison with PRBS ($2^{20}-1$) [69]

	8B/10B	**5B/6B**	**7B/8B**	**9B/10B**	**64B/66B**	**PRBS**($2^{20}-1$)
Overhead (%)	25.00	20.00	14.29	11.11	3.21	0.00
Line rate (Gb/s)	12.44	11.94	11.37	11.06	10.26	9.95
Maximum run length	5	6	7	7	64*	20
Disparity per codeword	0 or ± 2	0 or ± 2	0, ± 2 or ± 4	0, ± 1 or ± 2	N/A	N/A

$*$ The maximum run length is 64 when the input block to the 64B/6B encoder is a sequence of zeros. However when the input is a PRBS of length $2^n - 1$, the maximum run length is n.

Besides the aforementioned codings, many other DC-balanced line codings (such as, 8B/10B [80, 82], 5B/6B [83], 7B/8B [84], 9B/10B [85], and 64B/66B [86]) have attracted lots of attentions. In nB/mB line coding, n-bit blocks of data are coded into m-bit codewords, and n and m are integers and satisfy with 'm>n>0' [69]. The encoding process of 5B/6B, 7B/8B, 8B/10B, and 9B/10B codes are based on mapping blocks of data into predefined codewords, which needs to satisfy certain properties on run length, disparity constraints, etc. As for 64B/66B line coding, each 64-bit message is scrambled by a self-synchronous scrambler of polynomial $x^{58}+x^{39}+1$, after which a 2-bit overhead is added ('01' if the scrambled block is only data signal; '10' if the scrambled block is only control or a mix of data and control signals) [86]. Table 2.2 summarizes the basic characteristics of these line codes, where the line rate is the total transmission rate including the overhead, the run length is the number of identical contiguous ones or zeros in the signal stream, and the disparity is the difference in the number of ones and zeros between different codewords. As illustrated in the table, 64B/66B code has an overhead of only 3.12% but at the cost of poorer transition

density and longer run length compared to the other codes. Moreover, it is observed from Table 2.2 that there is a tradeoff between the low-frequency content depletion and bandwidth expansion: the decrease in the maximum run length corresponds to larger overhead, which consequently requires larger bandwidth for the transmission devices (e.g., drivers, DMLs, or receivers) and makes the system more vulnerable to the fiber dispersion.

2.4 Transmission Performance of Directly Modulated 1.5-μm VCSELs

In this section, the transmission results from some literatures with the utilization of directly modulated 1.5-μm VCSELs with direct detection are compared and listed in Table 2.3, where different terms like data rate, distance, BL product, modulation format, detection method and raw BER are compared. It is noted that the raw data rate listed represents the maximum data rate from a single VCSEL, which means the reported link transmission rate might be higher than the listed value if wavelength division multiplexing or polarization multiplexing is applied. The distance listed in the table is the total transmission distance in the link, which might include the use of dispersion compensation fibers.

10-Gb/s NRZ signal's transmission over 23.6-km SSMF and low BER without the use of digital singal processing (DSP) are achieved in [8], which thanks to the optical equalization applied in the transmission link. [87] achieves a BL product of 1000 Gb/s·km in a 10-Gb/s single-VCSEL based transmission link, where the dispersion-induced distortion caused by 80-km SSMF is compensated by the

application of 20-km DCF. In [88], 10.7-Gb/s NRZ signal is successfully transmitted through 20- and 51-km SSMFs at 10^{-9} and 10^{-3} BER targets, respectively. In [28], 10.9-Gb/s NRZ signal is successfully transmitted through 5-km SSMF. The authors in [89] realize 4.2-km SSMF transmission of 25-Gb/s NRZ signal, which is generated by a short-cavity VCSEL with 17-GHz bandwidth. It is noted that an EDFA was used at the receiver side. In [90], a BL product of 280 Gb/s·km is successfully demonstrated with MLSE receiver. The authors in [91] used a short cavity 18-GHz VCSEL to successfully demonstrate the 35-Gb/s error free transmission at back-to-back condition. The data rate is further increased to 40Gb/s in [92], where the optical filter is applied for optical equalization. Error free transmissions of 50- and 56-Gb/s NRZ signals' transmissions over 2-km SSMF and at back-to-back condition are successfully achieved in [55], respectively. A two-tap FFE driver is utilized in this work to precompensate the response of the non-uniform response of VCSEL. Besides NRZ modulation format, many other modulation formats are also applied for directly modulated 1.5-μm VCSEL-based optical links. In [28], 10-Gb/s 4-PAM signal is successfully transmitted through over 5-km SSMF. 50 Gb/s 4-PAM signal's transmission over 100-m SSMF with direct detection is successfully demonstrated in [93] and no DSP is utilized in this link. When the DSP is applied for chirp and dispersion compensation, the data rate of 4-PAM signal is further increased to 56 Gb/s and the transmission distance is extended to 2 km in [36]. In addition, the highest single VCSEL raw bit rate of 115 Gb/s is achieved with the utilization of discrete multi-tone modulation (DMT) having 223 subcarriers in [94], where direct detection and DSP are applied at the receiver side. When the bit rate is reduced to 95 Gb/s, the transmission distance can be extended to 4 km, which means that a 380-Gb/s·km BL

product is successfully achieved.

Table 2.3: Summary of transmission performance using directly modulated 1.5-μm VCSELs with direct detection

Modulation Formats	Single VCSEL Raw Bit Rate (Gb/s)	Distance	BL Product (Gb/s·km)	Receiver Detection	Raw BER	Reference
NRZ	10	23.6	236	Direct	$1e-10$	[8]
NRZ	10	100	1000	Direct	$1e-9$	[87]
NRZ	10.7	20	214	Direct	$1e-9$	[88]
NRZ	10.7	51	545.7	Direct	$1e-3$	[88]
NRZ	10.9	5	54.5	Direct	0	[28]
NRZ	25	4.2	105	Direct	0	[89]
NRZ	28	10	280	Direct (w DSP)	$2e-5$	[90]
NRZ	35	B2B	< 35	Direct	0	[91]
NRZ	40	1	40	Direct	0	[92]
NRZ	50	2	100	Direct	0	[55]
NRZ	56	B2B	< 56	Direct	0	[55]
PAM-4	10	5	50	Direct	$10e-5$	[28]
PAM-4	50	0.1	5	Direct	$9e-3$	[93]
PAM-4	56	2	112	Direct/ w DSP	$10e-3$	[36]
OFDM-QPSK	0.5	5	2.5	Direct	$1e-5$	[28]
DMT	95	4	380	Direct (w DSP)	$8e-3$	[94]
DMT	115	B2B	< 115	Direct (w DSP)	$8e-3$	[94]

2.5 Summary

In this chapter, I review literatures on direct modulation and VCSELs. In Section 2.1, I first make a comparison on direct modulation and external modulation, and then review the basic characteristics, advantages and limitations of VCSELs. Section 2.2 focuses on directly intensity modulation of VCSELs, in which I analyse the frequency

chirp in directly intensity modulated VCSELs and review different approaches to mitigate this problem. Section 2.3 concerns FSK modulation in VCSELs, which takes advantage of the frequency chirp but suffers from the non-uniform FM response of the VCSEL. Several methods have been reported to address the above issue, among which DC-balanced line codings show potential to effectively deplete the low frequency contents of the signals and utilize the uniform region of the FM response at higher frequency range. Finally, in Section 2.4, the transmission performance from literatures which use directly modulated 1.5-μm VCSELs with direct detection are compared.

Chapter 3

10-Gb/s Signals Transmission over 1.5-μm VCSEL-based Optical Access Link

3.1 Introduction

As mentioned in Section 1.2, one of the biggest concerns about the use of 1.5-μm VCSELs for optical access applications would be a tight power budget, which comes from low output power and dispersion-induced sensitivity degradation. Direct current modulation of laser diodes always accompanies a large frequency chirp originated from the dependence of the refractive index on the carrier density in lasers [67]. This issue is especially critical for VCSELs due to their short cavity length. Thus, 1.5-μm VCSEL signals become very sensitive to fiber dispersion especially when the ER of the signal is large [22]. As mentioned in Section 2.2.2, fiber dispersion can be compensated by using DCMs along the link [17], but the performance improvement achieved by using DCMs is not directly translated into additional power budget owing to the insertion loss of the module. Another straightforward way of reducing the frequency chirp is to reduce the ER of the signal. By operating the laser far beyond the threshold current

with a small ER, both the transient and adiabatic chirps can be reduced. However, this method is not helpful in improving the power budget of access networks due to its poor back-to-back performance.

Fig. 3.1(a) shows the BER curves measured by using a 1.54-μm, 10-Gb/s VCSEL at the back-to-back and after 20-km transmission over SSMF. The BER performance is measured by using a PIN receiver at two different ERs (i.e., 2 and 7 dB). When the ER is set to 7 dB, we have a receiver sensitivity (at BER=10^{-9}) of -15.8 dBm at the back-to-back operation. We can also observe clear eye opening in Fig. 3.1(b). Due to the large frequency chirp, however, we have an error floor at around 10^{-3} after 20-km transmission. The eye diagram in Fig. 3.1(c) also shows that the signal suffers severe dispersion-induced distortion after 20-km transmission. The dispersion-induced performance degradation can be ameliorated by reducing the ER. For example, when we reduce the ER to 2 dB, the error floor is lowered to 10^{-4} after the transmission. However, this improvement comes at the expense of the back-to-back performance: the receiver sensitivity (at BER=10^{-9}) of ER-2 dB signal at the back-to-back condition is around -10.7 dBm, which shows a 5-dB power penalty with respect to the 7-dB ER signal.

On the other hand, we can consider applying FSK modulation on VCSELs by making a good use of the frequency chirp and it can improve the dispersion-limited transmission distance of VCSELs [22]. The VCSEL first generates binary FSK-formatted signals, which are then converted into OOK signals by a DI. The mark wavelength of the FSK-formatted signals is aligned to one of the peaks of the DI's transmittance to give high transmittance to the marks but low transmittance to the spaces. As mentioned in Section 2.3, the main problem in this approach, however,

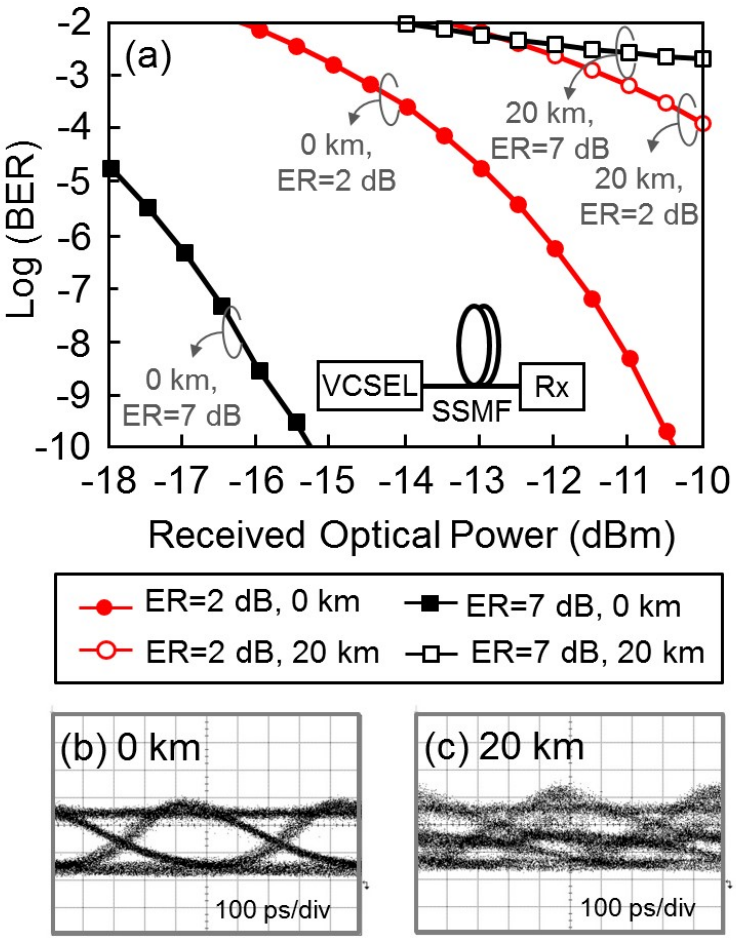

Figure 3.1: (a) BER curves measured by using a 1.54-μm directly-modulated VCSEL at back-to-back and after 20-km transmission. The inset shows the experimental setup for this measurement. Eye diagrams of 10.7-Gb/s OOK signals after (b) 0- and (c) 20-km transmissions, respectively.

is that VCSELs exhibit non-uniform FM response at low frequencies (e.g., $<$10 MHz), which in turn, causes severe signal degradation. This is because the thermal effect, which manifests itself from DC to tens of MHz, is out of phase with the carrier-induced FM effect spreading all over the VCSEL's FM bandwidth. We have reviewed some

approaches that can be applied to combat with this problem in Section 2.3. These approaches, however, either introduce additional cost and complexity to the system, or require large overhead when line coding is applied.

In addition, multilevel modulation format can also been considered to improve the dispersion tolerance of the transmission link. 4-PAM format has been extensively studied to double the data rate of VCSEL links [9, 10, 95]. For example, a 30-Gb/s 4-PAM transmission over an MMF link has been demonstrated by using a 0.85-μm VCSEL [26]. Recently, it has been demonstrated that a 1.55-μm VCSEL can be used to transmit a 10-Gb/s 4-PAM signal over 5-km SSMF [28]. A record 100-Gb/s 4-PAM transmission over 100-meter SSMF was also demonstrated by using polarization-division-multiplexed 1.55-μm VCSELs [9]. Thus, the use of 4-PAM modulation format for VCSEL links has been mainly focused on the doubling the data rate of short-reach optical links using band-limited VCSELs. It is worth noting that 4-PAM format is also a promising solution to improve the CD tolerance in 1.5-μm VCSEL links, since the quaternary modulation format doubles the symbol duration and shows higher spectral efficiency compared with the OOK signal at the same bit rate.

Electrical equalization is another technique which can be exploited to compensate for fiber dispersion of VCSEL links [12, 27, 29, 30]. With the aid of a DFE at the receiver side, 10-Gb/s OOK and 4-PAM transmissions over 300-meter polymer optical fiber were achieved by using a 0.85-μm VCSEL [30]. A record 55-Gb/s transmission of 0.85-μm OOK VCSEL signals was also demonstrated by using the electrical equalization at both the transmitter and receiver sides [12]. For 1.5-μm VCSELs, error-free transmissions of 10-Gb/s OOK signals over 40-km SSMF were

reported by using the electrical equalization at the receiver [29].

This chapter is divided into two parts. In the first part, we investigate the transmission performances of 10-Gb/s signals with DI in a 1.5-μm VCSEL-based optical access networks. When the DI is utilized, the FSK signals generated by the VCSEL will be converted to ASK signal and DC-balanced line codings are applied to improve the dispersion-limited performance of a 10-Gb/s OOK VCSEL link at 1.5 μm. It is noted that no electrical dispersion compensation is utilized in this work. Specifically, we firstly study the efficacy of DC-balanced line codings for 10-Gb/s VCSEL-based optical access networks, by comparing the transmission performance and bandwidth efficiency among various DC-balanced line coding schemes, including 7B/8B, 8B/10B, and 9B/10B. The bandwidth expansion of each code is taken into account to accurately assess the performance. Then, we optimize the FSR of DI in order to maximize the power budget of the 10-Gb/s VCSEL links. Finally, we try to further improve the power budget of the transmission link by replacing the PIN receiver with an APD receiver.

In the second part, we explore the possibility of realizing 10-Gb/s 1.5-μm VCSEL-based optical access networks using the OOK and 4-PAM modulation formats without DI. In this part, the electrical dispersion compensation is applied at the receiver side in order to maximize the power budget of 1.5-μm VCSEL links spanning tens of kilometers for optical access networks. The ER of the transmitted signals are also optimized in this experiment. The comparison between the performances of the OOK and 4-PAM VCSEL signals for optical access applications are also made in this part.

This chapter is organized as follows, Section 3.2 investigates the transmission performance of 10-Gb/s OOK signal with DI. The generation and basic characteristics

of the examined DC-balanced line codings are firstly introduced, followed by the experimental setup and results. Section 3.3 investigates and compares the transmission performances of 10-Gb/s OOK and 4-PAM signals without DI. An introduction of electrical equalization is firstly given, then followed by the experimental setup, theoretical analysis of power penalty and experimental results. Finally, this chapter is summarized in Section 3.4.

3.2 10-Gb/s OOK Signal Transmission over 1.5-μm VCSEL-based Optical Access Link with DI

3.2.1 DC-Balanced Line Coding

In this section, we give a brief introduction of various DC-balanced line codings, which aim to curb the occurrence of long consecutive identical bits without significantly increasing the overhead.

For 7B/8B [84], 8B/10B [82] and 9B/10B line codings [85]: they are based on mapping blocks of data into predefined codewords in order to satisfy the run length and disparity constraints, which are pre-defined in the coding lookup tables of each line coding. The run length is defined as the number of identical contiguous zeros or ones in the signal stream and the running disparity is defined as the difference between the number of zeros and ones in the codeword. Let's take 9B/10B as an example and explain its encoding process. In 9B/10B encoding process, 9 bits of data are translated into a 10-bit codeword, with a maximum run length of 7. The running disparity is controlled to maintain the DC balance during the encoding and mapping

process like follows: two look-up tables with positive and negative disparity are built up in advance. Only 512 10-bits codewords are used during this encoding process, which means nearly half of all 1024 10-bits codewords are discarded before encoding process by checking the disparity (i.e., the codewords with greater than 2-bits disparity in absolute value are first discarded). Therefore, only 252 balanced codewords, 210 codewords with disparity of 1, and 120 codewords pairs with disparity of 2 are kept. Then, 70 extra codewords are further discarded by checking the maximum run length: all codewords with beginning and trailing runs of 5 or more are dropped, which leaves us with 550 codewords. Moreover, the remaining codewords with beginning runs of 4 or ending runs of 4 are removed, after which the codewords are reduced to 520. Finally, 8 extra codewords are removed by re-checking the running disparity inside of each codepoints [85]. Fig. 3.2 shows the encoding process: for each 9-bit message, one of the look-up tables is selected to keep the running disparity of the output codewords as close to zero as possible. To be more specific, if the generated codeword has a positive running disparity, then the encoder will output a codeword that has zero or negative disparity; in contrast, if the generated codeword has a negative running disparity, then the encoder will output a codeword that has a zero or positive disparity. In summary, the running disparity will always be bounded and go towards zero. The overhead is 1/9 for 9B/10B line coding. Similarly, the 7B/8B and 8B/10B codes map 7-bit, and 8-bit blocks into predefined 8-bit, and 10-bit codewords, respectively.

Unlike the codes described above, the scramble-and-select coding is not based on mapping bit blocks into codewords. The scramble-and-select coding was proposed in [96] and the encoding procedure is illustrated in Fig. 3.3. Firstly, an uncoded 31-bit message is split into two ways and a 1-bit overhead of ‘0’ and ‘1’ is attached to each

of them, respectively. Both 32-bit codewords are then self-synchronously scrambled using a polynomial $g(x) = x^{21}+x^{19}+1$. Finally, we select one of the 32-bit codewords according to the selection rule by comparting the maximum run length (i.e., the number of identical consecutive '1's or '0's in a frame) and the mark rate (i.e., the ratio of total number of '1's to total number of bits in a frame) of the two codewords [96]. To be more specific: (1) if one of the two scrambled frames has a maximum run length smaller than the run length threshold set by the selector in advance, the corresponding frame is selected; (2) if none of them satisfies the run length requirement or both of them satisfy the constraints, the frame that has a mark rate closer to 0.5 would be selected. The overhead of this scramble-and-select line coding is 1/31. Table 3.1 summarizes the basic characteristics of the line codes examined in this chapter and the line rate is defined as the total transmission data rate including the overhead.

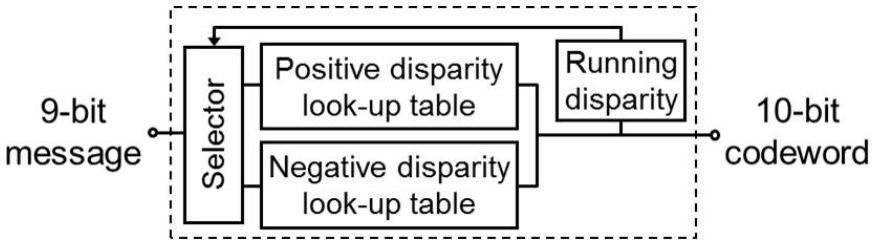

Figure 3.2: 9B/10B line encoder.

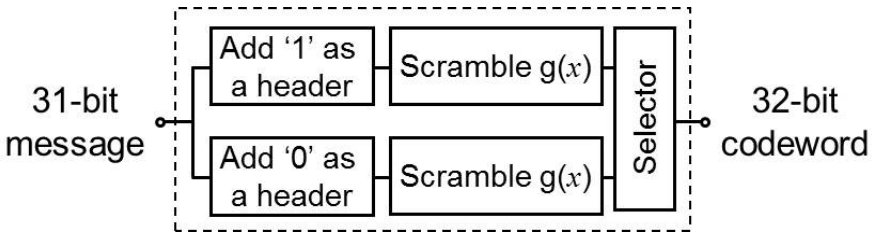

Figure 3.3: Scramble-and-select line encoder.

Table 3.1: Basic characteristics of the utilized line codes

	PRBS (2^{20}-1)	7B/8B	8B/10B	9B/10B	Scramble-and-select
Overhead(%)	0.00	14.29	25.00	11.11	3.22
Line rate (Gb/s)	9.95	11.37	12.44	11.06	10.27
Line rate (Gb/s)*	10.65	12.18	13.30	11.83	10.99
Maximum run length	20	7	5	7	31**
Disparity per codeword	N/A	0, ±2 or ±4	0, ±2	0, ±2 or ±4	31***

* The line rate here is further considered the 7% overhead of the Reed-Solomon (255, 239) forward-error correction.

** The maximum run length is 31 when the input block to the scramble-and-select encoder is a sequence of zeros. However when the input is a PRBS of length $2^n - 1$, the maximum run length is n.

*** When the input block of the scramble-and-select encoder is a sequence of zero.

3.2.2 Experimental Setup

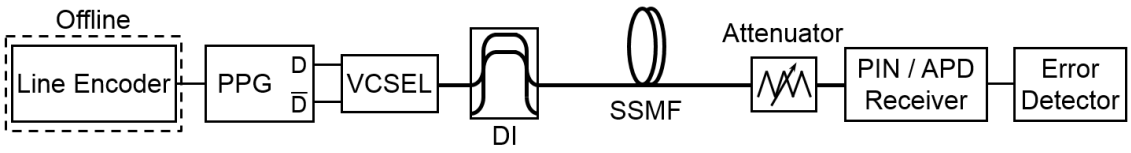

Figure 3.4: Experimental setup of 10-Gb/s OOK 1.5-μm VCSEL-based optical access link.

The experimental setup of 10-Gb/s OOK 1.5-μm VCSEL-based optical access link with DI and different line codes is depicted in Fig. 3.4. Non return-to-zero data with a PRBS length of $2^{20} - 1$ are first encoded offline and then uploaded to a pulse pattern generator (PPG). The generated differential pairs of the electrical signals are directly fed to a 1.54-μm VCSEL for direct modulation. The VCSEL used in the demonstration is an uncooled device housed in a TO-can packaging. The electro-optic

modulation bandwidth is measured to be 8 GHz. Fig. 3.5 shows the VCSEL's output power versus input current (L-I curve) characteristics at $25^{\circ}C$ and it is observed that the threshold current of the VCSEL used is around 4 mA. The VCSEL is biased at 14 mA and thus performs in a relative linear region [see Fig. 3.5]. At this bias condition, the output power is measured to be -1.2 dBm. There is no electrical amplifier to drive the VCSEL and the optimum driving current to the VCSEL is found to be 5.5-6.0 mApp. At this driving condition, the mark and space wavelengths are separated by half of the data rate, and thus a π phase shift occurs at every space [69]. The FSK signals at the output of the VCSEL are then sent to a DI to be converted into OOK signals with improved ERs. The FSR of the DI is varied to find out its optimum value. Every time we change the FSR of the DI, the phase of the DI is adjusted to minimize the BER by locating its peak at the marks' wavelength of the signal. The OOK signals after DI are then launched into SSMF and detected with a PIN/ APD receiver. The BER performance is directly calculated in the error detector by comparing the received samples with transmitted patterns.

It is noted that in this experiment, we try to compare the transmission performance among 7B/8B, 8B/10B and 9B/10B line codings. Due to the overhead of line coding, the line rates are set to be 11.37, 12.44, 11.06 Gb/s with 7B/8B, 8B/10B and 9B/10B codings, respectively (i.e., the raw data rate of PRBS signal is 9.95 Gb/s) [see Table 3.1]. When we replace the PIN receiver with an APD receiver and compare the transmission performance between 9B/10B and scramble-and-select line codings, 7% overhead of standard forward-error correction (FEC) is further considered. Therefore, the line rates are then set to be 10.99 Gb/s and 11.83 Gb/s for scramble-and-select and 9B/10B codings, respectively.

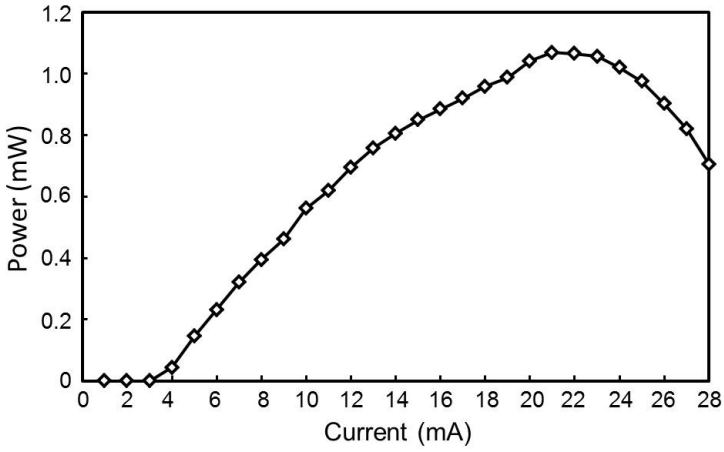

Figure 3.5: The L-I curve of the utilized VCSEL at 25°C.

3.2.3 Experimental Results

3.2.3.1 Evaluation of Different Line Codings

Fig. 3.6(a) and (b) show the BER performance when a DI with an FSR of 10.7 GHz is used. Without any line coding, error floors are observed at around 10^{-2} both for the back-to-back and 20-km transmission. This poor performance is attributed to the non-uniform FM response of the directly-modulated VCSEL. However, we observe a significant improvement in the BER performance with the line coding. The DC-balanced line coding depletes the low-frequency contents of the signal, and thus makes the whole spectrum of the signal reside in the uniform region of the VCSEL FM response. Even after applying line coding, however, we are unable to achieve a BER of 10^{-9} using this DI. This is because of the narrow optical filtering of the DI. As shown in Fig. 3.7, the 3-dB bandwidth of the DI is only 5.35 GHz (=10.7/2) and filtering the signal with this DI shrinks the signal bandwidth to 4 GHz. This bandwidth limitation of the signal is also evident from the eye closure in Fig. 3.8(a)-(d): the isolated marks

have a smaller eye opening than the long runs of marks. The BER performance can be greatly improved by using a DI with a 16.1-GHz FSR. Fig. 3.6(c) and (d) show that we can achieve decent receiver sensitivities (at BER=10^{-9}) ranging from -15.0 to -16.2 dBm when line coding is applied. The receiver sensitivity is further improved after 20-km transmission over SSMF. For example, we have 0.6-dB sensitivity improvement after the transmission when 9B/10B line coding is used. This improvement comes from the duobinary-like phase characteristics of the generated OOK signals after DI [97]. The eye diagram in Fig. 3.8(h) also shows wider eye opening after transmission. When we further increase the FSR of the DI, the BER performance of the VCSEL signals is slightly degraded. Fig. 3.6(e) and (f) show the BER curves measured with a 20-GHz-FSR DI. Compared to Fig. 3.6(c) and (d) where the DI has an FSR of 16.1 GHz, the receiver sensitivities are degraded by 0.3$\backsim$ 0.7 dB. Overall, 7B/8B and 9B/10B perform similarly but outperform 8B/10B, which has the highest line rate. It is interesting to note that the performance difference between the 9B/10B and 8B/10B decreases as the FSR of the DI increases. This is because the optical bandwidth of the signal after DI filtering increases with the FSR of the DI, which is evident from Fig. 3.7. We select 9B/10B as our coding scheme since it exhibits the best BER performance and has the lowest line rate.

3.2.3.2 Optimization of DI's FSR

Next, we optimize the FSR of the DI for our VCSEL-based link. We assume Reed-Solomon (255, 239) FEC with a 7% overhead. In this case, the line rate increases to 11.83 Gb/s after taking into account the overheads of FEC and 9B/10B coding [see Table 3.1]. We then measure the system performance using DIs with different FSRs

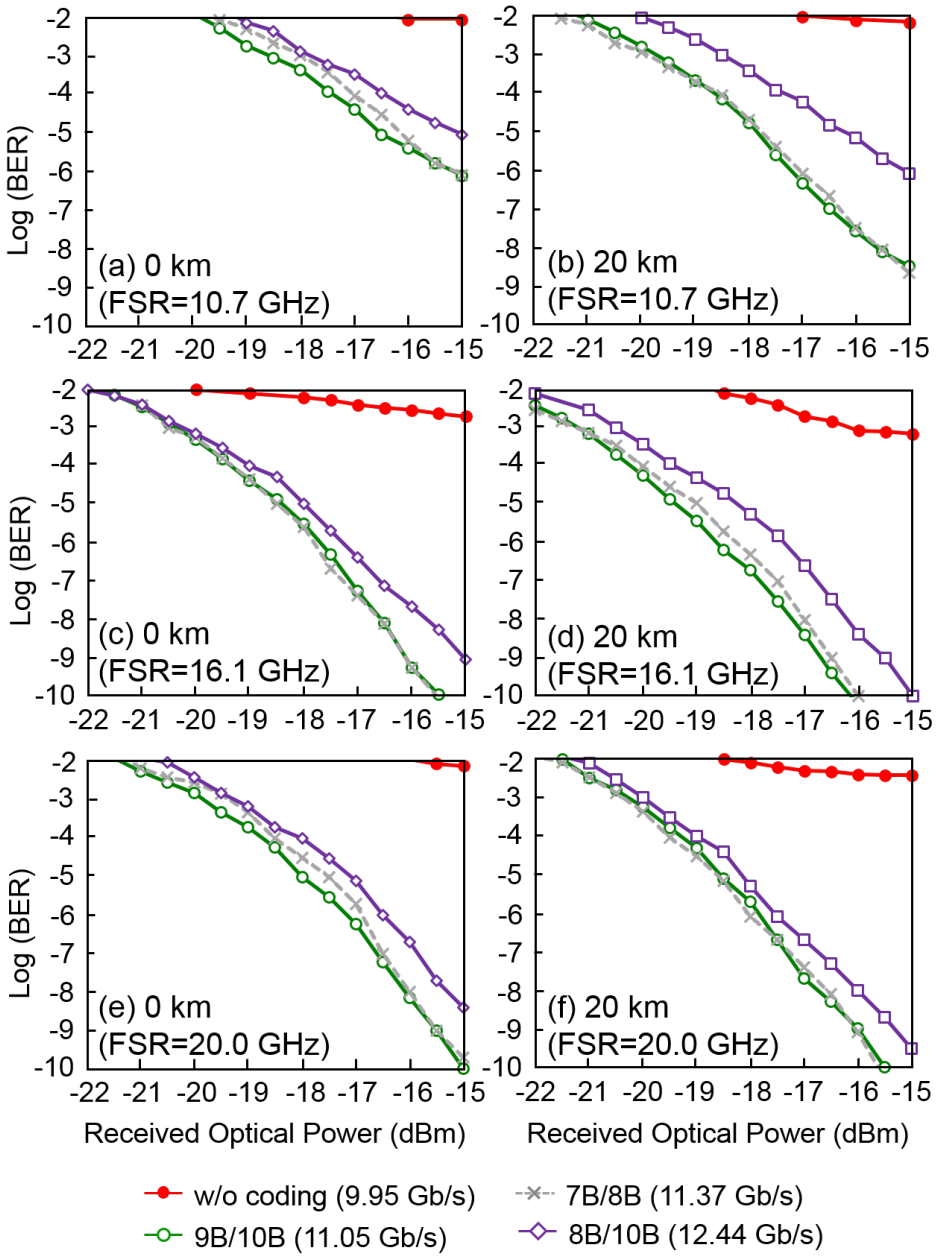

Figure 3.6: Measured BER curves of different line codings with different-FSR DIs.

and plot them in Fig. 3.9. The results show that the receiver sensitivities for both back-to-back and 20-km transmission are improved as we increase the FSR of the DI up to 16.1 GHz but start to decline if we further increase the FSR beyond 16.1 GHz.

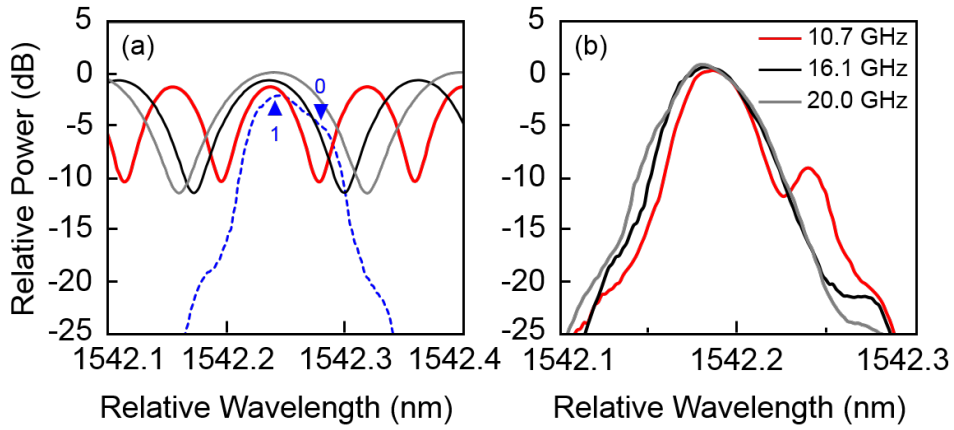

Figure 3.7: Measured optical spectra of the signals (a) at the DI input (dotted blue), and (b) at the DI output when the FSRs are 10.7, 16.1, and 20.0 GHz. Also shown in (a) is the wavelength response of the DI with different FSRs.

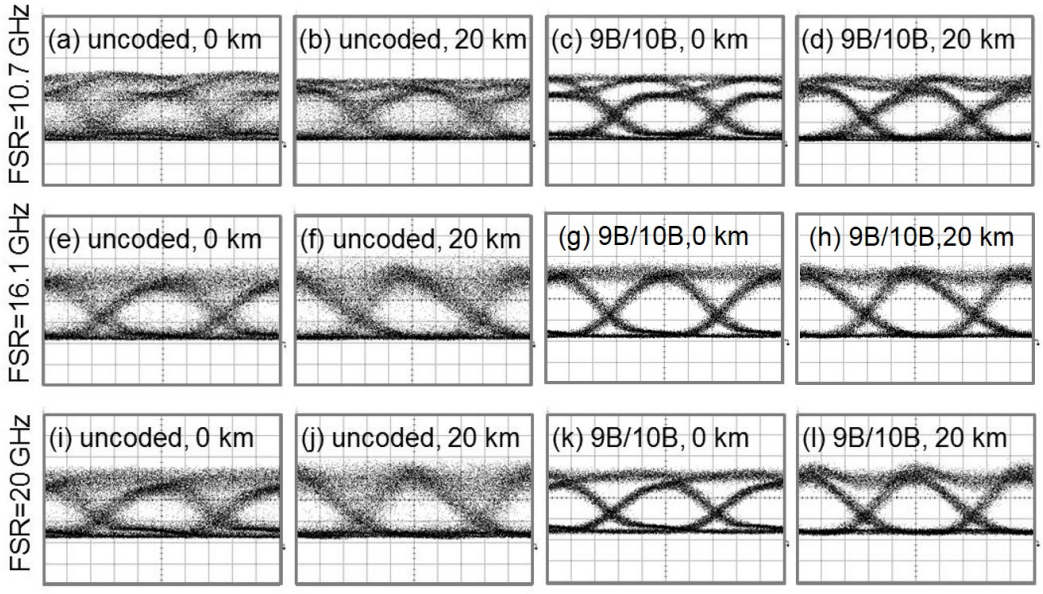

Figure 3.8: Measured optical eye diagrams.

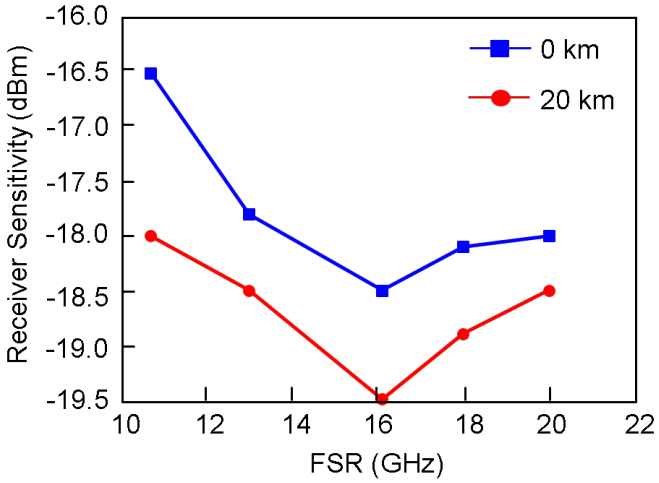

Figure 3.9: Receiver sensitivity as a function of the FSR of the DI. The receiver sensitivities are measured at the uncorrected BER of 1.8×10^{-4} and the line rate is 11.83 Gb/s, taking into account FEC and 9B/10B line coding.

Thus, the best BER performance is obtained with an FSR of 16.1 GHz. The reason for this performance behavior can be explained as follows: when the FSR is lower than 16.1 GHz, the signals at the DI output suffer from bandwidth limitation. On the other hand, when the FSR is above the optimal value, the ER is degraded due to the reduced suppression of the signal's 0-level which falls on the DI's skirt instead of its null in the spectrum [see Fig. 3.7 (a)]. To substantiate this explanation, we plot the ERs of the signals as a function of the FSR of the DI in Fig. 3.10. The ER is 11.5 dB when the FSR is 16.1 GHz, but it is degraded to 6.1 dB with the 20-GHz FSR. Fig. 3.10 also shows the insertion loss incurred by the DI. The insertion loss is 4.2 dB when a DI with 16.1-GHz FSR is used. This implies that considering a fiber launch power of -2.0 dBm, the system can accommodate a total link loss of 13.3 dB (=19.5$-$2$-$4.2) for 20-km SSMF link. It is worth noting that the conventional on-off keying scheme

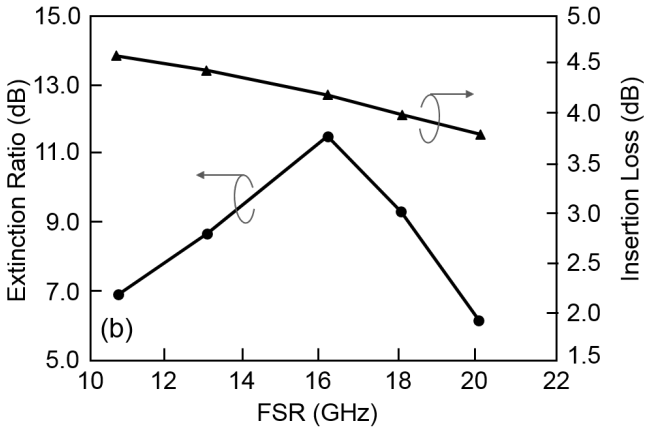

Figure 3.10: Extinction ratio of the VCSEL signals as a function of the FSR of the DI. The receiver sensitivities are measured at the uncorrected BER of 1.8×10^{-4} and the line rate is 11.83 Gb/s, taking into account FEC and 9B/10B line coding. Also shown in the figure is the insertion loss of the DI.

(e.g., 2-dB ER) has a power budget of only 8 dB (=10−2) [see Fig. 3.1]. Therefore, even with the insertion loss of the DI, the power budget is improved by >5 dB using the proposed scheme.

Lastly, we measure the dispersion tolerance of the VCSEL signals, as shown in Fig. 3.11. Thanks to a duobinary-like π phase change at every space, the signals can be transmitted over 50-km SSMF with less than 0.5-dB penalty. The best receiver sensitivity is obtained at 20 km.

3.2.3.3 Power Budget Improvement with APD Receiver

From Section 3.2.3.1 and 3.2.3.2, we find that the optimized transmission performance of OOK signals in 1.5-μm VCSEL-based optical access link is achieved by the utilization of 9B/10B line coding and 16.1-GHz DI. In this section, we replace the

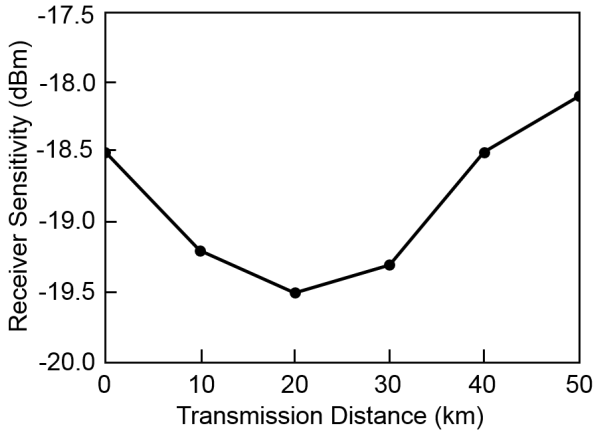

Figure 3.11: Measure dispersion tolerance of the VCSEL signals. The receiver sensitivities are measured at BER of 1.8×10^{-4}.

PIN receiver with an APD receiver in order to further improve the power budget of transmission link and further compare the transmission performance between 9B/10B and scramble-and-select line codings. We set the line rate of 9B/10B and scramble-and-select line coding to be 10.99 and 11.83 Gb/s, respectively, by assuming Reed-Solomon (255, 239) FEC with a 7% overhead [see Table 3.1].

Fig. 3.12 shows the measured BER curves. At the back-to-back operation [see Fig. 3.12(a)], we achieve a receiver sensitivity (BER=1.8×10^{-4}) of -29 dBm when the scramble-and-select line coding is employed. We achieve similar receiver sensitivity with 9B/10B coding. Decent performance of OOK signals after DI should be attributed to the use of DC-balanced line coding which depletes the low-frequency contents of the signal. Fig. 3.13 and Fig. 3.14 shows the measured electrical RF spectra of transmitted signals in the range of 50 MHz and 15 GHz, respectively. From these figures, we can observe that the 9B/10B coding depletes the low-frequency contents of the signal by $>$ 20 dB, whereas the scramble-and-select coding reduces the spectral contents of

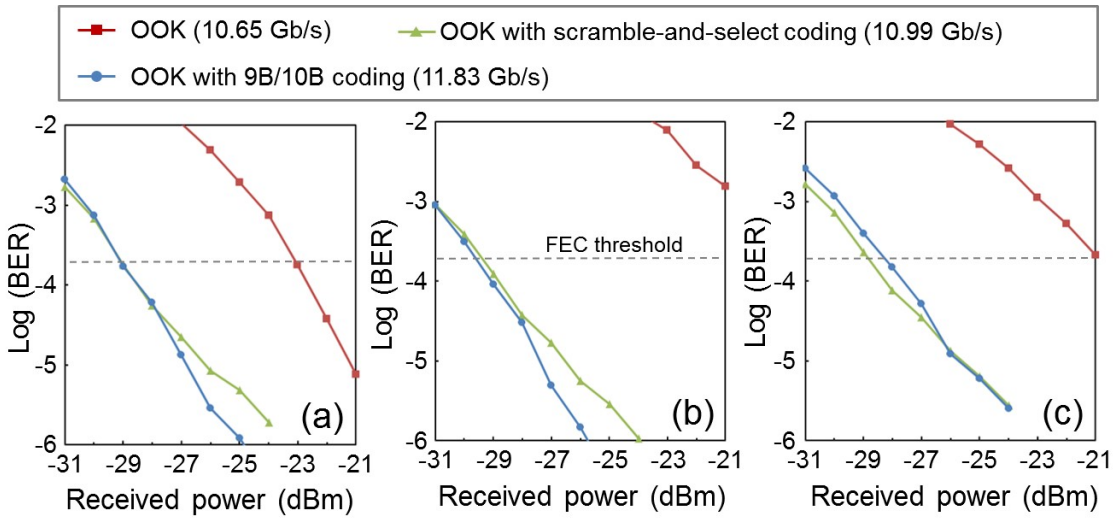

Figure 3.12: Measured BER as function of the received signal power at (a) 0 km, (b) 20 km, and (c) 40 km over SSMF.

the signal at 10 MHz by $\sim$ 10 dB, compared to the uncoded PRBS. These spectral depletions greatly help to utilize the flat portion of the FM response of the VCSEL. Without line coding, we observe an error floor at $> 10^{-3}$. The BER performance of the conventional OOK signals (i.e., without using DI) with an ER of 2.2 dB is also plotted in the Fig. 3.12 for comparison and the line rate is set to be 10.65 Gb/s. The receiver sensitivity is measured to be -23.0 dBm at the back-to-back operation, which can be improved by increasing the ER. However, as mentioned in Section 3.1: increasing the ER of the signals gives rise to large frequency chirp, which in turn, makes the OOK signal be severely degraded. After transmission over 20-km SSMF, the degraded BER performance of the OOK signal and degraded eye diagram in Fig. 3.15(l) confirms the above analysis. On the other hand, the OOK signals after DI exhibit slightly improved receiver sensitivity after 20-km transmission. This is because of the duobinary-like

phase characteristics of the generated signals [97]. The receiver sensitivities of the OOK signals after DI are measured to be better than -28 dBm after 40-km transmission. We can still observe clear eye opening of scramble-and-select and 9B/10B signals in Fig. 3.15 (d) and(i) after 40-km transmission, respectively.

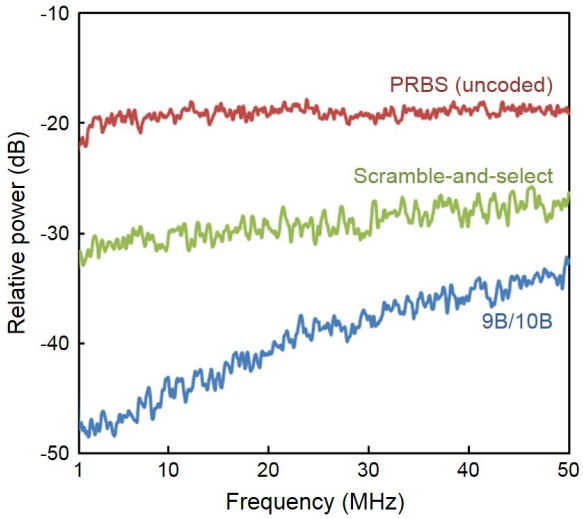

Figure 3.13: Measured RF spectra of the line coded and $2^{20} - 1$ PRBS signals at low-frequency range (< 50 MHz).

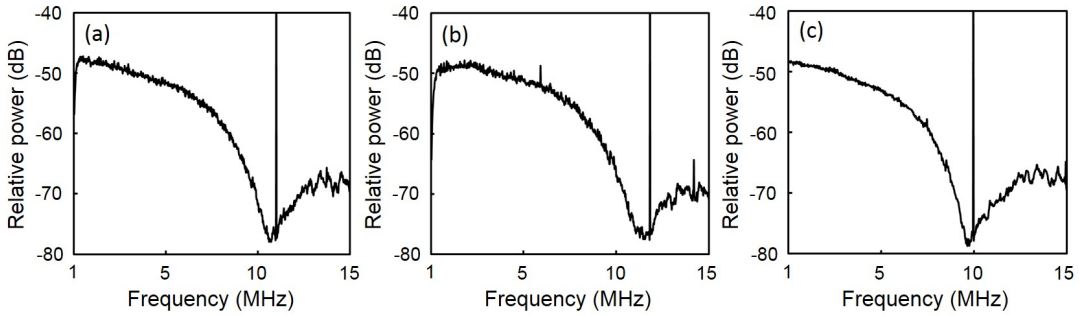

Figure 3.14: Measured RF spectra of (a) scramble-and-select, (b) 9B/10B, and (c) uncoded $2^{20} - 1$ PRBS signals.

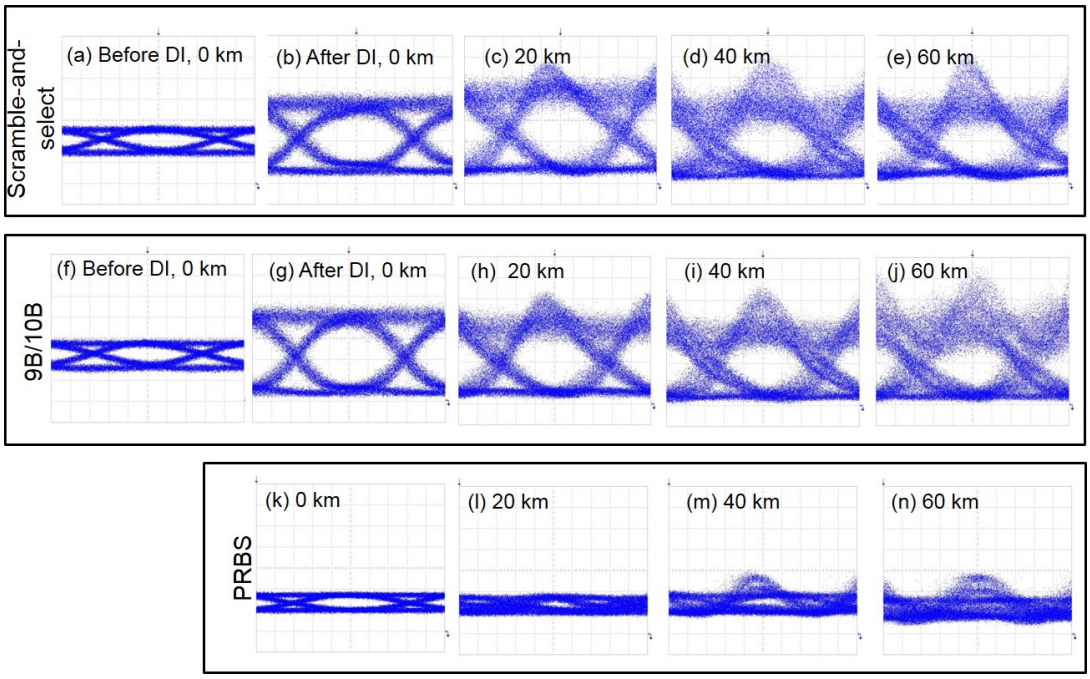

Figure 3.15: Optical eye diagrams of (a)-(e) scramble-and-select line coding, (f)-(j) 9B/10B line coding, and (k)-(n) OOK signals at different transmission length. (Horizontal: 15 ps/div, Vertical: 150 μw/div)

Fig. 3.16 shows the measured power budget (i.e., the fiber launch power minus the receiver sensitivity) as a function of the transmission distance over SSMF. For the OOK signals after DI, the DI is assumed to be co-located with the VCSEL at the transmitter side. Thus the insertion loss of the DI is removed from the power budget. When the DI is employed, it is observed that there is no performance difference between the scramble-and-select and 9B/10B codings. This is because that the performance degradation caused by relatively low spectral depletion of the scramble-and-select line coding is offset by its lower line rate compared with 9B/10B coding. We also observe that the OOK signals with DI exhibit a relatively uniform power budget performance

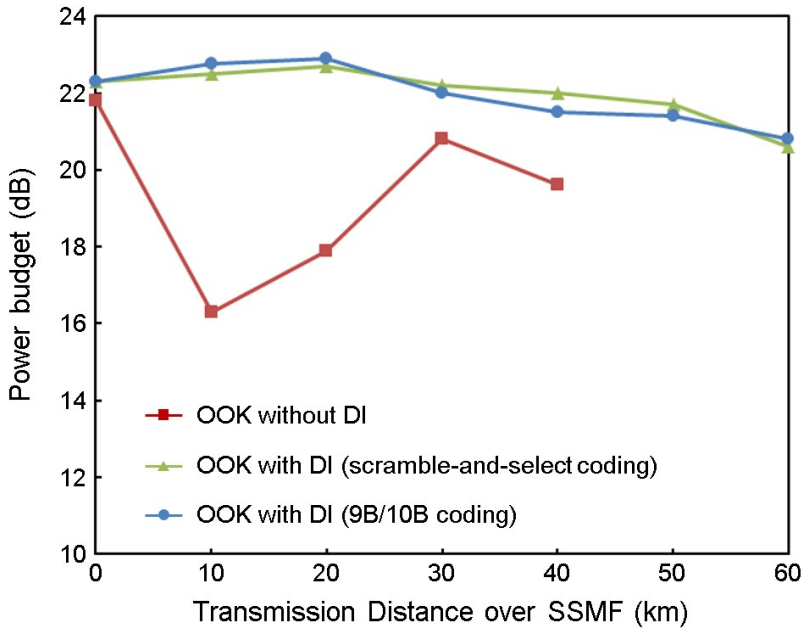

Figure 3.16: Power budget as a function of transmission distance. The insertion loss of the DI is removed from the budget.

up to 60 km. Clear eye opening of the signals after are still observed in Fig. 3.15(e) and (j) after 60-km transmission. Without DI, it is observed that the performance of conventional OOK signals is poor at 10 km but improved beyond, which reflects the effect of self-steeping, caused by the interplay between fiber dispersion and adiabatic chirp [88]. Nevertheless, the maximum transmission distance of the conventional OOK signal without DI is 40 km, beyond which is not achievable due to poor receiver sensitivity and loss of the fiber.

3.3 10-Gb/s OOK and 4-PAM Signals Transmission over 1.5-μm VCSEL-based Optical Access Link without DI

3.3.1 Adaptive Filter

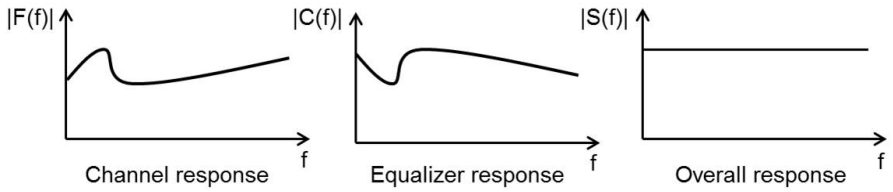

Figure 3.17: Concept of equalizer.

As mentioned before in Chapter 2, one issue of using long-wavelength VCSELs for optical access applications is their high susceptibility to fiber dispersion, which significantly limits the power budget of VCSEL-based optical access networks. It has been widely reported that adding equalizer is one effective method to compensate the dispersion-induced signal distortions in electrical domain [98, 99]. It is because that the equalizer can supply an inverse of the channel to the received signal, such that the combination of the channel and equalizer offers a flat frequency response as shown in Fig. 3.17.

However, in most practical transmission system, the transfer function is not known in advance and the channel's impulse response varies with time. Thus, static equalizers are not suitable for practical usage, although they are relatively cheap for implementation. Adaptive equalizer, which is a kind of filter that self-adjusts its transfer function to adapt to the time-varying prosperities of the communication

channel [99], becomes more appealing. In the rest of this section, we give a brief introduction of two types of adaptive filters: least mean square (LMS)-based transversal filter and decision-feedback equalizer that we will use for VCSEL-based optical access networks.

3.3.1.1 LMS-based Transversal Filter

LMS algorithm, based on minimizing the least-mean-square value of the error signal (difference between the desired and the actual signal), can be used for optimizing the adaptive filter coefficients. It has been widely applied in various applications due to its simplicity but highly effective in performance [98]. LMS-based filter can be built in a transversal (i.e. tapped delay line) structure, which is responsible for performing the filtering process. The illustration of the LMS-based transversal filter is given in Fig. 3.18, in which the weight control mechanism is responsible for performing the adaptive control process on the tap weight of the transversal filter. Since the filter coefficients are only adapted based on the error at the current time, it is a kind of stochastic gradient descent method. The LMS-based transversal filtering consists of two basic procedures: filtering process and adaptive process, which are discussed in details in the rest of this section.

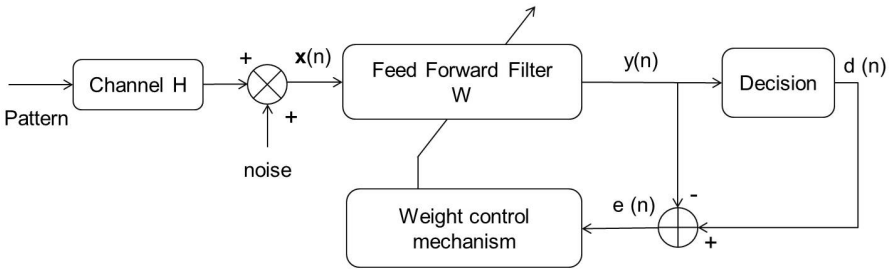

Figure 3.18: Block diagram of adaptive transversal filter.

The filtering process involves computing the output $y(n)$ of a linear filter in response to the input signal $\mathbf{x}(n)$, and generating an estimation error $e(n)$ by comparing $y(n)$ with a desired response as follows:

1. Filter output:

$$y(n) = \hat{\mathbf{w}}^H(n)\mathbf{x}(n) \tag{3.1}$$

2. Estimation error or error signal:

$$e(n) = d(n) - y(n) \tag{3.2}$$

where $\mathbf{x}(n)$ is the tap-input vector at time n, $y(n)$ is the filter output, and $d(n)$ is the decision value of $y(n)$ after passing the decision circuit.

The adaptive process involves the automatic adjustment of the coefficients of the filter according to the estimation error:

$$\hat{\mathbf{w}}(n+1) = \hat{\mathbf{w}}(n) + \mu_1 \mathbf{x}(n)e^*(n) \tag{3.3}$$

where μ_1 is the step size, and $\hat{\mathbf{w}}(n+1)$ is the estimated tap-weight vector at time $(n+1)$. If the prior knowledge of the tap-weight vector $\hat{\mathbf{w}}(n)$ is not available for computing $\hat{\mathbf{w}}(n+1)$, $\hat{\mathbf{w}}(n)$ is set to be $\mathbf{0}$. In order to properly set the initial value of $\hat{\mathbf{w}}(n)$, there usually exists a training process before normal signal reception, during which the transmitted pattern $p(n)$ is assumed to be known prior and takes place of $d(n)$. Note that the second term (i.e., $\mu_1 \mathbf{x}(n)e^*(n)$) in Eq. (3.3) represents the adjustment applied to the current estimate of the tap-weight vector $\hat{\mathbf{w}}(n)$.

The combination of above two processes constitutes a feedback loop: first, the LMS-based transversal filter is responsible for performing the filtering process; second, a mechanism is implemented for performing the adaptive control process on the tap weight of the transversal filter.

3.3.1.2 Decision-Feedback Equalization

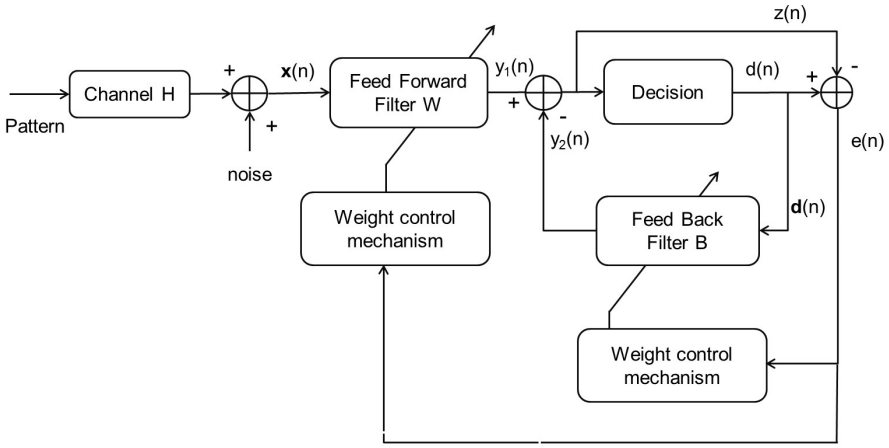

Figure 3.19: Block diagram of decision feedback equalizer.

The basic limitation of the transversal filter introduced in Section 3.3.1.1 is the poor performance on the channels having spectral nulls. A DFE is a kind of equalizer that arguments a linear equalizer by adding a filtered version of previous symbol estimates to the original filter output [98, 99]. Fig. 3.19 shows a simplified block diagram of DFE, which is composed of a forward transversal filter and a decision-feedback filter. The forward and feedback filters can be linear filters (e.g., transversal filters). The basic idea of a DFE is that if the previously detected symbols are known, then the ISI contributed by these symbols can be cancelled out exactly at the output of the forward filter by subtracting past symbols with appropriate weighting [98]. The tap weights of the forward and feedback filter can be adjusted simultaneously to fulfill certain criterion (e.g., LMS algorithm). The improved performance is possible to be achieved with the utilization of DFE, since the additional feedback filter allows more freedom in the selection of the feed-forward filter's coefficients, i.e., the exact

inverse of the channel response needs not be synthesized in the feed-forward filter. Therefore, excessive noise enhancement can be avoided and the sensitivity to sampler's phase is decreased.

Similar to Section 3.3.1.1, the adaptive filtering process of DFE is depicted as follows:

1. Filter output:

$$y_1(n) = \hat{\mathbf{w}}^H(n)\mathbf{x}(n) \tag{3.4}$$

$$y_2(n) = \hat{\mathbf{b}}^H(n)\mathbf{d}(n) \tag{3.5}$$

2. Estimation error:

$$e(n) = d(n) - z(n) \tag{3.6}$$

where $\mathbf{x}(n)$ is the tap-input vector at time n, $y_1(n)$ is the filter output of the feed forward part and $y_2(n)$ is the output of the decision feed back filter, and $z(n)$ is the difference between $y_1(n)$ and $y_2(n)$, which is then feed into the decision circuit for making a decision, i.e., $d(n)$. Note that $\mathbf{d}(n)$ is the decision input vector for the feed back filter at time n.

The adaptive process involves the automatic adjustment of the parameters of the filter both at the feed forward and feed back part according to the estimation error:

$$\hat{\mathbf{w}}(n+1) = \hat{\mathbf{w}}(n) + \mu_1\mathbf{x}(n)e^*(n) \tag{3.7}$$

$$\hat{\mathbf{b}}(n+1) = \hat{\mathbf{b}}(n) + \mu_2\mathbf{d}(n)e^*(n) \tag{3.8}$$

where μ_1 and μ_2 are the step sizes of feed forward filter and feed back filter, respectively. $\hat{\mathbf{w}}(n+1)$ is the estimated tap weight vector at time $(n+1)$. If the prior knowledge of the tap-weight vector $\hat{\mathbf{w}}(n)$ is not available for computing $\hat{\mathbf{w}}(n+1)$,

$\hat{\mathbf{w}}(n)$ is set to be $\mathbf{0}$. In order to properly set the initial value of $\hat{\mathbf{w}}(n)$, there usually exist a training process before normal signal reception, during which the transmitted pattern $p(n)$ is assumed to be known prior and takes place of $d(n)$. Similarly, $\hat{\mathbf{b}}(n+1)$ is the estimated tap weight vector of feedback part at time $(n+1)$. If the prior knowledge is not available, the tap-weight vector $\hat{\mathbf{b}}(n)$ is set to be $\mathbf{0}$.

Not that if an incorrect decision is made and fed to the feedback filter, this error will affect the following few symbols, which means the incorrect decision propagates through the feedback filter, i.e., error propagation. Therefore, it is possible that more errors are then generated. Fortunately, the error rate in most channels of interest is low enough that the overall performance degradation is not obvious [98, 99].

3.3.2 Experimental Setup

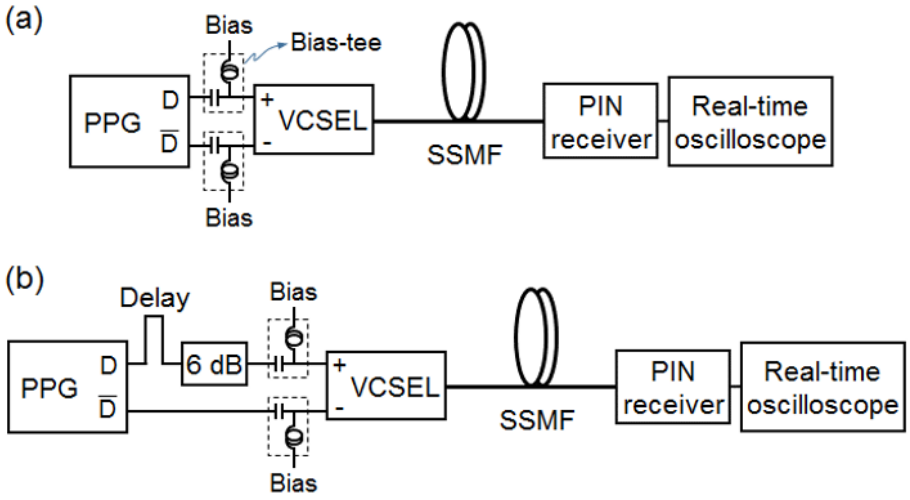

Figure 3.20: Experimental setups for transmission of (a) OOK and (b) 4-PAM signals.

Fig. 3.20(a) shows the experimental setup for transmission of 10.7-Gb/s OOK signal. A 1.5-μm VCSEL is directly modulated by a PRBS of length 2^{15}-1 from a

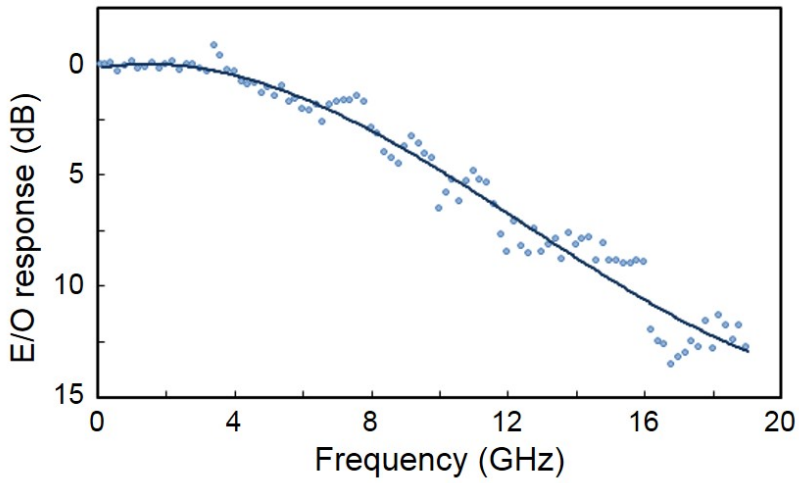

Figure 3.21: The EO response of the VCSEL used in the experiment.

PPG. The line rate is set to be 10.7 Gb/s in order to include 7% overhead of FEC. The VCSEL used in the experiment is an uncooled device housed in a TO-can package. Fig. 3.21 shows the measured electro-optic (E/O) response of the VCSEL at a bias current of 14 mA. The 3-dB E/O bandwidth of the device is measured to be 8 GHz. The output power of the VCSEL is about -2 dBm regardless of ER. After transmission over SSMF, the signal is detected by using a PIN detector. The received signal is then sampled by using a 50-Gsample/s oscilloscope for off-line signal processing and direct error counting. We also generate 4-PAM signals by using the same VCSEL. Fig. 3.20(b) shows the experimental setup for 4-PAM signal transmission. For the generation of the 4-PAM signal, one of the outputs from the PPG is 53-bit delayed (for decorrelation) and 6-dB attenuated with respect to the other output by using a microwave delay line and electrical attenuator, respectively. The two PRBSs are then directly fed to two electrical inputs of the VCSEL. The ER of the generated 4-PAM signal ε is defined as P_3/P_0, where P_3 is the optical power of the highest level and P_0 is the optical power of the lowest level. The ER of the signals can be tuned by adjusting the driving

amplitude from the PPG. It is worth noting that we do not use any electrical amplifiers and electrical power combiner for the generation of the 4-PAM signals. For BER measurement of the 4-PAM signal, we assume that the bits are mapped onto symbols using natural coding instead of the Gray coding due to the inherent characteristics of generating the 4-PAM signal using the aforementioned method [100].

3.3.3 Theoretical Power Penalty

In practical communication systems, the optical signal emitted by a transmitter has different powers at different signal levels, which is different from the theoretical analysis that no energy is contained in a '0' bit. Moreover, the optical signal degrades during its transmission through the fiber link. An example of such degradation is the signal distortion caused by chromatic dispersion. The minimum average optical power required by the receiver increases because of the above non-ideal conditions, and the increase in the average received power is referred as the power penalty [1]. In the following, we derive the relationship between the power penalty and the corresponding signal's ER.

Take 4-PAM signal as example, the relationship between the power penalty and the defined ER (i.e., the intensity ratio between the highest and lowest level) can be calculated from the following set of equations:

$$\varepsilon = \frac{P_3}{P_0} \tag{3.9}$$

$$I_0 = R_d \cdot P_0 \tag{3.10}$$

$$I_1 = R_d \cdot P_1 \tag{3.11}$$

$$I_2 = R_d \cdot P_2 \tag{3.12}$$

$$I_3 = R_d \cdot P_3 \tag{3.13}$$

$$Q = \frac{I_1 - I_0}{\sigma_0 + \sigma_1} = \frac{I_2 - I_1}{\sigma_1 + \sigma_2} = \frac{I_3 - I_2}{\sigma_2 + \sigma_3} \tag{3.14}$$

$$\overline{P}_{rec} = \frac{(P_0 + P_1 + P_2 + P_3)}{4} \tag{3.15}$$

$$\delta_{ex} = 10\log_{10}(\frac{\overline{P}_{rec}(\varepsilon)}{\overline{P}_{rec}(0)}) \tag{3.16}$$

where P_0, P_1, P_2, and P_3 are the optical power values from the lowest level to the highest level, and I_0, I_1, I_2, and I_3 are the corresponding photocurrents. R_d is the responsivity of the PIN receiver, and Q is the defined Q factor. $\overline{P}_{rec}$ is the averaged received power and the defined power penalty δ_{ex} can be calculated from $\overline{P}_{rec}$. Note that the root mean square (RMS) noise currents σ_0, σ_1, σ_2, and σ_3 depend on $\overline{P}_{rec}$ due to the dependence of the shot noise contribution on the received optical signal. However, all of them can be approximated by the thermal noise σ_T when receiver performance is dominated by thermal noise.

From Eq. (3.9) to (3.16), we can obtain the theoretical power penalty as

$$\delta_{ex} = 10\log_{10}(\frac{\varepsilon + 1}{\varepsilon - 1}) \tag{3.17}$$

The obtained theoretical power penalties of ER-3, ER-5, and ER-7 4-PAM signals from Eq. (3.17) is 3.01 dB, 1.76 dB and 1.25 dB, respectively. Therefore, the power penalty between ER-3 and ER-5 signals are calculated to be 1.25 dB, which decreases to 0.51 dB between ER-5 and ER-7 signals.

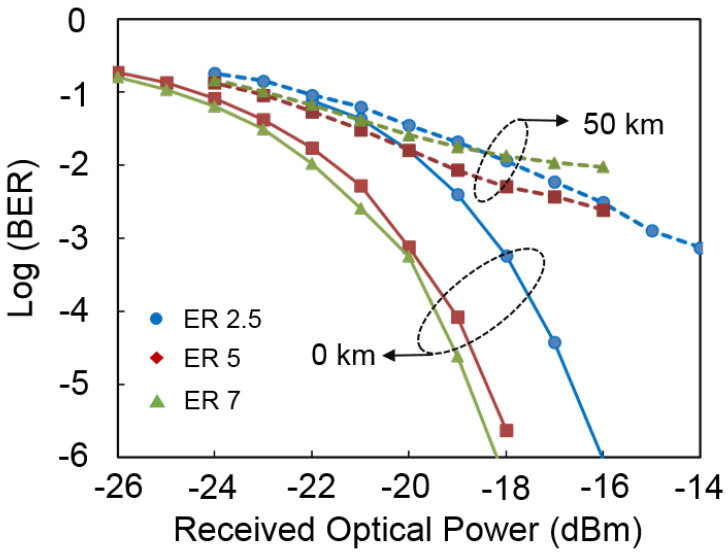

Figure 3.22: Measured BER curves of 10.7-Gb/s OOK signals after 0- and 50-km transmissions over SSMF, respectively, when no electrical equalization is applied at the receiver.

3.3.4 Experimental Results

3.3.4.1 Transmission Performance of 10.7-Gb/s OOK Signal

We first investigate the transmission performance of the 10.7-Gb/s OOK signal, when no electrical equalization is applied. Fig. 3.22 shows the measured BER curves at the back-to-back and after 50-km transmission, respectively. Here, we compare the BER performance among three ER values: 2.5, 5 and 7. In the back-to-back condition, we achieve best receiver sensitivities (BER$= 1.0 \times 10^{-3}$) at around -20.4 dBm for ER-7 signal, which are degraded to -20.1 dBm and -18.3 dBm for ER-5 and ER-2.5 signals, respectively. However, error floors are observed at around 10^{-2} and 10^{-3} for high-ER signals (i.e., ER-7 and ER-5 signals) after 50-km transmission over SSMF when no dispersion compensator is employed. For ER-2.5 signal, it can still achieve

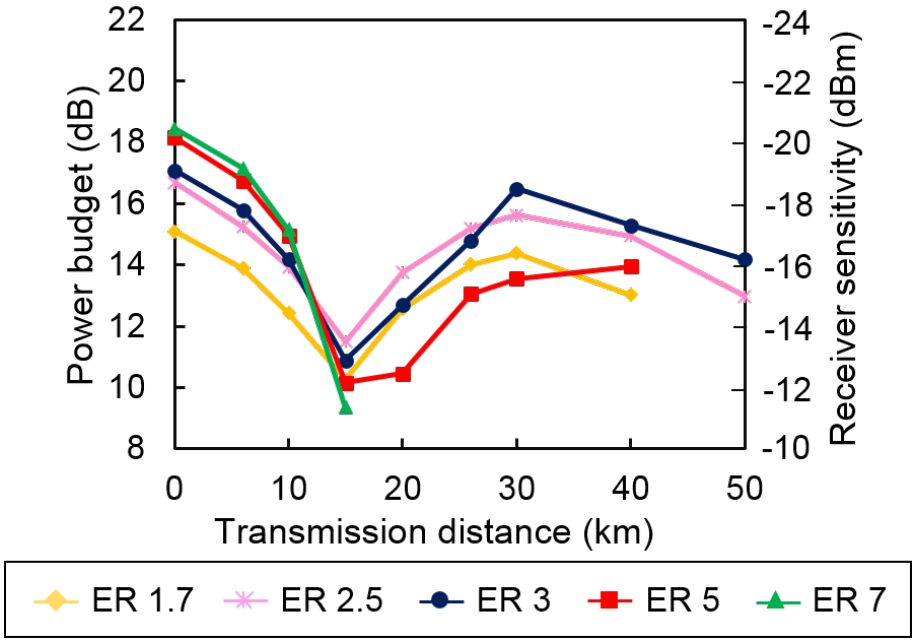

Figure 3.23: Measured power budget and receiver sensitivity of the 10.7-Gb/s OOK VCSEL link as a function of transmission distance over SSMF when no electrical equalization is applied at the receiver.

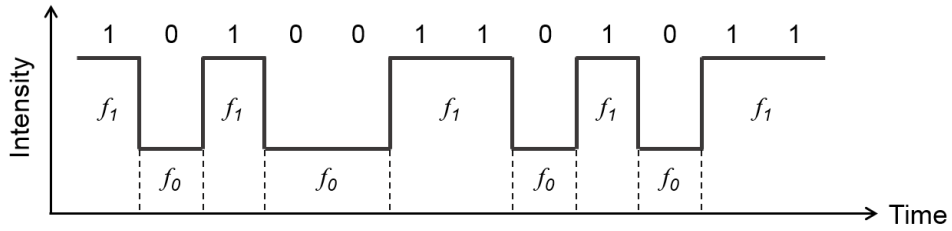

Figure 3.24: An OOK signal with a low ER generated by using a VCSEL. The marks and spaces emit different optical frequencies, f_1 and f_0, respectively, depending upon the modulation current of each intensity level.

BER at 10^{-3} with -14.57 dBm received power. The results show that low-ER signal has better receiver sensitivities than high-ER signals after transmission over SSMF. This is because that high-ER signal suffers more from dispersion-induced signal distortion

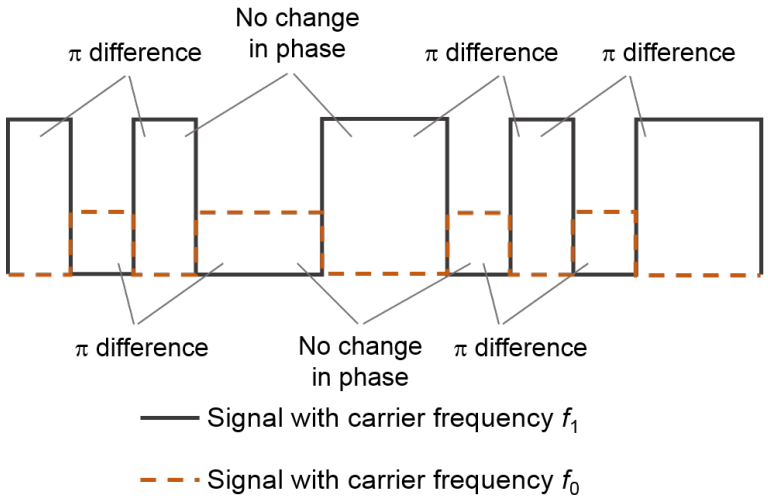

Figure 3.25: The OOK VCSEL signal can be decomposed into two high-ER signals, one with the carrier frequency f_1 and the other with f_0.

after transmission, as we mentioned earlier. Then we compare the measured power budget (i.e., the fiber launch power minus the receiver sensitivity at a BER of 10^{-3}) of the 10-Gb/s OOK signal as a function of the transmission distance when no electrical equalization is applied and the result is shown in Fig. 3.23. We vary the ER of the signal from 1.7 to 7 while keeping the bias current unchanged. The results show that as the transmission distance increases, the transmission performance is degraded up to 15 km at first. Then, there is a range of transmission distance where the receiver sensitivities are improved. This performance improvement can be explained as follows: when the VCSEL is biased at far above its threshold current and generates an OOK signal with a low ER, the adiabatic chirp dominates over the transient chirp at the output. In this case, the marks (i.e., '1's) and spaces (i.e. '0's) emit different optical frequencies, f_1 and f_0, respectively, depending upon the modulation current of each intensity level. Then, we can decompose this low-ER OOK signal into two

high-ER OOK signals, one with the carrier frequency of f_1 and the other with f_0. Fig. 3.24 illustrates the OOK signal with a low ER, which consists of the two frequencies. Fig. 3.25 shows that this signal can be decomposed into two signals. One is carried at f_1 and has the same data pattern as the original signal. On the other hand, the other signal carried at f_0 is complementary to the original signal. It should be noted that the signal with the carrier frequency f_1 has this carrier frequency only when it represents the marks. The carrier frequency is shifted to f_0 when the signal makes a transition to the spaces (even if the optical power is zero). Thus, the signal with the carrier frequency of f_1 experiences a phase shift every time it represents a space (i.e., a '0'). The amount of phase shift can be expressed as [97]:

$$\Delta\phi = \int_0^T 2\pi[f_1 - f_0]dt \tag{3.18}$$

where T is the bit duration. The signal with the carrier frequency f_0 also experiences the same amount of phase shift with the sign inverted every time it represents a space. Therefore, when the frequency separation between the marks and spaces is the half the data rate (i.e., $f_1 - f_0 = 1/2T$), this phase shift becomes π, and consequently the two signals carried at f_1 and f_0 have duobinary-like phase characteristics, as illustrated in Fig. 3.25. It is well known that the duobinary modulation format is robust against fiber's CD due to its phase reversal at every space [101]. This implies that the two signals carried at f_1 and f_0 also have high CD tolerance. The performance improvement in the presence of some amount of CD is a typical behavior of optical duobinary signals [102]. Since the fiber's CD is a linear phenomenon, the waveform of the original signal after transmission would be identical to the recombined waveform of these two signals after each being transmitted separately. Due to CD, however, a temporal walk-off between the two signals occurs

when they recombine after transmission. This temporal walk-off would give rise to bulges in the waveform of the recombined signal especially at the marks because the blue-shifted f_1 components travel faster than the red-shifted f_0 components in the anomalous dispersion region. This effect is introduced in a couple of references as the 'self-steepening effect' [103], [88]. Fig. 3.26 (a), (b), and (c) show the eye diagrams of the OOK signal after 0-, 15-, and 30-km transmissions, respectively. Pulse distortions caused by the self-steepening effect are observed after transmission. The VCSEL used in our experiment exhibits the frequency modulation coefficient of 0.96 GHz/mA. Since we need a peak-to-peak modulation current of 6 mA to generate the OOK signal with ER of 3, the π-phase shift occurs when the ER of the signal becomes $\sim$2.9. Fig. 3.23 shows that we can achieve the longest transmission distance when the ER of the signal is $\sim$3. This is consistent with the aforementioned explanation: the amounts of phase shift expressed in Eq. (3.18) become 0.90π and 1.08π when the ERs of the signal are 2.5 and 3, respectively. The power budgets after 50-km transmission are measured to be 13.0 and 14.2 dB for ERs of 2.5 and 3, respectively.

Next, we implement an off-line linear equalizer to compensate for fiber dispersion and improve the power budget of VCSEL-based transmission link. Fig. 3.27 shows the measured BER curves, when a 15-tap FFE is applied. In Fig. 3.27(a), we can observe that high-ER signals achieve better receiver sensitivities than low-ER signal at back-to-back condition. In addition, compared with Fig. 3.22, it is observed that the receiver sensitivities are improved by around 1 dB for different ER signals. However, after 70-km transmission, only ER-2.5 signal can achieve receiver sensitivity of -19.26 dBm [see Fig. 3.27(b)]. In addition, the receiver sensitivity is slightly improved compared to back-to-back condition [see Fig. 3.27(a)], which thanks to the OOK

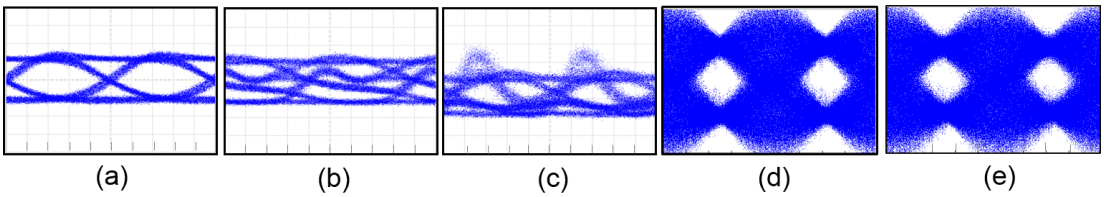

Figure 3.26: Eye diagrams of the 10.7-Gb/s OOK signal (a) at the back-to-back condition, (b) after 15-km transmission, and (c) after 30-km transmission, without electrical equalization; (d) after 70-km transmission when 15-tap transversal filter is applied; (e) after 80-km transmission when 15-tap FFE and 5-tap DFE is applied at the receiver side. The ER of the signal is 2.5.

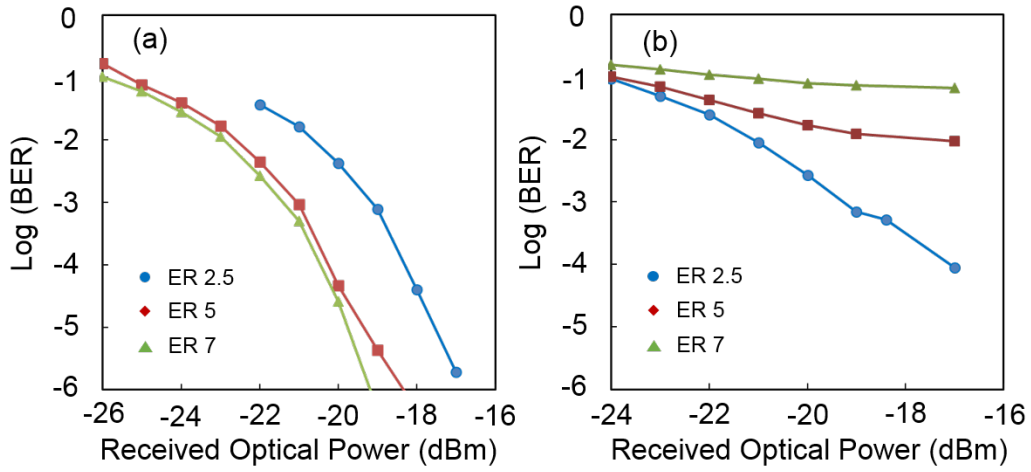

Figure 3.27: Measured BER curves of 10.7-Gb/s OOK signals after (a) 0- and (b) 70-km transmissions over SSMF, respectively, when 15-tap transversal filter is applied at the receiver.

signal's duobinary characteristics. Fig. 3.28 shows the power budget as a function of the transmission distance in the presence of post-detection linear equalization. We also utilize a 15-tap linear transversal filter in this figure. A longer-tap equalizer leads

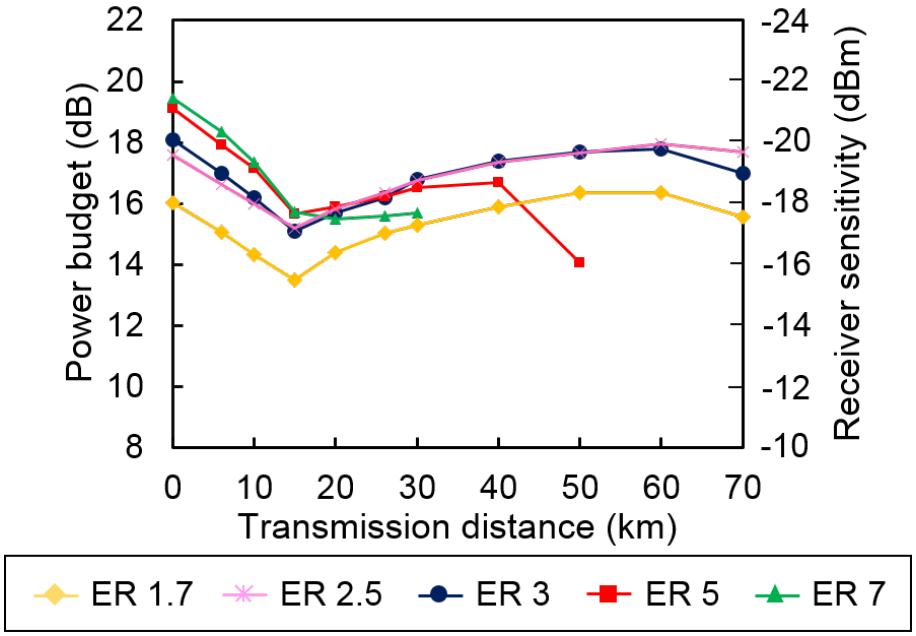

Figure 3.28: Measured power budget and receiver sensitivity of the 10.7-Gb/s OOK VCSEL link as a function of transmission distance over SSMF when 15-tap transversal filter is applied at the receiver.

to marginal improvement in our experiment. The use of the linear equalizer not only improves the dispersion-uncompensated transmission distance but it also increases the power budget at the B2B operation. For example, we observe around 1-dB improvement at 0 km for most of different-ER signals. We ascribe this to non-ideal frequency response of the VCSEL which is well-equalized by the transversal filter. Fig. 3.28 also shows that, compared to Fig. 3.23 (i.e, without using electrical equalization), the self-steeping effects happened at around 15 km are also alleviated by applying the electrical equalization, and the maximum transmission distance is successfully extended. Thus, we achieve 70-km transmission over SSMF using ER-1.7, -2.5 and -3 signals. The eye diagram in Fig. 3.26(d) also shows that we have clear eye opening

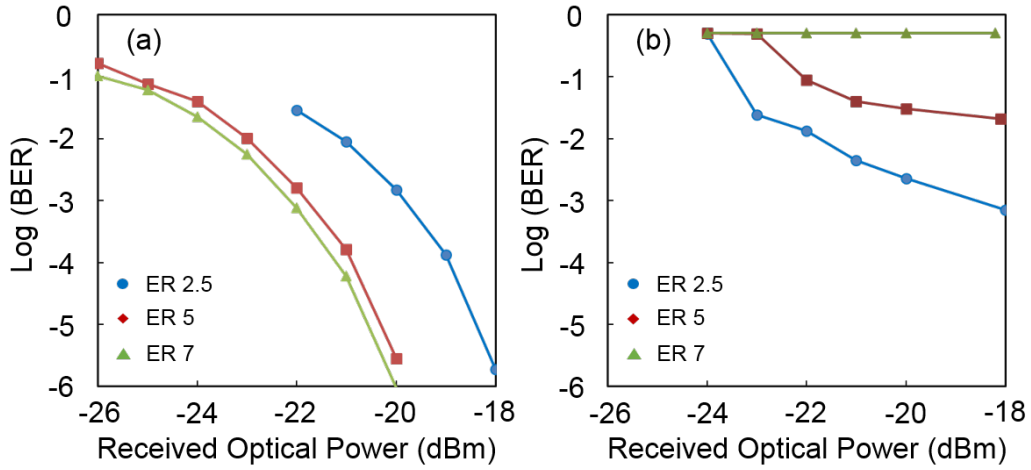

Figure 3.29: Measured BER curves of 10.7-Gb/s OOK signals after (a) 0- and (b) 80-km transmissions over SSMF, respectively, when 15-tap FFE and 5-tap DFE is applied at the receiver.

after 70-km transmission with help of equalization.

The power budget of transmission link can be further improved by utilization 15-tap FFE followed by 5-tap DFE and the corresponding results are shown in Fig. 3.29 and 3.30. In Fig. 3.29(a), we can observed that the receiver sensitivity is further improved to -22.2 dBm for ER-7 signal, which is -21.7 dBm and -19.9 dBm for ER-5 and ER-2.5 signals at the back-to-back condition, respectively. ER-2.5 signal successfully achieves 80-km transmission in presence of 15-tap FFE and 5-tap DFE. From Fig. 3.30, it is observed that we have 1.4∼1.8 dB improvement in the receiver sensitivities at the back-to-back condition, compared with Fig. 3.23. The maximum transmission distance is also greatly improved. We are able to successfully transmit the signal over 80-km long SSMF without optical dispersion compensation when the ERs of the signal are 1.7 and 2.5. Fig. 3.26(e) shows the eye diagram of the OOK signal with the ER of 2.5 after 80-km transmission in the presence of the equalizer. A

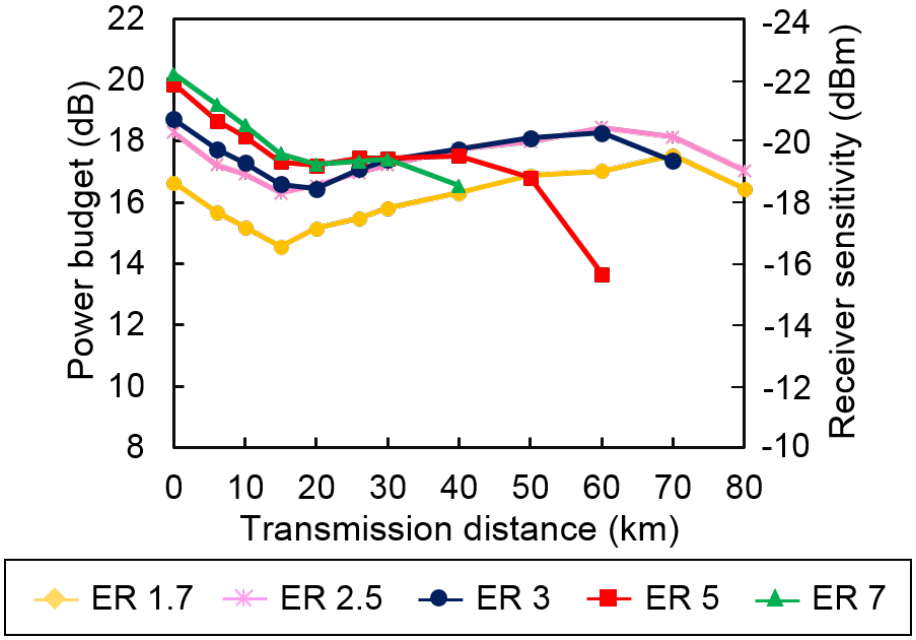

Figure 3.30: Measured power budget and receiver sensitivity of the 10.7-Gb/s OOK VCSEL link as a function of transmission distance over SSMF when 15-tap FFE and 5-tap DFE is applied at the receiver.

wide eye opening is observed at the output of the equalizer. The transmission longer than 80 km is not achievable due to the limited output power of the VCSEL.

3.3.4.2 Transmission Performance of 10.7-Gb/s 4-PAM Signal

Next, we investigate the transmission performance of the 10.7-Gb/s 4-PAM signal generated by using the VCSEL. Fig. 3.31 shows the measured BER curves without electrical equalization. We compared the BER performance among three values: 3, 5 and 7. For the 4-PAM signal, the ER is defined as the ratio between the highest and lowest intensity levels. In the back-to-back condition, ER-7 signal shows best receiver sensitivity of -16.4 dBm, however, the error floor at around 10^{-3} is observed for ER-7

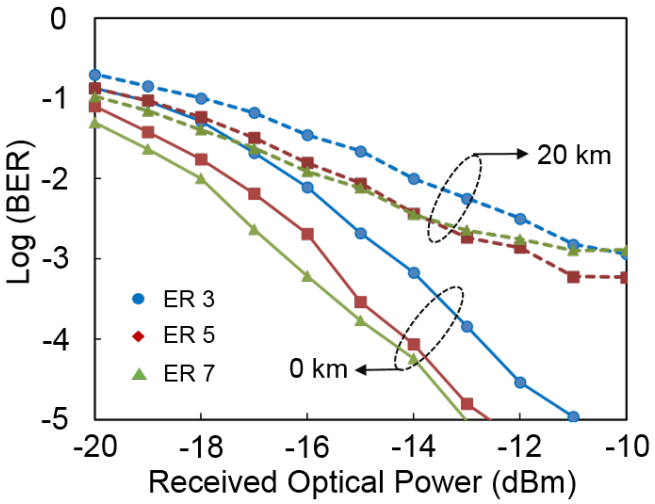

Figure 3.31: Measured BER curves of 10.7-Gb/s 4-PAM signals after 0- and 20-km transmissions over SSMF, respectively, when no electrical equalization is applied at the receiver.

signal after 20-km transmission. As for ER-5 and ER-3 signals, they are successfully achieve 20-km transmission without electrical equalization. Fig. 3.32 shows the measured power budget as a function of the transmission distance over SSMF in the absence of electrical equalizer. The figure shows that we can achieve a power budget of 14.4 dB for the 4-PAM signal with ER of 7 at the back-to-back condition, but it is reduced to 13.9 and 12.4 dB for the ER values of 5 and 3, respectively. This result agrees well with the theoretical analysis mentioned in Section 3.3.3, for example, the power budget difference between ERs of 7 and 5 is calculated to be 0.5 dB, which is the same as our measurement value. Fig. 3.32 shows that the transmission performance is degraded monotonically as the transmission distance is increased. It is interesting to note that the performance improvement observed from the 10.7-Gb/s OOK signal (when the SSMF distance ranges from 15 to 30 km) is not found for the 4-PAM signal.

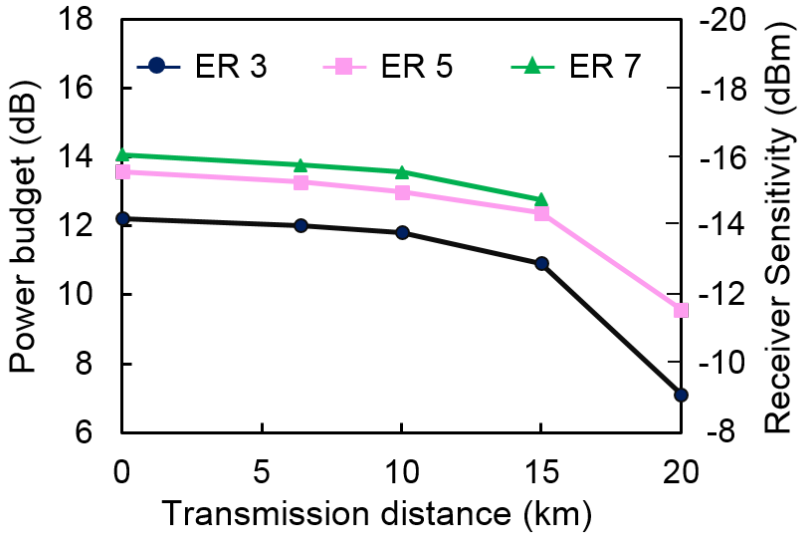

Figure 3.32: Measured power budget and receiver sensitivity of the 10.7-Gb/s 4-PAM VCSEL link as a function of transmission distance over SSMF when no electrical equalization is applied at the receiver.

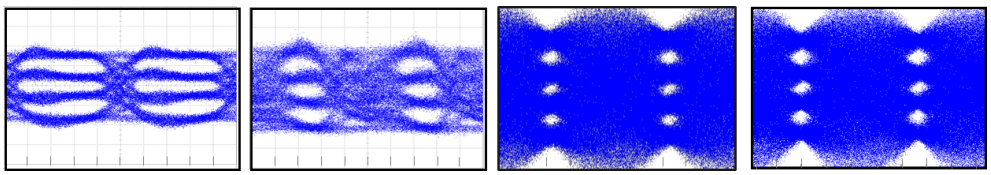

Figure 3.33: The Eye diagrams of the 10.7-Gb/s 4-PAM signal (a) at the back-to-back condition and (b) after 20-km transmission without EDC; (c) after 30-km transmission when 15-tap transversal filter is applied; (d) after 40-km transmission when 15-tap FFE and 5-tap DFE is applied. The ER of the signal is 3.

This should be attributed to the fact that the duobinary-like phase characteristics are not applicable to the quaternary signal. Fig. 3.32 also shows that we cannot achieve 20-km transmission over SSMF when the ER of the signal is 7. Since the spectral

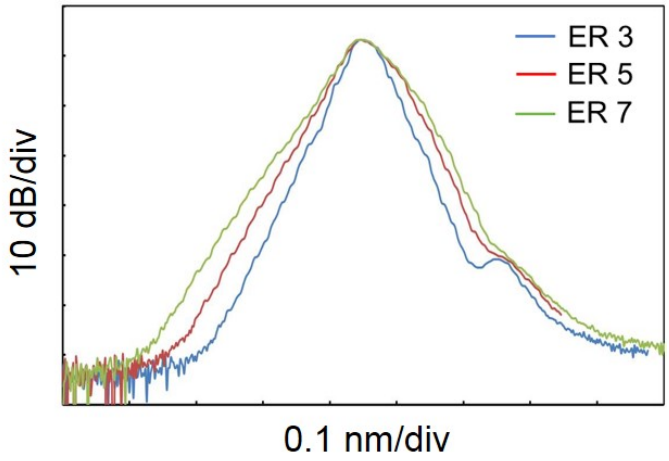

Figure 3.34: Optical spectrum of 4-PAM signals.

width of the VCSEL output increases with the ER of the signal, the 4-PAM signal with high ERs suffers more from the CD than low-ER 4-PAM signals. Fig. 3.33(a) and (b) show the eye diagrams of the 4-PAM signal after 0- and 20-km transmissions, respectively. It is observed from the eye diagram in Fig. 3.33(b) that the signal suffers from level-dependent skew after 20-km transmission. This is because of the interplay between the current-induced frequency chirp and CD. Since the carrier frequency increases with the intensity level at the output of the directly modulated VCSEL, the upper intensity levels travel faster than the lower ones in the anomalous dispersion region. The optical bandwidth measured by using an optical spectrum analyzer also confirms this explanation [see Fig. 3.34]. The 20-dB spectral width of the signal with ER of 7 is measured to be 29 GHz. However, the spectral widths are reduced to 25 and 19 GHz when the ERs of the signal are 5 and 3, respectively. Fig. 3.32 shows that the largest power budget of 9.8 dB is achieved after 20-km transmission using the 10.7-Gb/s 4-PAM signal with the ER of 5.

Fig. 3.35 and Fig. 3.36 show the transmission performance of the 4-PAM

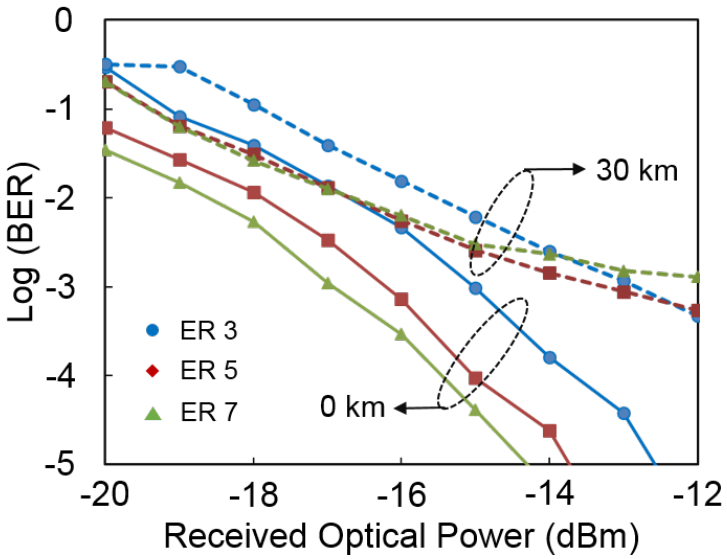

Figure 3.35: Measured BER curves of 10.7-Gb/s 4-PAM signals after 0- and 30-km transmissions over SSMF, respectively, when 15-tap transversal filter is applied at the receiver.

signal when we employ an LMS-based 15-tap transversal filter. Similarly to 10.7-Gb/s OOK signals shown in Section 3.3.4.1, the use of electrical equalization improves the dispersion tolerance of transmission link successfully. For example, we observe 1-dB receiver sensitivity improvement at 0 km for the ER-3 signal. In addition, the power budget degrades gradually as fiber length increases and the maximum transmission distance is extended by $>50\%$. Thus, we achieve 30-km transmission over SSMF for both ER-3 and ER-5 signals. The eye diagram in Fig. 3.33(c) also shows that we have clear eye opening after 30-km transmission with the help of equalization.

Fig. 3.37 and Fig. 3.38 show the transmission performance of the 10.7-Gb/s 4-PAM signal when we employ an LMS-based 15-tap FFE and 7-tap DFE. Compared with Fig. 3.31, the receiver sensitivities of different signals are improved more than

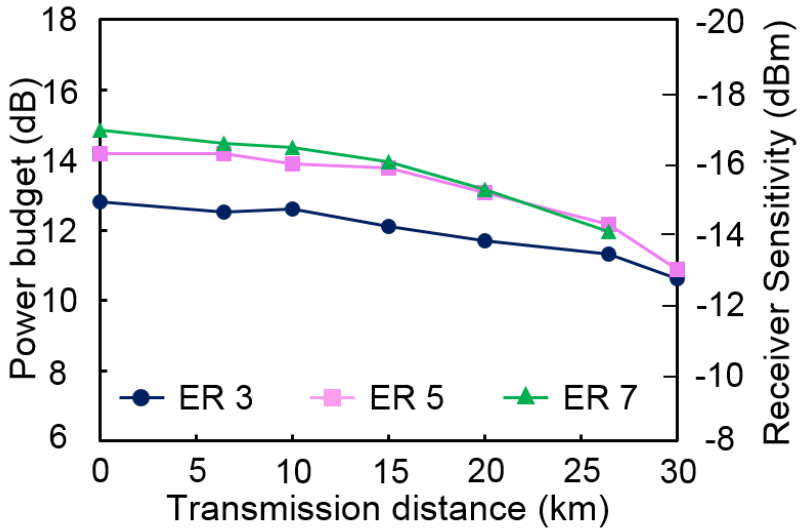

Figure 3.36: Measured power budget and receiver sensitivity of the 10.7-Gb/s 4-PAM VCSEL link as a function of transmission distance over SSMF when 15-tap transversal filter is applied at the receiver.

2 dB at back-to-back condition. Moreover, the maximum achievable transmission distance is doubled when the ER of the signal is 3, and thus reaches 40 km [see Fig. 3.38]. Fig. 3.33(d) shows the eye diagram of the signal after 40-km transmission. The power budget is measured to be 9.5 dB at 40-km transmission distance.

3.3.4.3 Performance Comparison Between 10.7-Gb/s OOK and 4-PAM Signals

Comparing the transmission performance between the 10.7-Gb/s OOK and 4-PAM signals plotted in Fig. 3.23, 3.28, 3.30 and Fig. 3.32, 3.36, 3.38, we find that the OOK signal vastly outperforms the 4-PAM signal when the ER of each signal is optimized. For example, in the back-to-back condition without using the electrical equalization, the optical modulation amplitude (OMA) of the OOK signal having an ER of 3 is measured to be -18.9 dBm, whereas the OMA of the 4-PAM signal, defined as the

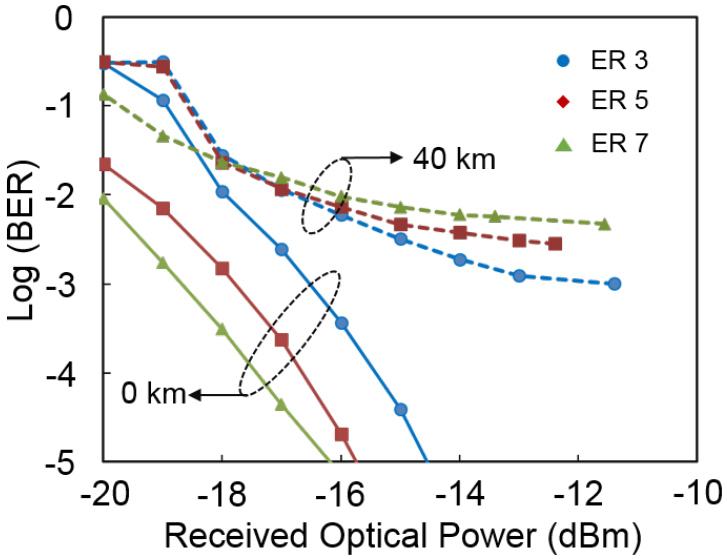

Figure 3.37: Measured BER curves of 10.7-Gb/s 4-PAM signals after 0- and 40-km transmissions over SSMF, respectively, when 15-tap FFE and 7-tap DFE is applied at the receiver.

power difference between the highest and lowest levels, is -14.2 dBm, when the ER of the 4-PAM signal is 5. The superior performance of the OOK signal to that of 4-PAM signal is also retained in the presence of electrical equalization. We achieve 80-km transmission by using the OOK signal but the maximum achievable distance is reduced to 40 km for the 4-PAM signal when the electrical equalizers with the similar number of taps are utilized. This is because even though the 4-PAM signal has a twice longer symbol duration than the OOK signal, the 4-PAM signal is not able to take the advantage of the duobinary-like phase characteristics. Therefore, unlike the signals generated by using chirp-free external modulators [104], the use of 4-PAM modulation format (instead of the OOK format) does not help to improve the CD tolerance for 1.5-μm VCSEL signals. It is worth noting that since the phase characteristics of the

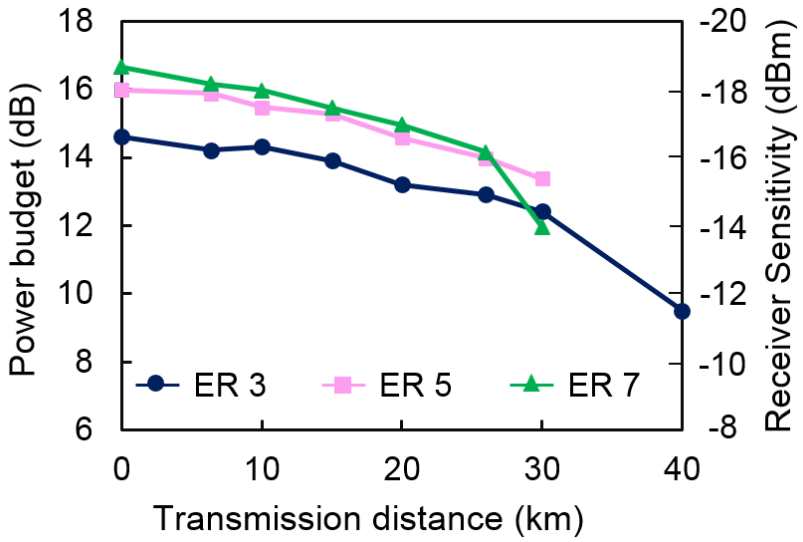

Figure 3.38: Measured power budget and receiver sensitivity of the 10.7-Gb/s 4-PAM VCSEL link as a function of transmission distance over SSMF when 15-tap FFE and 7-tap DFE is applied at the receiver.

signals are irrelevant to the line rate, these conclusions would be applicable to other line rates.

Finally, the maximum transmission distances achieved by using the 10.7-Gb/s OOK and 4-PAM signals when the ER of each signal is optimized are summarised in Table 3.2. When the electrical equalizer is used at the receiver, the ER of the signal should be slightly reduced to maximize the transmission distance.

3.4 Summary

In this chapter, we have explored both optical and electrical dispersion compensation methods to enhance the transmission performance of 1.5-μm, 10-Gb/s VCSEL link. In the first part, we have utilized DI at the transmitter side for FSK-to-ASK signal

Table 3.2: Maximum transmission distance of the OOK and 4-PAM signals when the ER of each signals is optimized

Line rate (Gb/s)	Modulation format	Without equalization		With 15-tap transversal filter		With 15-tap FFE and 5-tap DFE	
		ER	Maximum reach (km)	ER	Maximum reach (km)	ER	Maximum reach (km)
10.7	OOK	3	50	2.5	70	2.5	80
10.7	4-PAM	5	20	5	30	3	40

conversion and compared the transmission performance of various line codes. We take the bandwidth expansion induced by the overhead of each line code into consideration for fair comparison. Among the line codes we tested, 9B/10B and scramble-and-select line codings exhibit similar and outstanding performance. This is because 9B/10B and scramble-and-select line codings can greatly deplete the low-frequency spectral contents of the signals, yet they expand the bandwidth a bit. Then, we also optimize the FSR of the DI for our VCSEL-based link. The results show that the best BER performance is obtained with an FSR of 16.1 GHz. With a PIN receiver, 50-km transmission over SSMF with less than 0.5-dB power penalty is successfully achieved with 9B/10B line coding and 16.1-GHz DI. The power budget of the transmission link is further improved by 5 dB when the PIN receiver is replaced by an APD receiver. Moreover, by taking the loss of the DI away, we have still improved the power budget of the VCSEL link by 6 dB after 10-km transmission, compared with the conventional OOK signals without DI.

In the second part, we have investigated and compared the transmission performance of 10.7-Gb/s OOK and 4-PAM signals in 1.5-μm VCSEL-based optical access link without DI. Thanks to the optimized ER and the use of post-detection

electrical equalization, we have achieved 80- and 40-km transmissions over SSMF using the OOK and 4-PAM modulation formats, respectively. Larger than 9-dB power budgets are achieved by both signals after the transmission. Our experimental comparison between the OOK and 4-PAM signals shows that the OOK format is better suited for 1.5-μm VCSEL based optical access networks since not only the OOK transceivers are much simpler to be implemented than 4-PAM counterparts but also does it outperform the 4-PAM format in term of CD tolerance, which thanks to its duobinary-like phase characteristics.

In conclusion, the use of optical dispersion compensation (e.g., the application of DI for FSK to ASK conversion) and electrical dispersion compensation (e.g., the utilization of FFE and DFE at receiver side) both effectively improve the dispersion tolerance of 1.5-μm VCSEL-based optical access link effectively. We believe that directly modulated 1.5-μm VCSELs could be used to implement point-to-point and low-splitting ratio (e.g., $<$10) time-division-multiplexed 10-Gb/s passive optical networks in a cost-effective manner, with the help of effective dispersion compensation.

Chapter 4

25-Gb/s Signals Transmission Using 1.5-μm 10G-Class VCSEL for Optical Access Network

4.1 Introduction

In order to meet the insatiable demands for transmission capacity in optical access networks, it is envisaged that the current optical access networks based on 10-Gb/s transmission are upgraded to 25 Gb/s or higher data rate in the near future [105, 106]. However, it is still challenging to implement 25-Gb/s transmission links in a cost-effective manner because they typically require expensive high-speed optical transceivers and are also susceptible to fiber chromatic dispersion. Thus, the conventional way of implementing the 25-Gb/s transmission systems operating in the 1.55-μm window is to utilize external modulators and/or DCMs. However, these devices and modules might be still too expensive to be used for the cost-effective implementation of optical access networks. In addition, they inevitably incur an insertion loss (e.g., 2∼3 dB for DCMs and ∼4 dB for MZMs), which in turn, serve to reduce the power budget of the links in comparison with dispersion-uncompensated

transmission links utilizing directly modulated lasers. Thus, in order to bring down the cost per bit of 25-Gb/s systems lower than that of 10-Gb/s systems, it is necessary to utilize highly cost-effective optical transmitters such as VCSELs, but not to employ DCMs.

In this chapter, we explore the possibility of utilizing a highly cost-effective 1.5-μm VCSEL for optical access networks based on 25-Gb/s transmission. In particular, in order to further enhance their cost-effectiveness, we utilize a TO-can packaged VCSEL developed for low-cost 10 Gb/s applications. We aim to maximize the transmission distance of 25-Gb/s 4-PAM and OOK signals over SSMF without using bulky and lossy DCMs. We also try to compare the transmission performance between OOK and 4-PAM signals. In addition, we investigate the transmission performances of OOK signals obtained from two different transmitter schemes: with and without a DI at the output of the directly modulated VCSEL. When the DI is used, the FSK signal from the VCSEL is converted into the OOK signal having an improved ER [13]. The electrical equalization technique is employed at the receiver to compensate for the dispersion-induced signal distortions and band-limitation of the VCSEL.

This chapter is organized as follows: Section 4.2 gives a brief introduction on the experimental setups for both 25-Gb/s 4-PAM and OOK signals' transmission. Then, the experimental results are illustrated and discussed in Section 4.3. We first discuss the transmission performance of 25-Gb/s 4-PAM signal without DI in Section 4.3.1, followed by the experimental results of 25-Gb/s OOK signals without and with the utilization of DI in Section 4.3.2 and Section 4.3.3, respectively. Finally, this chapter is summarized in Section 4.4.

4.2 Experimental Setup

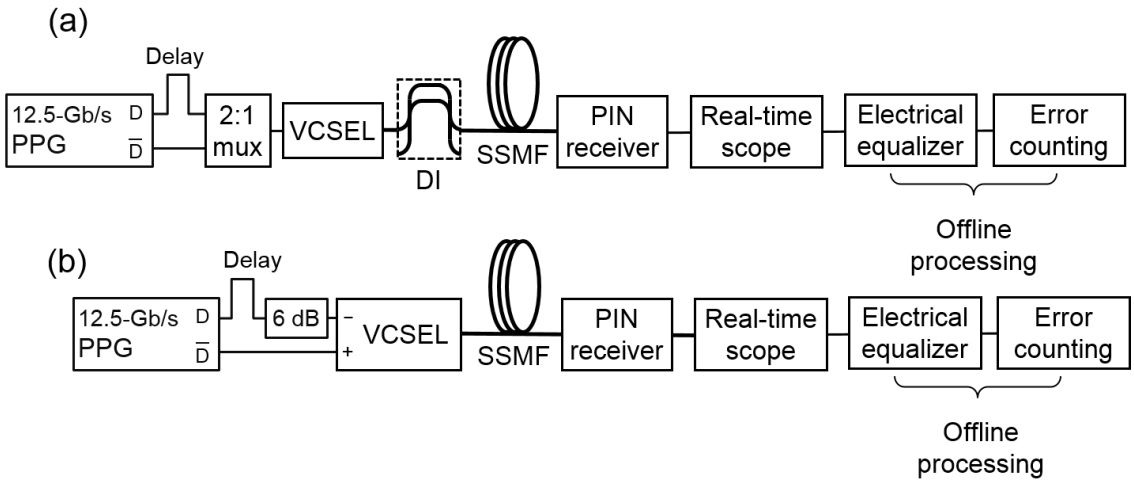

Figure 4.1: Experimental setups for transmissions of 25-Gb/s (a) OOK and (b) 4-PAM signals, respectively.

Fig. 4.1(a) shows the experimental setup for the transmission of the 25-Gb/s OOK signal. A PPG first generates 12.5-Gb/s NRZ electrical signals. The two complementary PRBS signals (length=2^{15}-1), one of which is 63-bit delayed with respect to the other for decorrelation, are then time-division-multiplexed to be fed directly to a 1.54-μm VCSEL. No electrical amplifier is used for driving the VCSEL. The output voltage of the multiplexer (MUX) is adjusted by using an electrical attenuator to vary the ER of the optical signals. The VCSEL used in the experiment is a TO-can packaged device, as shown in the inset of Fig. 4.2. This device emits an optical power of -0.8 dBm when biased at 14 mA. Fig. 4.2 shows the measured E/O response of this device. The 3-dB modulation bandwidth is measured to be around 7 GHz. Thus, this laser diode is rated for 10-Gb/s applications. The output of the

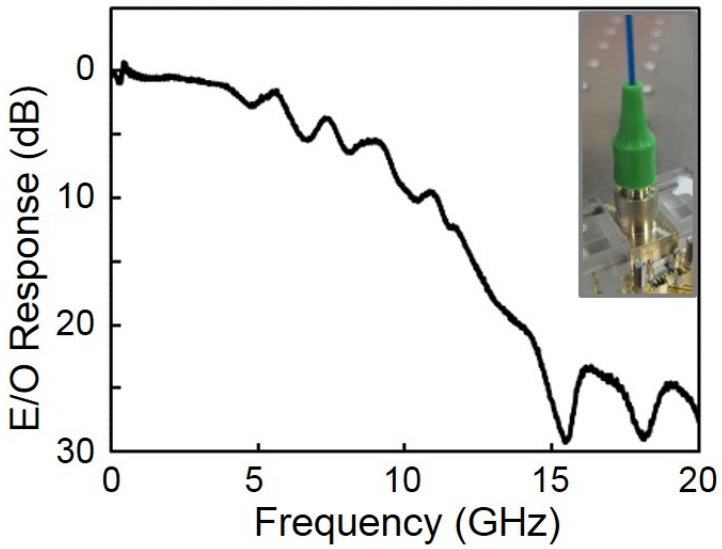

Figure 4.2: Measured E/O response of the VCSEL used in the experiment. The inset shows the photograph of the VCSEL.

VCSEL signal is fed to a DI before transmission over SSMF. The phase of the DI is adjusted such that the wavelength of the VCSEL is aligned to one of quadrature points of the DI's transmittance curve. Then the spaces (i.e., '0's) experience a larger loss by the DI than the marks (i.e., '1's) since the spaces' wavelength is longer than the marks' wavelength due to the adiabatic chirp of the VCSEL. As a result, the ER of the signal is enhanced after the DI. However, it has been shown that VCSELs exhibit non-uniform FM response at low frequencies due to the thermal effect, which in turn, causes severe signal degradations when the FSK-to-OOK conversion is undertaken (for example by using the DI) [13]. This problem can be alleviated by utilizing a DC-balanced line coding which depletes the low-frequency contents of the signal [69]. In our experimental demonstration, a line coding is not employed due to the low-frequency depletion of the signal when the driving signal was generated by multiplexing two complementary signals. However, in a real system, a line coding such as 9B/10B

and scramble-and-select coding should be applied to the signal to combat the signal degradations associated with the non-uniform FM response of the VCSEL [32, 107]. After transmission, the signals are detected at a PIN receiver (bandwidth: 40 GHz) and then sampled by using a digital sampling scope (sampling rate: 100 Gsample/s) for offline processing. In order to compensate for the signal distortions caused by the fiber dispersion and limited bandwidth of VCSEL, we employ a half-symbol-spaced 17-tap FFE followed by a 7-tap DFE.

Fig. 4.1(b) shows the experimental setup for 25-Gb/s 4-PAM transmission. One of the electrical paths from the PPG is delayed by 62 bits (for decorrelation) and attenuated by 6 dB with respect to the other using a microwave delay line and electrical attenuator, respectively. Two 12.5-Gb/s PRBSs are then directly sent to two electrical inputs of the VCSEL. Note that no electrical amplifier and power combiner is used for the generation of the 4-PAM signal. After the detection of the signal by using a PIN detector (bandwidth: 10 GHz), we sample the detected signal at 50 Gsample/s and carry out off-line signal processing. For electrical dispersion compensation, we apply a 15-tap FFE and 7-tap DFE to the signal. Such an electrical equalizer with low power consumption could be implemented cost-effectively by using the CMOS technology [108, 109]. We directly count the number of bit errors, assuming that bits are pair-wise mapped onto symbols according to the natural coding instead of the Gray coding due to the inherent characteristics of generating the 4-PAM signal using the aforementioned method [35].

It should be noted that the output power of the VCSEL is fixed to be -0.8 dBm throughout the experiment regardless of the presence of DI. No optical amplifier is, nevertheless, employed. Therefore, we explore the possibility of utilizing 1.5-μm

VCSELs for optical access network under the constraint of their inherently low output power.

4.3 Experimental Results

4.3.1 Transmission Performance of 25-Gb/s 4-PAM Signal without DI

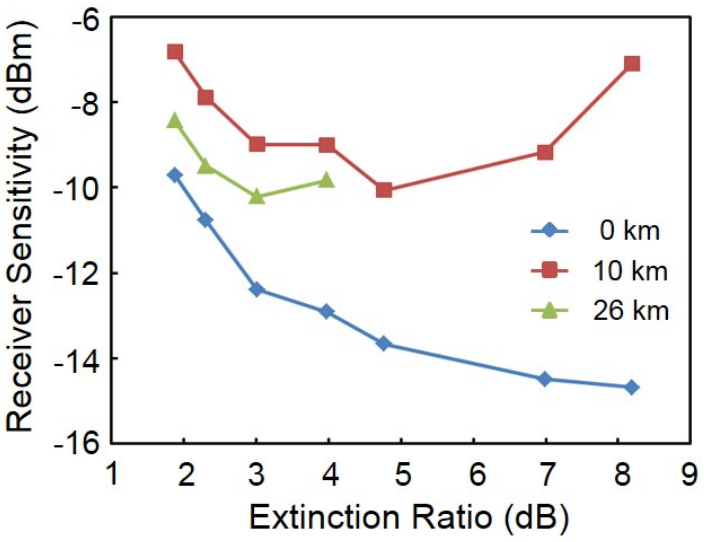

Figure 4.3: Measured receiver sensitivity as a function of the extinction ratio for 25-Gb/s 4-PAM signals at different transmission distances.

We first investigate the transmission performance of 25-Gb/s 4-PAM signals. No DI is applied during the transmission link. Fig. 4.3 shows the measured receiver sensitivities (at BER=10^{-3}) of the 25-Gb/s 4-PAM signals as a function of ERs for various transmission distances. Here, the ER of the 4-PAM signal is defined as the ratio between the highest and lowest intensity levels. As we increase the ER of the OOK

signal, the receiver sensitivity is improved in the back-to-back condition. However, due to large frequency chirp of high-ER signals, the optimum ER which gives us the best receiver sensitivity shifts towards a lower value as the transmission distance increases. For example, when the transmission distance is 10 km, the optimum ER is 4.8 dB for 4-PAM signal, however, the value decreases to 3 dB as the transmission distance increases to 26 km. Based on the results found in Fig. 4.3, we set the ER of the 4-PAM signal to be 3.0 dB. Fig. 4.4 shows the measured BER curves for the 4-PAM signals after 0-km and maximum transmissions (i.e., 35-km). The receiver sensitivity (at BER=10^{-3}) in the back-to-back condition is measured to be -12.4 dBm. After 35-km transmission over SSMF, we observe a transmission penalty of 2.3 dB. In addition, we are not able to reach the BER lower than 10^{-3} after 35-km transmission for 4-PAM signals, since the error floor is observed for longer transmission distance (>35 km). Fig. 4.5(c) shows the eye diagram of the signal measured at the receiver after 35-km transmission and with electrical equalization. It shows that the eye diagram is degraded after 35-km transmission, when compared with the eye diagram in back-to-back condition [see Fig. 4.5(b)].

4.3.2 Transmission Performance of 25-Gb/s OOK Signal without DI

Next, we investigate the transmission performance of the 25-Gb/s OOK signal generated by using the 10G-class VCSEL without using the DI. Fig. 4.6 shows the measured receiver sensitivities (at BER=10^{-3}) of the signal as a function of ER for various transmission distances. The ER is defined as the intensity ratio between long marks and long spaces at the output of the VCSEL and thus the effects of

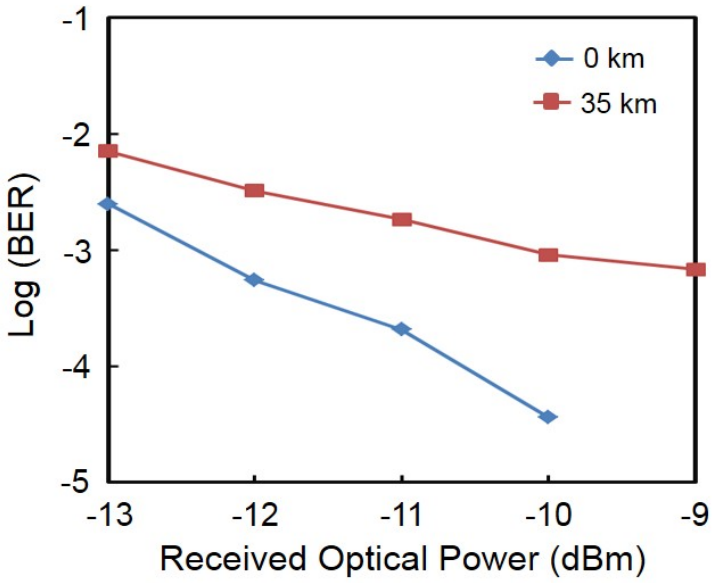

Figure 4.4: Measured BER as a function of the received signal power at 0 km and after maximum transmission (i.e., 35 km) for 25-Gb/s 4-PAM signal.

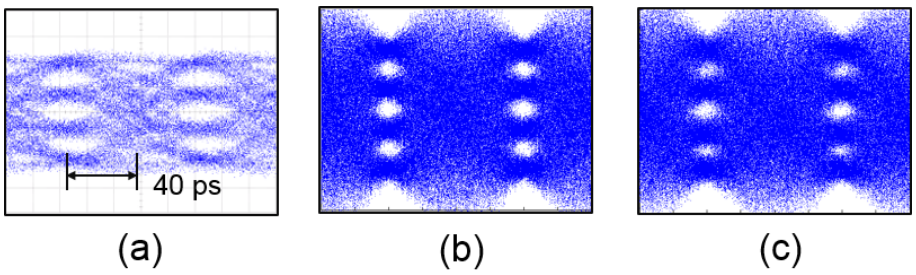

Figure 4.5: (a) Optical eye diagram of the 25-Gb/s 4-PAM signals at the output of VCSEL. Eye diagrams of the 25-Gb/s 4-PAM signals measured at the receiver when the electrical equalization is applied (b) after 0- and (c) 35-km transmissions. The ER of the signal is 3.0 dB and the received signal power is -10 dBm.

band-limitation are excluded. A similar tendency of the receiver sensitivities with respect to the ER is observed to the OOK signal: the receiver sensitivity is firstly improved with the increasing ER in the back-to-back condition. However, the optimal

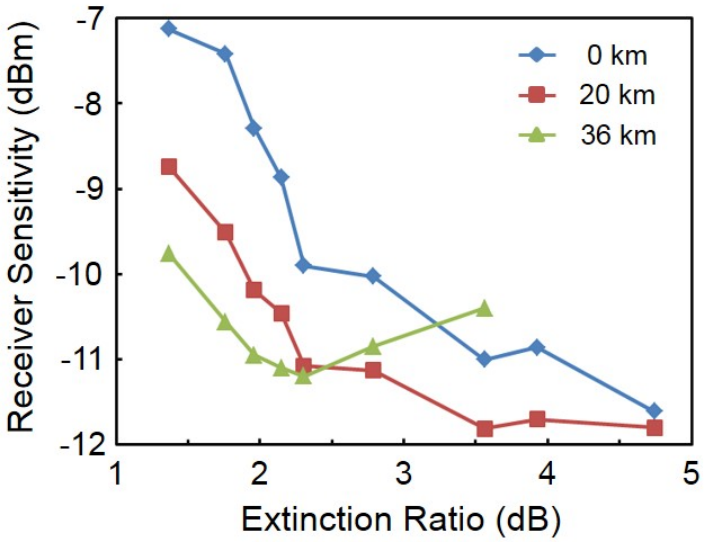

Figure 4.6: Measured receiver sensitivity as a function of the extinction ratio for 25-Gb/s OOK signals at different transmission distances without using DI.

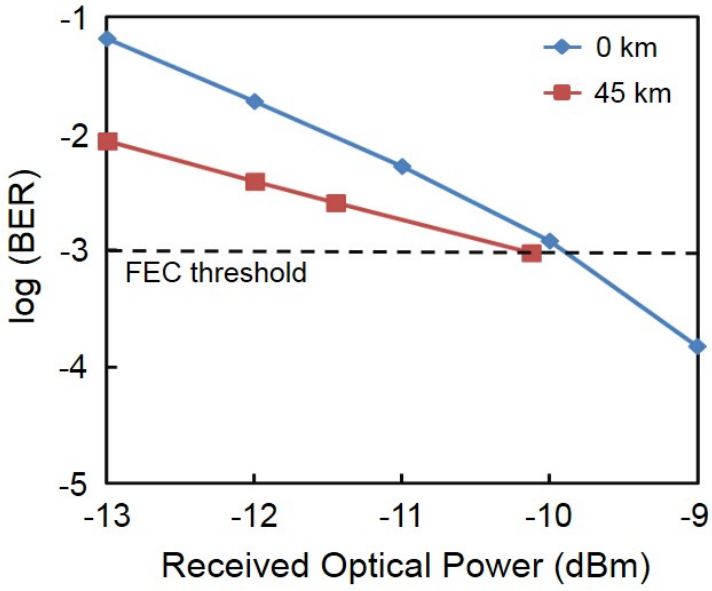

Figure 4.7: Measured BER as a function of the received signal power at 0 km and after maximum transmission (i.e., 45 km) for 25-Gb/s OOK signal without using DI.

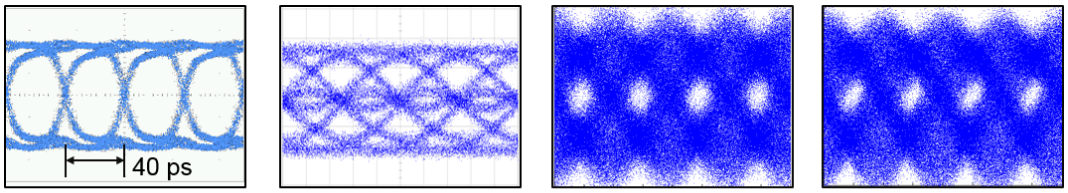

Figure 4.8: (a) Eye diagram of the 25-Gb/s NRZ electrical signal driving the VCSEL. (b) Eye diagram of the 25-Gb/s OOK signal measured at the output of the VCSEL. Eye diagrams of the OOK signals measured at the receiver when the electrical equalization is applied (c) after 0- and (d) 45-km transmissions. The ER of the signal is 2.3 dB and the received signal power is -10 dBm.

ER is found to be 3.6 dB after 20-km transmission but it is decreased to 2.3 dB after 36-km transmission.

Based on the results obtained from Fig. 4.6, we set the ER of the OOK signal to be 2.3 dB. Fig. 4.7 shows the BER curves of the OOK signal after 0- and 45-km transmissions. The receiver sensitivity in the back-to-back condition is measured to be -9.9 dBm. Due to the limited bandwidth of the VCSEL, the eye diagram at the output of the VCSEL is severely closed as shown in Fig. 4.8(b), even though the eye diagram of the NRZ electrical signal driving the VCSEL is widely open [shown in Fig. 4.8(a)]. However, when the electrical equalizer is employed at the receiver, the eye diagram is open, as displayed in Fig. 4.8(c). After 45-km transmission over SSMF, we can barely achieve a BER lower than the FEC threshold of 10^{-3} due to the low output power of the VCSEL. Nevertheless, the receiver sensitivity after 45-km transmission is slightly improved compared to that in the back-to-back condition and is measured to be -10.1 dBm. We were not able to measure the BER performance beyond -10 dBm after 45-km

transmission due to the low output power of the VCSEL (i.e., -0.8 dBm). Fig. 4.8(d) shows the eye diagram of the signal measured at the receiver after 45-km transmission with electrical equalization. It shows that the eye diagram is not noticeably degraded after the transmission. It can be ascribed to the π-phase difference of the marks when a single space is sandwiched between them [110]. This makes the phase characteristics of the 25-Gb/s OOK signal similar to those of duobinary signal, which is known to be resilient to fiber chromatic dispersion.

4.3.3 Transmission Performance of 25-Gb/s OOK Signal with DI

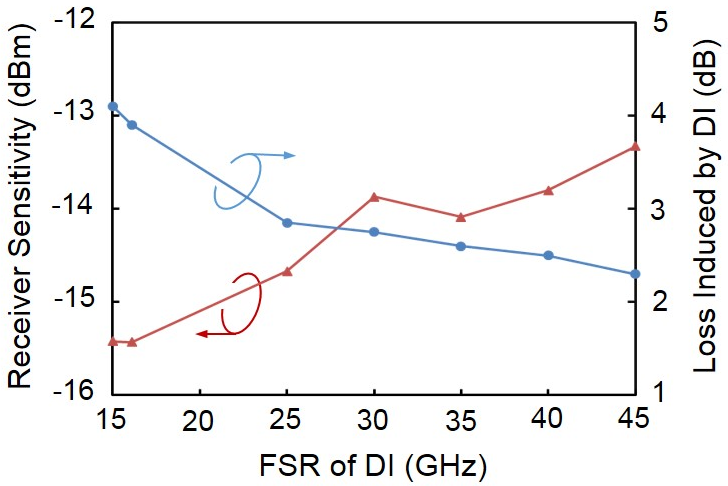

Figure 4.9: Receiver sensitivity of 25-Gb/s OOK signal measured after 20-km transmission as a function of the FSR of DI. Also shown in this plot is the insertion loss incurred by the DI.

Next, we insert the DI at the output of the VCSEL and investigate the transmission performance of the 25-Gb/s OOK signal. In this case, it is important to optimize the FSR of DI to maximize the transmission distance. It should be noted that the ER

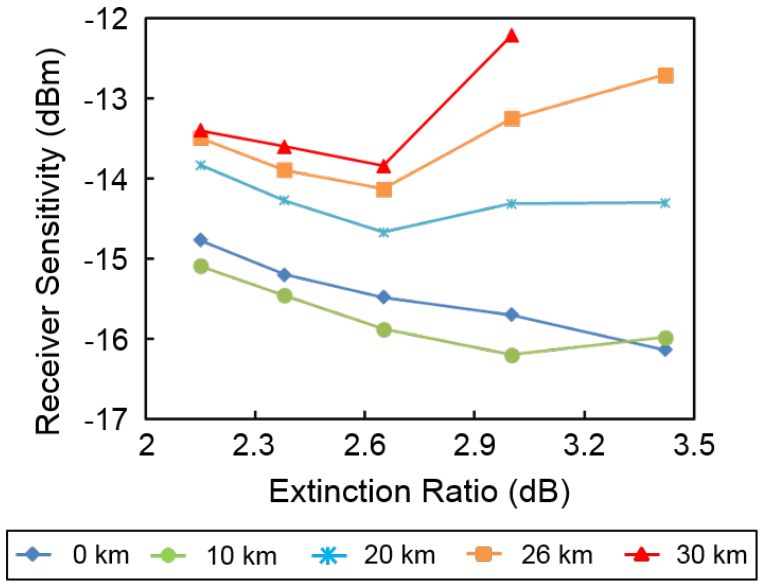

Figure 4.10: Receiver sensitivity as a function of the ER (at the output of the VCSEL) for various transmission distances when the FSR of DI is 25 GHz.

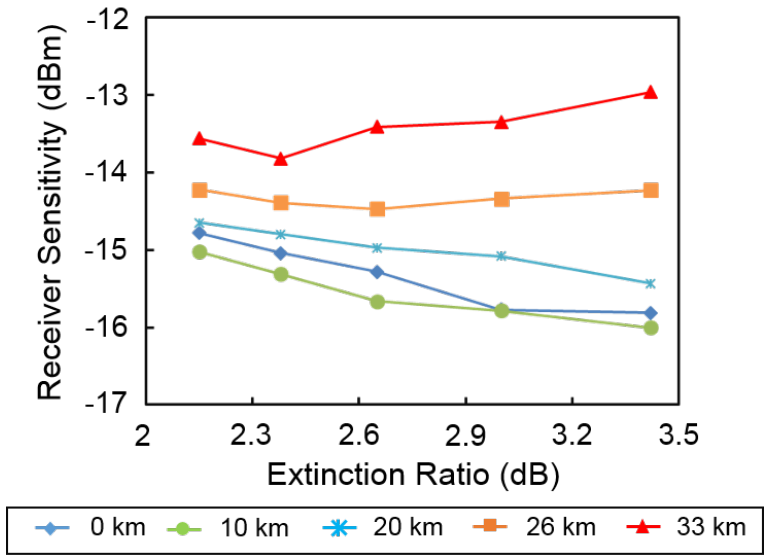

Figure 4.11: Receiver sensitivity as a function of the ER (at the output of the VCSEL) for various transmission distances when the FSR of DI is 16.1 GHz.

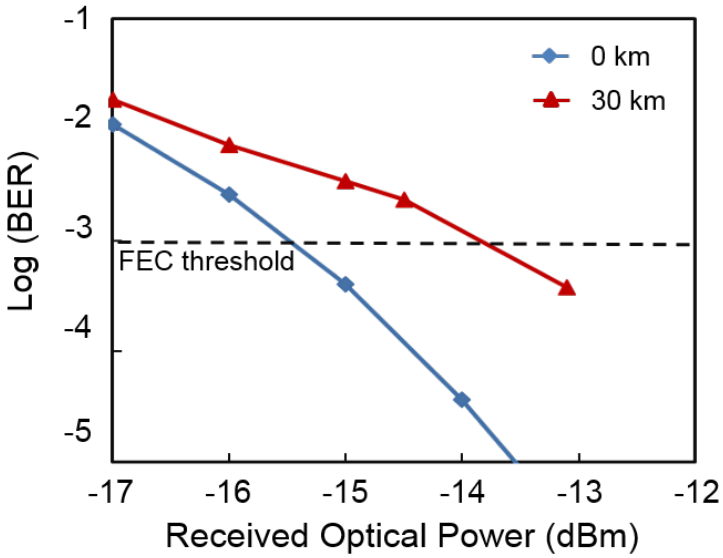

Figure 4.12: BER curves of the 25-Gb/s OOK signal having an ER of 2.7 dB at the output of the VCSEL after 0- and 30-km transmissions. The FSR of the DI is 25 GHz in this measurement.

of the signal in the presence of DI refers to the value at the output of the VCSEL (i.e., at the input of the DI) unless otherwise stated. Fig. 4.9 shows the measured receiver sensitivity after 20-km transmission as a function of the FSR of DI. Also shown in this figure is the insertion loss incurred by the DI. The ER of the signal is adjusted to achieve the best receiver sensitivity every time we tune the FSR of DI. The results show that the best receiver sensitivity is achieved when the FSR of DI is around 16 GHz. However, when the FSR of DI is smaller than 15 GHz, the insertion loss incurred by the DI increases significantly, which is undesirable for optical access networks because a large loss of DI reduces the fiber launch power and thus the power budget of networks. Thus, we optimize the ER of the signal for two FSR values: 16.1 and 25 GHz.

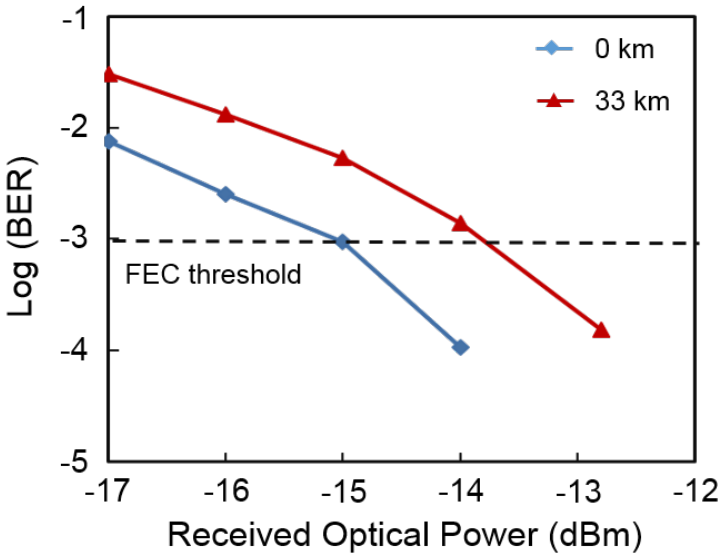

Figure 4.13: BER curves of the 25-Gb/s OOK signal having an ER of 2.4 dB at the output of the VCSEL after 0- and 33-km transmissions. The FSR of the DI is 16.1 GHz in this measurement.

Fig. 4.10 and Fig. 4.11 show the measured receiver sensitivities of the 25 Gb/s OOK signal as a function of the ER (at the output of the VCSEL) when the FSRs of DI are 25 and 16.1 GHz, respectively. A similar tendency we found in Fig. 4.6 is also observed in Fig. 4.10: the optimum ER for the best receiver sensitivity is decreased as the transmission distance increases. The optimum ER for the maximum transmission distance of 30 km is found to be 2.7 dB. When the FSR of DI is changed to 16.1 GHz [see Fig. 4.11], the maximum transmission distance of 33 km is achieved by the signal with ER of 2.4 dB.

Fig. 4.12 shows the measured BER curves for the 25-Gb/s OOK signal when the FSR of DI is 25 GHz and the ER is 2.7 dB. The receiver sensitivities after 0- and 30-km transmissions are measured to be -15.5 and -13.8 dBm, respectively. Thus,

the transmission penalty after 30-km transmission is 1.7 dB. As for the transmission performance of 25-Gb/s OOK signal (with ER of 2.4 dB) when the FSR of DI is 16.1 GHz is utilized, we can observe from the BER curves in Fig. 4.13 that the receiver sensitivity in back-to-back condition is measured to be -15 dBm. The maximum transmission distance is extended to 33 km, and the receiver sensitivity is degraded by 1.1 dB after 33-km transmission.

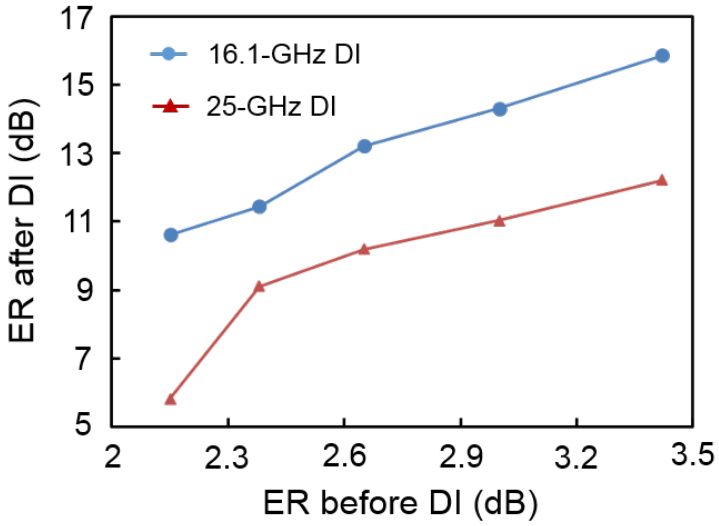

Figure 4.14: ER measured after the DI versus ER before the DI.

Compared to the receiver sensitivity measured without using the DI in the back-to-back condition [see Fig. 4.7], we have around 5.6-dB sensitivity improvement by using 25-GHz DI. The reasons for this improvement are twofold. First, the use of DI significantly increases the ER of the signal at the output of the DI. The ER of the signal is improved by the difference of DI's transmittance between the marks' and spaces' wavelengths. Fig. 4.14 shows the ER measured at the output of the DI versus the ER measured at the input of the DI. Since the wavelength difference between the marks and spaces linearly increases with the driving current due to the adiabatic chirp

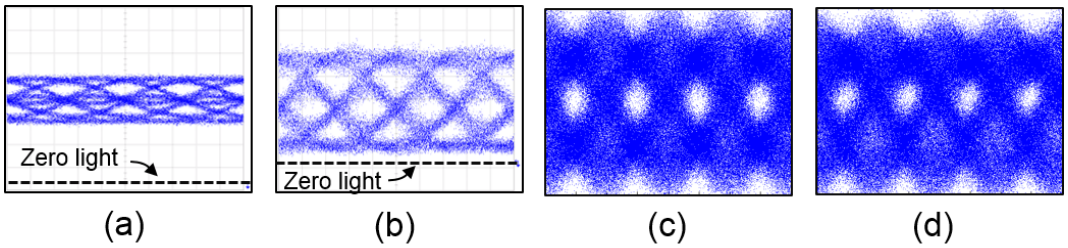

Figure 4.15: Optical eye diagrams of the 25-Gb/s OOK signals (a) before the DI, (b) after the DI. Eye diagrams of the 25-Gb/s OOK signals measured at the receiver when the electrical equalization is applied (c) after 0- and (d) 30-km transmissions. The FSR of the DI is 25 GHz. The ER of the signal is 2.7 dB and the received signal power is -15 dBm.

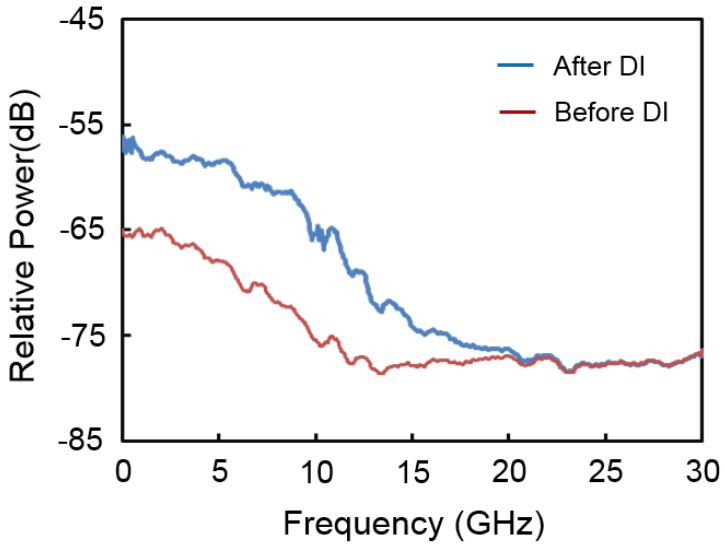

Figure 4.16: RF spectra of the 25-Gb/s signals measured before and after the DI. The ER of the signal is 2.7 dB and the FSR of the DI is 25 GHz.

of the VCSEL, it also increases with the ER at the output of the VCSEL. Thus, we can achieve a bigger improvement in ER by using the DI as the ER of the VCSEL output increases. Also, a DI having a smaller FSR exhibits a steeper transmittance

slope with respect to wavelength and thus a bigger improvement in ER. For example, we increase the ER of the 25-Gb/s OOK signal by 8.8 dB when a DI having an FSR of 25 GHz is employed for the OOK signal with a 3.4-dB ER. It is further improved by additional 3.6 dB when the FSR of DI is changed to 16.1 GHz. Second, the DI also serves to alleviate the signal distortions caused by the limited bandwidth of VCSEL. Fig. 4.15(a) and (b) show the eye diagrams measured at the input and output of the DI, respectively. They clearly show that eye opening is improved and the ER of the signal is dramatically enhanced after the DI. In addition, we can still observe clear eye opening of 25-Gb/s OOK signal after 30-km transmission in Fig. 4.15 (d), when the FSR of DI is 25 GHz and the ER of the signal is 2.7 dB. The RF spectra of the 25-Gb/s OOK signals measured before and after the DI depicted in Fig. 4.16 also show that the DI compensates partly for the band-limitation of the VCSEL. We believe this is because of the high-pass-filter characteristics of the DI for directly modulated semiconductor optoelectronic devices [111].

4.3.4 Performance Comparison between 25-Gb/s 4-PAM and OOK Signals

Finally, we compare the transmission performances among 25-Gb/s 4-PAM signal generated without DI and the 25-Gb/s OOK signals generated with and without DI. Fig. 4.17 shows the receiver sensitivity of the different signals as a function of the transmission distance. Firstly, in the absence of DI, the results show that there is a range of transmission distances where the receiver sensitivities are improved for both the OOK and 4-PAM signals. We attribute this to the effects of the self-steeping and duobinary-like-phase characteristics of the directly modulated signals [29, 35].

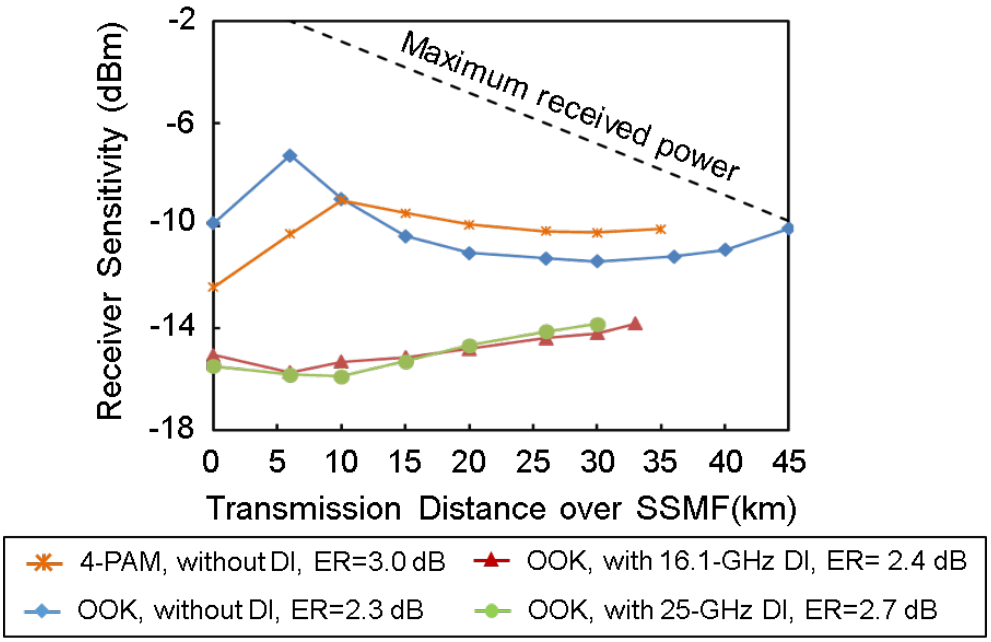

Figure 4.17: Measured receiver sensitivity of the 25-Gb/s 4-PAM and OOK signals as a function of transmission distance over SSMF without and with DI (16.1- and 25-GHz FSR), respectively. The corresponding ERs measured at the output of the VCSEL are 3.0, 2.3, 2.4, and 2.7 dB, respectively.

The results also show that when the transmission distance is less than 10 km, the 4-PAM signal exhibits better receiver sensitivities than the conventional OOK signal without DI. This is because of poor eye opening of the OOK signal [due to the limited bandwidth of the VCSEL as shown in the inset of Fig. 4.8(b)]. However, the OOK signal outperforms the 4-PAM signal after 10 km and beyond, and is successfully transmitted over 45-km-long SSMF with a negative transmission penalty. On the other hand, when the DI is employed, the receiver sensitivity is gradually degraded as the transmission distance increases [111]. The results show that the use of DI significantly improves the receiver sensitivity of the 25-Gb/s OOK signal up to 30 km. This is

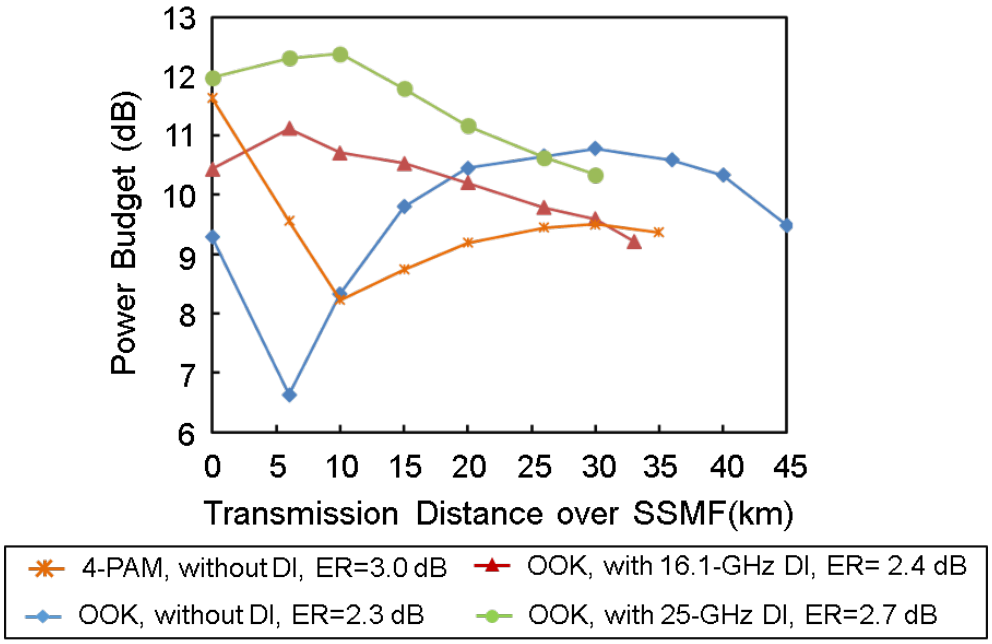

Figure 4.18: Measured power budget of the 25-Gb/s 4-PAM and OOK signals as a function of transmission distance over SSMF without and with DI (16.1- and 25-GHz FSR), respectively. The corresponding ERs measured at the output of the VCSEL are 3.0, 2.3, 2.4, and 2.7 dB, respectively.

certainly because of the improvement in ER and (partial) compensation of the VCSELs band-limitation, as explained in the previous subsection. Due to the dispersion-induced signal distortions, however, transmission distances longer than 33 km are not achieved by using the DI. For example, we observe error floors over 2×10^{-3} after 35-km transmission and are not able obtain BERs lower than the FEC threshold. On the other hand, the maximum transmission distance of 45 km is achieved without using the DI. Thus, we achieve a BL product of 1125 Gb/s·km without using optical dispersion compensation. By comparing with the results listed in Table 2.3, we believe this is the highest BL product ever reported for directly-detected single VCSEL. It is worth

mentioning that the maximum transmission distance is limited by the low output power of the VCSEL instead of the signal distortions caused by fiber chromatic dispersion when no DI is applied. Thus, we expect to further increase the maximum transmission distance by utilizing an APD receiver and/or by inserting an optical amplifier in the link [112].

It is important to note that the use of DI at the output of the VCSEL raises two problems: insertion loss of the DI and wavelength alignment between the DI and VCSEL. We can justify the use of DI for optical access networks as long as the sensitivity improvement brought by the DI is larger than its insertion loss. To answer this question, we plot the power budget of the transmission link as a function of transmission distance in Fig. 4.18. The power budget is defined as the maximum optical loss that the transmission link can accommodate and is calculated by the fiber launch power minus the receiver sensitivity. Since the output power of the VCSEL is set to be -0.8 dBm throughout the experiment, the fiber launch power should be decreased by the insertion loss of the DI (see Fig. 4.9 for the insertion loss of the DI) when the DI is employed. The results show that the sensitivity improvement achieved by using the DI is offset partly by the insertion loss of DI. For example, the use of DI brings 1.1- and 2.7-dB advantages in terms of power budget over the case without using the DI when the FSRs of the DI are 16.1 and 25 GHz, respectively, even though the sensitivity improvement is about 5.5 dB in the back-to-back case. In addition, larger power budget is still achieved by OOK signals with 25-GHz DI compared with 25-Gb/s 4-PAM signals, however, 4-PAM signals shows larger power budget than OOK signals with 16.1-GHz DI in back-to-back condition. Nonetheless, we can still achieve a largest power budget up to 25 km by using a DI having a 25-GHz FSR. For typical

optical access network covering up to 20 km, we can achieve a power budget larger than 11 dB by using a DI with an FSR of 25 GHz.

The wavelength alignment between the DI and VCSEL can be achieved by locking the VCSELs wavelength to one of DI's transmission peaks. This can be realized, for example, by applying a low-frequency tone to the VCSEL and minimizing the amplitude of the tone signal after detecting it at one of the outputs of the DI [113, 114]. Multiple VCSELs operating at different wavelengths could be frequency-locked to the transmission peaks of a single DI for wavelength-division multiplexed passive optical networks [115]. Thus, the placement of DI at the transmitter side rather than at the receiver side greatly facilitates the wavelength alignment between the DI and VCSELs.

4.4 Summary

We have explored the possibility of utilizing 1.5-μm, 10G-class VCSELs for the cost-effective implementation of optical access networks based on 25-Gb/s transmission. To further enhance the cost-effectiveness and secure a large power budget for optical access networks, we employed simple modulation formats, i.e., OOK and 4-PAM, and direct detection, but did not employ bulky and lossy dispersion compensation modules. In order to improve the power budget of 25-Gb/s OOK VCSEL based transmission, two different transmitter designs are considered: with and without DI. The extinction ratio of the signals and the free-spectral range of DI are optimized to maximize the transmission distance.

The experimental results can be summarized as follows. For 25-Gb/s 4-PAM signals, which suffer less bandwidth limitation from 10G-class VCSEL, successful

transmission over 35-km-long SSMF can be achieved with 15-tap FFE and 7-tap DFE. As for the OOK signals without using DI, 45-km transmission over SSMF is successfully achieved with similar tap of equalizer at the receiver side. A BL product of 1125 Gb/s·km without using optical dispersion compensation is successfully achieved. We believe this is the highest BL product ever reported for directly-detected single VCSEL. This result shows that while generated by using a 1.5-μm 10G-class VCSEL and electrical equalization being employed at the receiver, OOK signals not only perform better in terms of dispersion tolerance but also are easier to be implemented than the 4-PAM counterparts.

On the other hand, when a DI is utilized for the 25-Gb/s OOK VCSEL-based transmission system, the maximum transmission distance is limited to 33 km. But compared to the case without using the DI, we are able to improve the power budget of the system up to 25 km at the expense of the cost of the DI. For example, a power budget larger than 11 dB can be achieved in a typical optical access network covering up to 20 km with a DI having a free-spectral range of 25 GHz at the output of the VCSEL. Thanks to the periodicity of the DI's transmittance with respect to wavelength, a single DI can be shared among multiple channels in wavelength-division-multiplexed optical access networks.

In sum, with the help of electrical equalization and optical dispersion compensation, 1.5-μm, 10G-class VCSELs can be implemented for low-splitting ratio (e.g., $<$10) passive optical networks operating at 25 Gb/s cost-effectively.

Chapter 5

Conclusions and Future Works

5.1 Conclusions

This thesis is devoted to exploring the possibility of utilizing 1.5-μm VCSEL for the applications of optical access networks. I summarize the main contributions of this thesis as follows.

In Chapter 3, we experimentally demonstrate the power budget improvement of a 10-Gb/s VCSELs link with optical and electrical dispersion compensations. In the first part of Chapter 3, the FSK signals generated by directly modulated VCSEL are converted to ASK signals with an improved ER by utilizing DI. The FSR of the DI is optimized. In order to use the flat region of the VCSEL's FM response, we investigate and compare the transmission performance among different line codings with low DC characteristics: 7B/8B, 8B/10B, 9B/10B and scramble-and-select line codings. The bandwidth expansion induced by the coding overhead of each line code is taken into consideration for a fair comparison. Among the examined codes, 9B/10B and scramble-and-select line codings show similar and excellent performance. By

taking into the insertion loss of the DI, we achieve a power budget improvement by $>$ 5 dB with the utilization of OOK modulation format and DI, when compared with a conventional OOK VCSEL link without DI. 50-km transmission over SSMF with less than 0.5-dB power penalty is successfully achieved. When we replace the PIN receiver with an APD receiver, the power budget of the VCSEL link is further improved by 5 dB. The maximum transmission distance is then extended to 60 km with a relatively uniform power budget. Therefore, applying FSK modulation and suitable DC line coding for directly modulated VCSEL can be beneficial for implementing cost-effective 10-Gb/s access transmission systems.

In the second part of Chapter 3, we present a systematic study on the transmission performance of 10.7-Gb/s OOK and 4-PAM signals generated by a directly modulated 1.5-μm VCSEL without DI. We optimize the ER of signals, and employ the electrical equalization technique at the receiver. Thanks to the optimized ER and electrical equalization, 80- and 40-km transmissions over SSMF are successfully achieved by using the OOK and 4-PAM signals, respectively. The performance comparison between the OOK and 4-PAM signals indicates that the OOK format is better suited for 1.5-μm VCSEL-based optical access networks with better tolerance to the CD, which thanks of the duobinary-like phase characteristics that OOK signal has. In addition, the OOK transceivers are much simpler to implement than the 4-PAM counterparts.

In Chapter 4, it is shown that 25-Gb/s signals can be accommodated with a 7-GHz-bandwidth VCSEL. Simple modulation formats (i.e., OOK and 4-PAM) and direct detection are implemented. In addition, two different transmitter schemes for OOK signals (i.e., without and with DI at the output of VCSEL) are investigated in order to maximize the power budget of transmission link. Note that the ER of

signals and FSRs of DI are optimized throughout the experiment. Firstly, without the utilization of DI, we can successfully achieve 35- and 45-km transmissions over SSMF by utilizing 25-Gb/s 4-PAM and OOK signals, respectively. A BL product of 1125 Gb/s·km is successfully achieved without using optical dispersion compensation. We believe this is the highest BL product ever reported for directly-detected VCSELs. Furthermore, the power budget of the 25-Gb/s OOK VCSEL-based optical access link is improved up to 25 km with DI, although the maximum transmission distance is limited to 33 km. In particular, a power budget larger than 11 dB is achieved in a typical optical access network covering up to 20 km. Thanks to the periodicity of the DI's transmittance with respect to wavelength, a single DI can be shared among multiple channels in WDM optical access networks.

The findings of this thesis would be useful for the implementation of short or intermediate haul (e.g., $<$ 50 km) transmission links and cost-sensitive optical access networks with low splitting ratios, by utilizing 1.5-μm VCSELs. The data rate is supported up to 25 Gb/s with the utilization of 10G-class VCSEL. The use of delay interferometer can successfully improve the dispersion tolerance of transmission links, and the use of DC-balanced line codings can not only well compensate the non-uniform frequency response of VCSELs at low frequencies but also be beneficial for cost-sensitive access applications, since it is a digital solution and can be used with the commercially available VCSELs without replacing the deployed fiber links or the existing devices at the transceiver sides. In addition, the utilization of electrical dispersion compensation can also effectively alleviate both dispersion-induced and band limitation-induced distortions in 1.5-μm 10G-class VCSEL-based access links.

5.2 Future Works

I highlight several future work directions in the following which I deem important and worthy of further investigations by extending the results presented in this thesis.

5.2.1 Wavelength Locking Between DI and Laser Signal

In the proposed systems in Chapter 3 and 4, one potential problem is that the central frequency of the VCSEL is sensitive to temperature fluctuation and the phase of DI also changes over time. In order to align the laser wavelength precisely to the transmittance of the DI, we can consider monitoring the operating wavelength of the laser diode. This monitoring process can be realized by using a FP etalon-based monitoring module along with a low-frequency electrical tone signal [116]. To be more specific, the VCSEL is first modulated with a small sinusoidal current, i.e., the tone signal with a unique frequency that is lower than tens of MHz. This tone signal would not interfere with the data signal, since the low frequency spectral contents of the data signal are depleted due to the applied DC-balanced line coding. The output signal from the photodiode is then sampled and processed through a fast Fourier transform (FFT) algorithm, after which the optical frequency can be calculated from the relationship between the pilot signal and transmitted signal. In addition, for the wavelength-division-multiplexed directly modulated system, the optical frequency monitoring can also be achieved by arranging different channels with different channel-by-channel tone frequency and then observing the ratio of the amplitudes of nearby pilot tones. With the observed wavelength shift between the VCSEL and DI, we can significantly improve the reliability of the system to ensure that the laser wavelength is locked to the DI and the ER of the signal is optimized.

5.2.2 Nonlinear Equalization at the Receiver Side

In this thesis, we mainly consider the frequency chirp and chromatic dispersion induced signal distortions in directly modulated VCSEL-based transmission system. In many cases, besides the chirp effect and chromatic dispersion, the signal distortions may also come from other factors: (1) limited bandwidth of devices; (2) signal-to-signal beating noise (SSBN); (3) fiber nonlinearities [117]. We can consider applying Volterra filter, which is a well-know time-domain nonlinear compensation scheme, to compensate for these distortions simultaneously [118]. The mth sample of the output signal waveform after the three-kernels Volterra filter is represented as:

$$y(m) = \sum_{l_1=0}^{L_1-1} w_1(l_1)x(m-l_1) + \sum_{l_1=0}^{L_2-1}\sum_{l_2=0}^{l_1-1} w_2(l_1,l_2)x(m-l_1)x(m-l_2) + \sum_{l_1=0}^{L_3-1}\sum_{l_2=0}^{l_1-1}\sum_{l_3=0}^{l_2-1} w_3(l_1,l_2,l_3)x(m-l_1)x(m-l_2)x(m-l_3) \quad (5.1)$$

where $x(m-l_i)$ is the $(m-l_i)^{th}$ sample of the received signal, $w_k(l_1)$, $w_k(l_1,l_2)$, $w_k(l_1,l_2,l_3)$ are the 1^{st}, 2^{nd} and 3^{rd} order weighting factor, and L_1, L_2, and L_3 are the corresponding memory length. The first term in Eq. (5.1) indicates a linear filter, and the second and third terms are designed to deal with SSBN and fiber nonlinearities, respectively. Even though taking more nonlinear terms into consideration might obtain better performance, the computational complexity will also increase dramatically [118]. Usually, three-kernels Volterra filtering already can achieve desirable performance. By using the nonlinear Volterra filter, it is believed that not only linear distortions but also nonlinear distortions can both be well compensated and the transmission performance of long-wavelength VCSEL-based optical access link will be further improved.

5.2.3 Duobinary 4-PAM Signal Transmission over 1.5-μm VCSEL-based Optical Access Link

In Chapter 3 and 4, we compare the transmission performance between 4-PAM and OOK signals on 10.7- and 25-Gb/s data rate, respectively. The result shows that OOK signal outperforms the 4-PAM signal on higher dispersion tolerance and longer transmission distance over SSMF, which is because the duobinary characteristics of OOK signals are not observed from 4-PAM signals. This duobinary characteristics can well compensate the dispersion-induced signal distortions after transmission over SSMF. In addition, duobinary signal is also known as a partial response modulation scheme, which can effectively improve the spectral efficiency [119]. Therefore, we can consider applying duobinary 4-PAM signal to improve the data rate and dispersion tolerance of 4-level signal in 1.5-μm VCSEL-based access link. The generation of duobinary 4-PAM signal can be realized by passing through a low pass filter (LPF) (e.g., Bessel filter [120]) or it can also be realized by utilization of bandwidth-limited transmitters, which is similar to the method in Chapter 4. With the utilization of the spectral-efficient duobinary 4-PAM modulation formats, it is expected that higher data rate and better dispersion tolerance can be achieved in 1.5-μm VCSEL-based optical access link.

Bibliography

[1] G. P. Agrawal, *Fiber-optic communication system*, 4th ed. John Wiley&Sons. Inc, 2010.

[2] J. Chesnoy, *Undersea Fiber Communication Systems*, 2nd ed. New York, US: Academic Press, 2015.

[3] J. Zheng and H. T. Mouftah, "Media access control for Ethernet passive optical networks: an overview," *IEEE Commun. Magazine*, vol. 43, no. 2, pp. 145–150, Feb. 2005.

[4] S. Gaede and C. G. Schaeffer, "Overview of optical monitoring in next generation optical access networks," in *Proc. Photonic Networks*, Leipzig, Germany, May 2011, paper 15.

[5] H. Ying, H. Lu, C. Li, C. Lin, and P. Peng, "A 20-km/60-Gb/s two-way PON based on directly modulated two-stage injection-locked 1.55-μm VCSEL transmitters and negative dispersion fibers," *IEEE Photonics Journal*, vol. 7, no. 1, pp. 1–10, Feb. 2015.

[6] L. Liao, D. S. Rubio, M. Morse, A. Liu, D. Hodge, D. Rubin, U. D. Keil, and T. Franck, "60 Gbits error-free 4-PAM operation with 850 nm VCSEL," *Optical Express*, vol. 13, no. 8, pp. 3129–3135, Apr. 2005.

[7] J. Liu, M. Beals, A. Pomerene, S. Bernardis, R. Sun, J. Cheng, L. C. Kimerling, and J. Michel, "Waveguide-integrated, ultralow-energy GeSi electro-absorption modulators," *Nature Photonics*, vol. 2, no. 7, pp. 433 – 437, May 2008.

[8] T. Gibbon, K. Prince, T. Pham, A. Tatarczak, C. Neumeyr, E. Rnneberg, M. Ortsiefer, and I. T. Monroy, "VCSEL transmission at 10 Gb/s for 20 km single mode fiber WDM-PON without dispersion compensation or injection locking," *Opt. Fiber Technol.*, vol. 17, no. 1, pp. 41 – 45, Jan. 2011.

[9] R. Rodes, J. Estaran, B. Li, M. Muller, J. B. Jensen, T. Gruendl, M. Ortsiefer, C. Neumeyr, J. Rosskopf, K. J. Larsen, M. C. Amann, and I. T. Monroy, "100 Gb/s VCSEL data transmission link," in *Proc. OFC*, Los Angeles, CA, Mar. 2012, paper PDF5D.I0.

[10] K. Szczerba, P. Westbergh, M. Karlsson, P. Andrekson, and A. Larsson, "60 Gbits error-free 4-PAM operation with 850 nm VCSEL," *Elect. Lett.*, vol. 49, no. 15, pp. 953–955, Jul. 2013.

[11] C. Chang-Hasnain, in *Optical Fiber Telecommunications*, 4th ed. New York, US: Academic Press, 2002, pp. 668–670.

[12] D. Kuchta, A. Rylyakov, C. Schow, J. Proesel, C. Baks, C. Kocot, L. Graham, R. Johnson, G. Landry, E. Shaw, A. MacInnes, and J. Tatum, "A 55 Gb/s directly modulated 850 nm VCSEL-based optical link," in *Proc. IPC*, Burlingame, CA, Sep. 2012, paper PD1.5.

[13] Z. Al-Qazwini, J. Zhou, and H. Kim, "1.5-μm, 10-Gb/s VCSEL link for optical access applications," *IEEE Photon. Technol. Lett.*, vol. 25, no. 22, pp. 2160–2163, Nov. 2013.

[14] X. Zhao, "*Optical injection locking on vertical-cavity surface-emitting lasers (VCSELs): physics and applications*," PhD Thesis, University of California, Berkeley, 2003.

[15] B. Zhang, X. Zhao, L. Christen, and D. Parekh, "Adjustable chirp injection-locked 1.55-μm VCSELs for enhanced chromatic dispersion compensation at 10-Gbit/s," in *Proc. OFC*, San Diego, CA, Feb. 2008, paper OWT7.

[16] P. Boffi, A. Boletti, A. Gatto, and M. Martinelli, "VCSEL to VCSEL injection lockig for uncompensated 40-km transmission at 10 Gb/s," in *Proc. OFC*, San Diego, CA, Mar. 2009, paper JThA32.

[17] W. Hofmann, L. Gruner-Nielsen, E. Ronneberg, G. Bohm, M. Ortsiefer, and M. Amann, "1.55-μm VCSEL modulation performance with dispersion-compensation fibers," *IEEE Photon. Technol. Lett.*, vol. 21, no. 15, pp. 1072–1074, Sep. 2009.

[18] C. W. Chow, L. Xu, C. H. Yeh, H. K. Tsang, W. Hofmann, and M. C. Amann, "40-Gb/s upstream transmitters using directly modulated 1.55-μm VCSEL array for high-split-ratio PONs," *IEEE Photon. Technol. Lett.*, vol. 22, no. 5, pp. 347–349, Mar. 2010.

[19] K. Prince, M. Ma, T. B. Gibbon, and I. T. Monroy, "Demonstration of 10.7-Gb/s transmission in 50-km PON with uncooled free-running 1550-nm VCSEL," in *Proc. CLEO*, San Jose, CA, May 2010, paper ATuA2.

[20] K. Prince, M. Ma, T. B. Gibbon, C. Neumeyr, E. Rnneberg, M. Ortsiefer, and I. T. Monroy, "Free-running 1550 nm VCSEL for 10.7 Gb/s transmission in 99.7

km PON," *Journal of Optical Communications and Networking*, vol. 3, no. 5, pp. 399–403, May 2011.

[21] T. Gibbon, K. Prince, C. Neumeyr, E. Ronneberg, M. Ortsiefer, and I. T. Monroy, "10 Gb/s 1550 nm VCSEL transmission over 23.6 km single mode fiber with no dispersion compensation and no injection locking for WDM PONs," in *Proc. OFC*, San Diego, CA, Mar. 2010, paper JThA30.

[22] Z. Al-Qazwini, M. Thollabandi, and H. Kim, "1.55-μm, 10-Gb/s VCSEL transmission for optical access networks," in *Proc. OECC*, Kyoto, Japan, Jun. 2014, paper MP1-4.

[23] A. E. Willner, M. Kuznetsov, I. P. Kaminow, J. Stone, L. W. Stulz, and C. A. Burrus, "FM and FSK response of tunable two-electrode DFB lasers and their performance with noncoherent detection," *IEEE Photon. Technol. Lett.*, vol. 1, no. 12, pp. 1041–1135, Aug. 1989.

[24] S. Alexander, D. Welford, and D. Marquis, "Passive equalization of semiconductor diode laser frequency modulation," *Journal of Lightwave Technology*, vol. 7, no. 1, pp. 11–23, Jan. 1989.

[25] K. Hasebe, Y. Mada, T. Sakairi, T. Sakaguchi, A. Matsutani, and F. Koyama, "High-speed optical modulation based on frequency-modulated VCSELs and optical filters," in *Proc. ICIPRM*, Newport Beach, CA, May 2009, paper Thb1.5.

[26] K. Szczerba, P. Westbergh, E. Agrell, M. Karlsson, P. Andrekson, and A. Larsson, "Comparison of intersymbol interference power penalties for OOK and 4-PAM in short-range optical links," *IEEE J. Lightw. Technol.*, vol. 31, no. 22, pp. 3525–3534, Oct. 2013.

[27] J. Ingham, R. Penty, I. White, P. Westbergh, J. Gustavsson, A. Haglund, and A. Larsson, "32 Gb/s multilevel modulation of an 850 nm VCSEL for next-generation datacommunication standards," in *Proc. CLEO*, Baltimore, MD, May 2011, paper CWJ2.

[28] F. Karinou, L. Deng, R. Lopez, K. Prince, J. Jensen, and I. Monroy, "Performance comparison of 850-nm and 1550-nm VCSELs exploiting OOK, OFDM, and 4-PAM over SMF/MMF links for low-cost optical interconnects," *Opt. Fiber Technol.*, vol. 19, no. 3, pp. 206–212, Feb. 2013.

[29] N. Nishiyama, C. Caneau, J. D. Downie, M. Sauer, and C. E. Zah, "10-Gbps 1.3 and 1.55-μm InP-based VCSELs: 85°C 10-km error-free transmission and room temperature 40-km transmission at 1.55-μm with EDC," in *Proc. OFC*, Anaheim, CA, Mar. 2006, paper PDP23.

[30] F. Breyer, S. Lee, S. Randel, and N. Hanik, "Comparison of OOK- and PAM-4 modulation for 10 Gbit/s transmission over up to 300 m polymer optical fiber," in *Proc. OFC/NFOEC*, San Diego, CA, Feb. 2008, paper OWB5.

[31] C. Peucheret, *Direct and External Modualtion of Light*. Experimental Note, Technical University of Denmark, 2009.

[32] Z. Al-Qazwini and H. Kim, "Line coding to enhance the performance of 10-Gbps CPFSK-ASK directly modulated signals," *Opt. Express*, vol. 18, no. 8, pp. 8360–8366, Apr. 2010.

[33] C. Wilmsen, H. Temkin, and L. Coldren, *Vertical-Cavity Surface-Emitting Lasers*. Cambridge University Press, New York, 1999.

[34] A. Karim, S. Bjorlin, J. Piprek, and J. E. Bowers, "Long-wavelength vertical-cavity lasers and amplifiers," *IEEE Journal of Selected Topics in Quantum Electronics*, vol. 6, no. 6, pp. 1244–1253, Nov. 2000.

[35] J. Tatum, D. Gazula, L. A. Graham, J. K. Guenter, R. H. Johnson, J. King, C. Kocot, G. D. Landry, I. Lyubomirsky, A. N. MacInnes, E. M. Shaw, K. Balemarthy, R. Shubochkin, D. Vaidya, M. Yan, and F. Tang, "VCSEL-based interconnects for current and future data centers," *IEEE J. Lightw. Technol.*, vol. 33, no. 4, pp. 727–732, Nov. 2014.

[36] F. Karinou, C. Prodaniuc, N. Stojanovic, M. Ortsiefer, A. Daly, R. Hohenleitner, B. Kogel, and C. Neumeyr, "Directly PAM-4 modulated 1530-nm VCSEL enabling 56 Gb/s/λ data-center interconnects," *IEEE Photon. Technol. Lett.*, vol. 27, no. 17, pp. 1872–1875, Sep. 2015.

[37] S. H. Bae, H. Kim, and Y. C. Chung, "Transmission of 51.56-Gb/s OOK signal over 15 km of SSMF using directly-modulated 1.55-μm DFB laser," in *Proc. OFC*, Anaheim, CA, Mar. 2016, paper Tu2J.5.

[38] S. Nakamura, M. Shirao, and M. Nogami, "Uncooled 25.78 Gb/s transmission over 10 km using a 1.3 m directly modulated DFB laser in a TO-CAN package," in *Proc. OECC*, Niigata, Japan, Jun. 2016, paper WD3-3.

[39] L.-S. Yan, C. Yu, Y. Wang, T. Luo, L. Paraschis, Y. Shi, and A. E. Willner, "40-Gb/s transmission over 25 km of negative-dispersion fiber using asymmetric narrow-band filtering of a commercial directly modulated DFB laser," *IEEE Photonics Technology Letters*, vol. 17, no. 6, pp. 1322–1324, June 2005.

[40] C. J. Chang-Hasnain, "Optically-injection locked tunable multimode VCSEL for WDM passive optical networks," in *International Nano-Optoelectronics Workshop*, Shonan Village, Aug. 2008, paper 98-99.

[41] E. Wong, C. A. Chan, M. P. I. Dias, M. Mueller, and M. C. Amann, "Low-power transmitters for green access networks," in *Photonics Global Conference*, Singapore, Dec. 2012, paper 1-6.

[42] T. L. Koch and R. A. Linke, "Effect of nonlinear gain reduction on semiconductor laser wavelength chirping," *App. Phys. Lett.*, vol. 48, no. 10, pp. 613–615, Jan. 1986.

[43] I. P. Kaminow and T. Li, *Optical Fiber Telecommunications IV A: Components*, 4th ed. USA, Academic Press, 2002.

[44] P. Krehlik, "Characterization of semiconductor laser frequency chirp based on signal distortion in dispersive optical fiber," *Opto-Electronics Review*, vol. 14, no. 2, pp. 119–124, Jun. 2006.

[45] B. Hakki, "Evaluation of transmission characteristics of chirped DFB lasers in dispersive optical fiber," *IEEE Journal of Lightwave Technology*, vol. 10, no. 7, pp. 964–970, Aug. 2002.

[46] S. Hu and F. Koyama, "Chirp reduction and modulation bandwidth enhancement of transverse coupled cavity VCSEL," in *Proc. OECC*, Shanghai, China, Jul. 2015, paper 1-3.

[47] H. Dalir and F. Koyama, "29 GHz directly modulated 980 nm vertical-cavity surface emitting lasers with bow-tie shape transverse coupled cavity," *App. Phys. Lett.*, vol. 103, no. 9, pp. 1–4, Aug. 2013.

[48] S. Hu, X. Gu, and F. Koyama, "Low chirp operation of transverse-coupled-cavity VCSELs," in *Proc. CLEO*, San Jose, CA, Jun. 2016, paper SF1L.4.

[49] B. Jopson and A. Gnauck, "Dispersion compensation for optical fiber systems," *IEEE Communications Magazine*, vol. 33, no. 6, pp. 96–102, Jun. 1995.

[50] S. Warm, C. A. Bunge, T. Wuth, and K. Petermann, "Electronic dispersion precompensation using a directly modulated laser," in *Proc. ECOC*, Brussels, Sep. 2008, paper P.4.07.

[51] N. Henmi, T. Saito, and T. Ishida, "Prechirp technique as a linear dispersion compensation for ultrahigh-speed long-span intensity modulation directed detection optical communication systems," *IEEE Journal of Lightwave Technology*, vol. 12, no. 10, pp. 1706–1719, Oct. 1994.

[52] T. Saito, N. Henmi, S. Fujita, M. Yamaguchi, and M. Shikada, "Prechirp technique for dispersion compensation for a high-speed long-span transmission," *IEEE Photon. Technol. Lett.*, vol. 3, no. 1, pp. 74–76, 1991.

[53] D. M. Kuchta, A. V. Rylyakov, C. L. Schow, J. E. Proesel, C. Baks, P. Westbergh, J. S. Gustavsson, and A. Larsson, "64Gb/s transmission over 57m MMF using an NRZ modulated 850nm VCSEL," in *Proc. OFC*, San Francisco, CA, Mar. 2014, paper Th3C.2.

[54] D. M. Kuchta, A. V. Rylyakov, C. L. Schow, J. E. Proesel, C. W. Baks, P. Westbergh, J. S. Gustavsson, and A. Larsson, "A 50 Gb/s NRZ modulated 850 nm VCSEL transmitter operating error free to 90 °C," *IEEE Journal of Lightwave Technology*, vol. 33, no. 4, pp. 802–810, Oct. 2014.

[55] D. Kuchta, T. Huynh, F. Doany, L. Schares, C. Baks, C. Neumeyr, A. Daly, K. Benjamin, J. Rosskopf, and M. Ortsiefer, "Error-free 56 Gb/s NRZ modulation of a 1530 nm VCSEL link," *IEEE Journal of Lightwave Technology*, vol. 34, no. 14, pp. 3275 – 3282, Jul. 2016.

[56] D. M. Kuchta, F. E. Doany, L. Schares, C. Neumeyr, A. Daly, B. Kogel, J. Rosskopf, and M. Ortsiefer, "Error-free 56 Gb/s NRZ modulation of a 1530 nm VCSEL link," in *Proc. ECOC*, Valencia, Sep. 2015, paper 1-3.

[57] I. Tomkos, D. Chowdhury, J. Conradi, D. Culverhouse, K. Ennser, C. Giroux, B. Hallock, T. Kennedy, A. Kruse, S. Kumar, N. Lascar, I. Roudas, M. Sharma, R. S. Vodhanel, and C. C. Wang, "Demonstration of negative dispersion fibers for DWDM metropolitan area networks," *IEEE Journal of Selected Topics in Quantum Electronics*, vol. 7, no. 3, pp. 439–460, Jun. 2001.

[58] X. Cheng, Y. J. Wen, Z. Xu, X. Shao, Y. Wang, and Y. Yeo, "10-Gb/s WDM-PON transmission using uncooled, directly modulated free-running 1.55-μm VCSELs," in *Proc. ECOC*, Brussel, Sep. 2008, paper P.6.02.

[59] L. Chrostowski, C.-H. Chang, and C. J. Chang-Hasnain, "Enhancement of dynamic range in 1.55-μm VCSELs using injection locking," *IEEE Photonics Technology Letters*, vol. 15, no. 4, pp. 498–500, Apr. 2003.

[60] A. Gatto, A. Boletti, P. Boffi, and M. Martinelli, "Adjustable-chirp VCSEL-to-VCSEL injection locking for 10-Gb/s transmission at 1.55 μm," *Opt. Express*, vol. 17, no. 24, pp. 21 748–21 753, Nov. 2009.

[61] X. Zhao, D. Parekh, E. K. Lau, H.-K. Sung, M. C. Wu, W. Hofmann, M. C. Amann, and C. J. Chang-Hasnain, "Novel cascaded injection-locked 1.55-μm

VCSELs with 66 GHz modulation bandwidth," *Opt. Express*, vol. 15, no. 22, pp. 14 810–14 816, Oct. 2007.

[62] H. B. Zhang, X. W. Yi, Q. W. Zhang, Y. Ling, M. L. Deng, E. Hugues-Salas, R. P. Giddings, Y. Hong, M. Wang, and J. M. Tang, "Robust real-time 15.125 Gb/s adaptive optical OFDM transmissions over 100 m OM2 MMFs utilizing directly modulated VCSELs subject to optical injection locking," *Opt. Express*, vol. 22, no. 1, pp. 1163–1171, Jan. 2014.

[63] W. Idler, A. Klekamp, R. Dischler, and B. Wedding, "Advantages of frequency shift keying in 10 Gb/s systems," in *Proc. IEEE/LEOS*, Jul. 2004, paper 51-52.

[64] E. Forestieri and G. Prati, "Analysis of delay-and-multiply optical FSK receivers with line-coding and non-flat laser FM response," *IEEE Journal on Selected Areas in Communications*, vol. 13, no. 3, pp. 543–556, Apr. 1995.

[65] S. Kobayashi, Y. Yamamoto, M. Ito, and T. Kimura, "Direct frequency modulation in AlGaAs semiconductor lasers," *IEEE Transactions on Microwave Theory and Techniques*, vol. 30, no. 4, pp. 428–441, Apr. 1982.

[66] W. V. Sorin, K. W. Chang, G. A. Conrad, and P. R. Hernday, "Frequency domain analysis of an optical FM discriminator," *J. Lightwave Technol.*, vol. 10, no. 6, pp. 787–793, Jun. 1992.

[67] P. Gambini, N. P. Caponio, M. Puleo, and E. Vezzoni, "Accurate measurement of the FM response in magnitude and phase of different DFB laser structures," in *Proc. SPIE*, vol. 17, Feb. 1990, pp. 41 – 45.

[68] R. S. Vodhanel, A. F. Elrefaie, M. Z. Iqbal, R. E. Wagner, J. L. Gimlett, and S. Tsuji, "Performance of directly modulated DFB lasers in 10-Gb/s ASK, FSK,

and DPSK lightwave systems," *IEEE Journal of Lightwave Technology*, vol. 8, no. 9, pp. 1379 – 1386, Sep. 1990.

[69] Z. Al-Qazwini and H. Kim, "Line coding for 10-Gb/s directly modulated lasers," in *Proc. OFC*, San Diego, CA, Mar. 2010, paper OThW8.

[70] L. S. Yan, Y. Wang, B. Zhang, C. Yu, J. McGeehan, L. Paraschis, and A. E. Willner, "Reach extension in 10-Gb/s directly modulated transmission systems using asymmetric and narrowband optical filtering," *Opt. Express*, vol. 13, no. 13, pp. 5106–5115, Jun. 2005.

[71] A. Agarwal, S. Banerjee, D. F. Grosz, A. P. Kung, D. N. Maywar, A. Gurevich, and T. H. Wood, "Ultrahigh-capacity long-haul 40-Gb/s WDM transmission with 0.8-b/s/Hz spectral efficiency by means of strong optical filtering," *IEEE Photon. Technol. Lett.*, vol. 15, no. 3, pp. 470–472, Mar. 2003.

[72] A. Malacarne, V. Sorianello, A. Daly, K. Benjamin, M. Ortsiefer, C. Neumeyr, M. Romagnoli, and A. Bogoni, "Performance analysis of 40 Gb/s transmission based on directly modulated high-speed 1530-nm VCSEL," *IEEE Photon. Technol. Lett.*, vol. 28, no. 16, pp. 1735–1738, Apr. 2016.

[73] S. Alexander and D. Welford, "Equalisation of semiconductor diode laser frequency modulation with a passive network," *Electronics Letters*, vol. 21, no. 9, pp. 361–362, Apr. 1985.

[74] R. S. Vodhanel, B. Enning, and A. F. Elrefaie, "Bipolar optical FSK transmission experiments at 150 Mbit/s and 1 Gbit/s," *Journal of Lightwave Technology*, vol. 6, no. 10, pp. 1549–1553, Oct. 1988.

[75] T. Muoi, "Receiver design for digital fiber optic transmission systems using Manchester (biphase) coding," *IEEE Transactions on Communications*, vol. 31, no. 5, pp. 608–619, May 1983.

[76] P. W. Hooijmans, M. T. Tomesen, and A. van de Grijp, "Penalty free biphase linecoding for pattern independent FSK coherent transmission systems," *Journal of Lightwave Technology*, vol. 8, no. 3, pp. 323–328, Mar. 1990.

[77] R. Forster, "Manchester encoding: opposing definitions resolved," *Engineering Science and Education Journal*, vol. 9, no. 6, pp. 278–280, Dec. 2000.

[78] H. Tsushima, S. Sasaki, R. Takeyari, and K. Uomi, "Alternate-mark-inversion optical continuous phase FSK heterodyne transmission using delay-line demodulation," *Journal of Lightwave Technology*, vol. 9, no. 5, pp. 666–674, May 1991.

[79] R. Gangopadhyay, S. P. Mazumder, P. Cochrane, and E. Forestieri, "Performance analysis of a direct detection receiver for AMI-coded CPFSK signals," *IEEE Photonics Technology Letters*, vol. 7, no. 5, pp. 552–554, May 1995.

[80] P. Baroni, V. Miot, A. Carena, and P. Poggiolini, "8B10B line coding to mitigate the non-uniform FM laser response of direct modulated CPFSK transmitter," *Opt. Express*, vol. 16, no. 10, pp. 7279–7284, May 2008.

[81] "Bipolar encoding," https://en.wikipedia.org/wiki/Bipolar_encoding#Alternate_mark_inversion, 2016.

[82] A. X. Widmer and P. A. Franaszek, "A DC-balanced, partitioned-block,8B/10B transmission code," *IBM J. Research and Develop.*, vol. 27, no. 5, pp. 440–451, Sep. 1983.

[83] A. Elahi, "A fault tolerant indexed 5B/6B code," in *Proc. of IEEE Southeastcon '96. Bringing Together Education, Science and Technology*, Tampa, FL, Apr. 1996, paper 281-283.

[84] X. Widmer, "DC balanced 7B/8B, 9B/10B, and partitioned DC balanced 12B/14B, 17B/20B, and 16B/18B transmission codes," US Patent 6614369B1, Mar. 2003.

[85] F. Effinberger, F. Yu, Z. Wang, and J. Gao, "A 9B10B line code for 2.5 Gb/s upstream PONs," in *Proc. OFC*, San Diego, CA, Mar. 2009, paper JWA90.

[86] R. Walker and R. Dugan, "64B/66B low-overhead coding proposal for serial links," iEEE802.3ah (10GE) Task Force, 2000.

[87] Y. Rao, C. Chase, M. C. Y. Huang, S. Khaleghi, M. R. Chitgarha, M. Ziyadi, D. P. Worland, A. E. Willner, and C. J. Chang-Hasnain, "Continuous tunable 1550-nm high contrast grating VCSEL," in *Proc. CLEO*, San Jose, CA, May 2012, paper CTh5C.3.

[88] F. Fidler, C. Hambeck, P. Winzer, and W. Leeb, "410-Gb/s CWDM transmission using VCSELs from 1531 nm to 1591 nm," in *Proc. ECOC*, Cannes, France, pp. 521–522.

[89] M. Michael, H. Werner, N. Alexey, and M. Alex, "1.55 μm high-speed VCSELs enabling error-free fiber-transmission up to 25 Gbit/s," in *Proc. ISLC*, Kyoto, Japan, Sep. 2010, paper 156-157.

[90] F. Karinou, N. Stojanovic, G. Goeger, C. Xie, M. Ortsiefer, A. Daly, R. Hohenleitner, B. Kgel, and C. Neumeyr, "28 Gb/s NRZ-OOK using 1530-nm VCSEL, direct detection and mlse receiver for optical interconnects," in *Proc. IOIC*, San Diego, CA, Apr. 2015, paper 20-21.

[91] W. Hofmann, M. Muller, P. Wolf, A. Mutig, T. Grundl, G. Bouhm, D. Bimberg, and M.-C. Amann, "40 Gbit/s modulation of 1550 nm VCSEL," *Electron. Lett.*, vol. 47, no. 4, pp. 270–271, Feb. 2011.

[92] A. Malacarne, V. Sorianello, A. Daly, B. Kogel, M. Ortsiefer, S. Melo, C. Neumeyr, M. Romagnoli, and A. Bogoni, "High-speed long wavelength VCSELs for energy-efficient 40Gbps links up to 1 km without error correction," in *Proc. OFC*, Los Angeles, CA, Mar. 2015, paper Tu2H.1.

[93] R. Rodes, M. Mueller, B. Li, J. Estaran, J. B. Jensen, T. Gruendl, M. Ortsiefer, C. Neumeyr, J. Rosskopf, K. J. Larsen, M. Amann, and I. T. Monroy, "High-speed 1550 nm VCSEL data transmission link employing 25 GBd 4-PAM modulation and hard decision forward error correction," *J. Lightwave Technol.*, vol. 31, no. 4, pp. 689–695, Feb. 2013.

[94] C. Xie, P. Dong, S. Randel, D. Pilori, P. Winzer, S. Spiga, B. Kogel, C. Neumeyr, and M.-C. Amann, "Single-vcsel 100-Gb/s short-reach system using discrete multi-tone modulation and direct detection," in *Proc. OFC*, Los Angeles, CA, Mar. 2015, paper Tu2H.2.

[95] K. Szczerba, P. Westbergh, J. Karout, J. Gustavsson, A. Haglund, M. Karlsson, P. Andrekson, E. Agrell, and A. Larsson, "30 Gbps 4-PAM transmission over 200 m of MMF using an 850 nm VCSEL," *Opt. Express*, vol. 19, no. 26, pp. B203–B208, Dec. 2011.

[96] S. Takahashi, T. Okamura, and A. Tajima, "The fastest response burst-mode transmission scheme using small redundant scrambler and AC-coupled receiver with fast baseline response," in *Proc. OFC/NFOEC*, San Diego, CA, Mar. 2010, paper OThE7.

[97] H. Kim, S. K. Kim, H. Lee, S. Hwang, and Y. Oh, "A novel way to improve the dispersion-limited transmission distance of electroabsorption modulated lasers," *IEEE Photon. Technol. Lett.*, vol. 18, no. 8, pp. 947–949, Apr. 2006.

[98] S. Haykin, *Adaptive filter theory*. Prentice Hall, 2002.

[99] G. Malik and A. S. Sappal, "Adaptive equalization algorithms: an overview," *IJACSA*, vol. 2, no. 3, pp. 62–67, Mar. 2011.

[100] K. Szczerba, P. Westbergh, J. Karout, J. S. Gustavsson, A. Haglund, M. Karlsson, P. A. Andrekson, E. Agrell, and A. Larsson, "4-PAM for high-speed short-range optical communications," *J. Opt. Commun. Netw.*, vol. 4, no. 11, pp. 885–894, Nov. 2012.

[101] H. Kim, C. Yu, and D. T. Neilson, "Demonstration of optical duobinary transmission system using phase modulator and optical filter," *IEEE Photon. Technol. Lett.*, vol. 14, no. 7, pp. 1010–1012, Jul. 2002.

[102] H. Kim, G. Lee, H. Lee, S. Kim, I. Kang, S. Hwang, and Y. Oh, "On the use of 2.5-Gb/s Mach-Zehnder modulators to generate 10-Gb/s optical duobinary signals," *Photon. Technol. Lett.*, vol. 16, no. 11, pp. 2577–2579, Oct. 2004.

[103] P. Corvini and T. Koch, "Computer simulation of high-bit-rate optical fiber transmission using single-frequency lasers," *IEEE J. Lightw. Technol.*, vol. LT-5, no. 11, pp. 1591–1595, Nov. 1987.

[104] S. Walklin and J. Conradi, "Multilevel signaling for increasing the reach of 10 Gb/s lightwave systems," *IEEE J. Lightw. Technol.*, vol. 17, no. 11, pp. 2235–2248, Nov. 1999.

[105] H. Zhang, S. Fu, J. Man, W. Chen, X. Song, and L. Zeng, "4×25Gb/s 4-PAM modulation with commercial 10Gbps TOSA and ROSA for 100Gb/s-PON," in *Proc. OFC/NFOEC*, San Francisco, CA, Mar. 2014, paper M2I.3.

[106] Z. Li, L. Yi, X. Wang, and W. Hu, "28 Gb/s duobinary signal transmission over 40 km based on 10 GHz DML and PIN for 100 Gb/s PON," *Opt. Express*, vol. 23, no. 16, pp. 20 249–20 256, Aug. 2015.

[107] S. Chong, S. Li, Z. Al-Qazwini, S. Takahashi, T. Okamura, A. Tajima, and H. Kim, "Directly modulated laser transmitter using scramble-and-select-based line coding with low overhead," in *Proc. OECC*, Kaohsiung, Jul. 2011, paper 8E1-5.

[108] J. S. Eng and C. Kocot, *Optical Fiber Telecommunications VIA*. Academic Press, 2013.

[109] L. Graham, H. Chen, D. Gazula, T. Gray, J. Guenter, B. Hawkins, R. Johnson, C. Kocot, A. MacInnes, G. Landry, and J. Tatum, "The next generation of high speed VCSELs at Finisar," in *Proc. SPIE*, San Francisco, CA, Feb. 2012, paper 827602.

[110] J. Zhou, C. Yu, and H. Kim, "Transmission performance of OOK and 4-PAM signals using directly modulated 1.5-μm VCSEL for optical access network," *IEEE J. Lightw. Technol.*, vol. 33, no. 15, pp. 3243–3249, Jun. 2015.

[111] H. Kim, "10-Gbps operation of RSOA using a delay interferometer," *IEEE Photon. Technol. Lett.*, vol. 22, no. 18, pp. 1379–1381, Oct. 2010.

[112] J. Zhou, C. Yu, and H. Kim, "10-Gb/s, 20-km VCSEL optical access link at 1.5 μm with 23-dB power budget," in *Proc. OFC/NFOEC*, San Francisco, CA, Mar. 2014, paper W2A.2.

[113] Y. Chung and T. Shay, "Frequency stabilization of a diode laser to a Fabry-Perot interferometer," *Optical Engineering*, vol. 27, no. 5, pp. 424–427, Nov. 1988.

[114] J. Li, K. Worms, R. Maestle, D. Hillerkuss, W. Freude, and J. Leuthold, "Free-space optical delay interferometer with tunable delay and phase," *Opt. Express*, vol. 19, no. 12, pp. 11 654–11 666, Jun. 2011.

[115] H. Kim, "Transmission of 10-Gbps directly modulated RSOA signals in single-fiber loopback WDM PONs," *IEEE Photon. Technol. Lett.*, vol. 23, no. 14, pp. 965–967, Jul. 2011.

[116] K. J. Park, S. K. Shin, and Y. C. Chung, "Simple monitoring technique for WDM networks," *Electronics Letters*, vol. 36, no. 6, pp. 415–417, Mar. 1999.

[117] X. Li, S. Zhou, H. Ji, M. Luo, Q. Yang, L. Yi, R. Hu, C. Li, S. Fu, A. Arokiaswami, W.-D. Zhong, and C. Yu, "Transmission of 4×28-Gb/s PAM-4 over 160-km single mode fiber using 10G-class DML and photodiode," in *Proc. OFC*, Anaheim, CA, Mar. 2016, paper W1A.5.

[118] H.-Y. Chen, C.-C. Wei, H.-H. Chu, Y.-C. Chen, I.-C. Lu, and J. Chen, "An EAM-based 50-Gbps 60-km OFDM system with 29-dB loss budget enabled by SSII cancellation or Volterra filter," in *Proc. ECOC*, Cannes, Sep. 2014, paper P.3.21.

[119] T. Zuo, L. Zhang, E. Zhou, G. N. Liu, and X. Xu, "112-Gb/s duobinary 4-PAM transmission over 200-m multi-mode fibre," in *Proc. ECOC*, Valencia, Sep. 2015, paper 1-3.

[120] L. F. Suhr, J. J. V. Olmos, B. Mao, X. Xu, G. N. Liu, and I. T. Monroy, "Direct modulation of 56 Gbps duobinary-4-PAM," in *Proc. OFC*, Los Angeles, CA, Mar. 2015, paper Th1E.7.